iScience

CellPress

Article

Alzheimer Aβ Assemblies Accumulate in Excitatory Neurons upon Proteasome Inhibition and Kill Nearby NAKα3 Neurons by Secretion

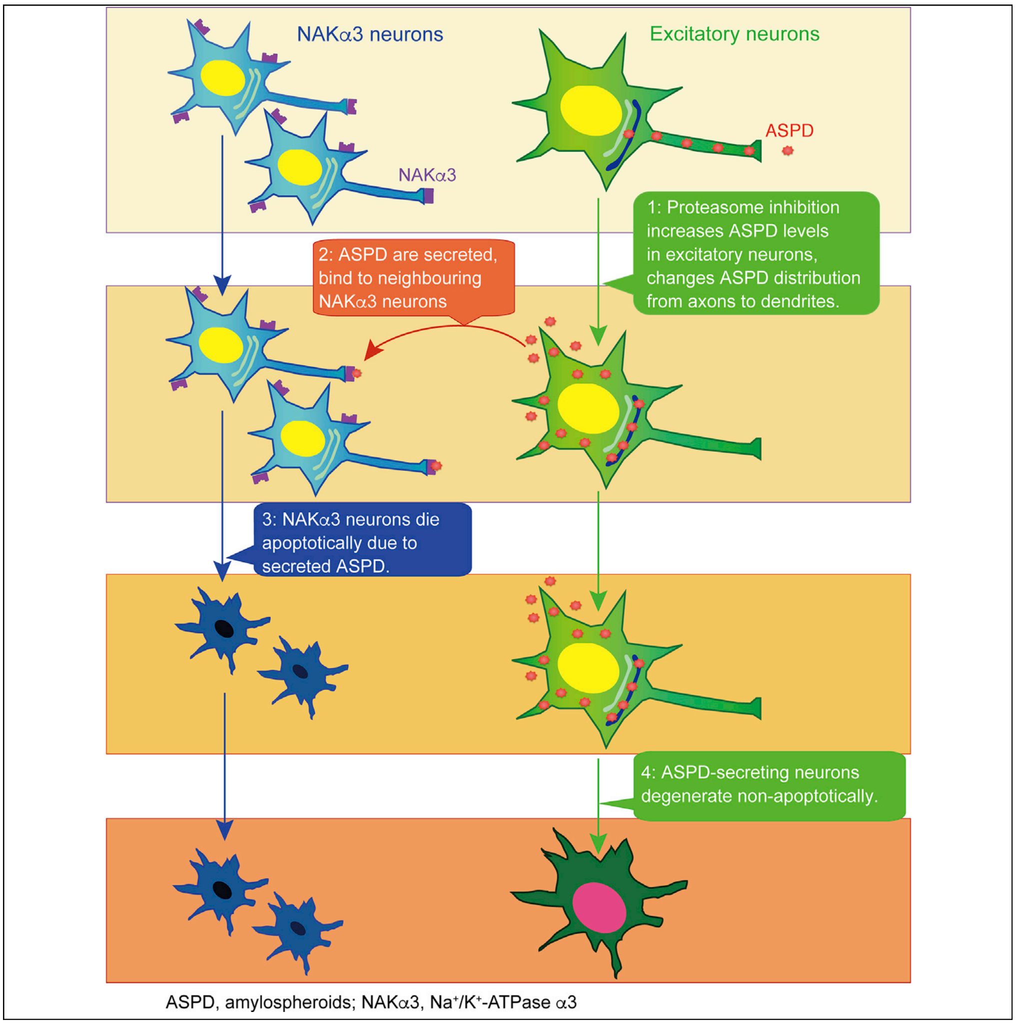

Hitomi Komura, Shota Kakio, Tomoya Sasahara, ..., Shin-ichi Muramatsu, Isao Kii, Minako Hoshi

minako.hoshi.9w@lmls-kobe.org

HIGHLIGHTS

Proteasome inhibition increases ASPD in excitatory neurons by increasing APP and Aβ

Proteasome inhibition shifts the Aβ and ASPD distribution from axons to dendrites

ASPDs are secreted and kill surrounding ATPase α3 neurons by cell surface binding

Following apoptosis in α3 neurons, ASPD-accumulating neurons die non-apoptotically

Komura et al., iScience *13*, 452–477
March 29, 2019
https://doi.org/10.1016/j.isci.2019.01.018

iScience

CellPress

Article

Alzheimer Aβ Assemblies Accumulate in Excitatory Neurons upon Proteasome Inhibition and Kill Nearby NAKα3 Neurons by Secretion

Hitomi Komura,[1,2,9] Shota Kakio,[1,2,9] Tomoya Sasahara,[1,2] Yoshie Arai,[1,2] Naomi Takino,[3] Michio Sato,[4] Kaori Satomura,[1,2] Takayuki Ohnishi,[1,2] Yo-ichi Nabeshima,[5] Shin-ichi Muramatsu,[3,6] Isao Kii,[7] and Minako Hoshi[8,9,10,*]

SUMMARY

We identified ∼30-mer amyloid-β protein (Aβ) assemblies, termed amylospheroids, from brains of patients with Alzheimer disease (AD) as toxic entities responsible for neurodegeneration and showed that Na^{+},K^{+}-ATPase α3 (NAKα3) is the sole target of amylospheroid-mediated neurodegeneration. However, it remains unclear where in neurons amylospheroids form and how they reach their targets to induce neurodegeneration. Here, we present an *in vitro* culture system designed to chronologically follow amylospheroid formation in mature neurons expressing amyloid precursor protein bearing early-onset AD mutations. Amylospheroids were found to accumulate mainly in the *trans*-Golgi network of excitatory neurons and were initially transported in axons. Proteasome inhibition dramatically increased amylospheroid amounts in *trans*-Golgi by increasing Aβ levels and induced dendritic transport. Amylospheroids were secreted and caused the degeneration of adjacent NAKα3-expressing neurons. Interestingly, the ASPD-producing neurons later died non-apoptotically. Our findings demonstrate a link between ASPD levels and proteasome function, which may have important implications for AD pathophysiology.

INTRODUCTION

Alzheimer's disease (AD) impairs neural networks involved in cognitive function by affecting synaptic connections and causing neuronal degeneration (Kouchi et al., 1998; Parthasarathy et al., 2015; Serrano-Pozo et al., 2011). Amyloid-β protein (Aβ), a small protein produced physiologically by proteolytic cleavages of the amyloid precursor protein (APP) (Haass et al., 2012), has been long considered to play a primary role in this process (Hardy and Selkoe, 2002). Aβ has the ability to form a range of structurally distinct assemblies, which exert different toxic functions via different targets (Benilova et al., 2012; Chiti and Dobson, 2009; Glabe, 2008; Hardy and Selkoe, 2002; Hoshi et al., 2003; Jarosz-Griffiths et al., 2016; Klein et al., 2001; Matsumura et al., 2011; Noguchi et al., 2009; Ohnishi et al., 2015; Roychaudhuri et al., 2009; Walsh and Selkoe, 2007). However, in neurons, the subcellular site and the regulation mechanism of Aβ production still remain to be determined (Haass et al., 2012), as do the mechanisms of Aβ assembly into neurotoxic structures and the manner in which these structures encounter their target neurons.

We previously identified a population of neurotoxic Aβ assemblies, amylospheroids (ASPD), stable assemblies containing approximately 30 monomers (Hoshi et al., 2003; Matsumura et al., 2011; Noguchi et al., 2009; Parthasarathy et al., 2015). ASPD bind to the neuron-specific α3 subunit of the Na^{+}, K^{+}-ATPase pump (NAKα3), with a K_d in the low nanomolar range, and induce neurodegeneration by impairing the pump activity (Ohnishi et al., 2015). Importantly, ASPD concentration correlated with disease severity and progression in patients (Ohnishi et al., 2015). Interestingly, ASPD levels were high in the cerebral cortex, where NAKα3-expressing neurons were lost, whereas their levels were low in the cerebellum, where NAKα3-expressing neurons were preserved. These findings showed that NAKα3 was a neurotoxic target of ASPD and also suggested a difference in the ability to form ASPD between brain regions (Ohnishi et al., 2015).

In vitro studies have shown that the pathway of ASPD assembly from Aβ monomers is distinct from those of other Aβ oligomers (Matsumura et al., 2011). A key question remaining was how ASPD formation occurred

[1]Department of Brain and Neurodegenerative Disease Research, Institute of Biomedical Research and Innovation, Foundation for Biomedical Research and Innovation at Kobe, Kobe 650-0047, Japan

[2]TAO Health Life Pharma Co., Ltd., Med-Pharma Collaboration Bldg, Kyoto University, 46-29 Yoshida Shimoadachi-cho, Sakyo-ku, Kyoto 606-8501, Japan

[3]Division of Neurology, Jichi Medical University, Shimotsuke 329-0498, Japan

[4]Meiji University, Graduate School of Agriculture, Meiji University, Kawasaki 214-8571, Japan

[5]Department of Gerontology, Institute of Biomedical Research and Innovation, Foundation for Biomedical Research and Innovation at Kobe, Kobe 650-0047, Japan

[6]Center for Gene & Cell Therapy, The Institute of Medical Science, University of Tokyo, Tokyo 108-0071, Japan

[7]RIKEN Center for Life Science Technologies, Division of Bio-Function Dynamics Imaging, Kobe 650-0047, Japan

[8]Department of Anatomy and Developmental Biology, Graduate School of Medicine, Kyoto University, Kyoto 606-8501, Japan

[9]These authors contributed equally

[10]Lead Contact

*Correspondence: minako.hoshi.9w@lmls-kobe.org

https://doi.org/10.1016/j.isci.2019.01.018

in vivo. We reasoned that because the primary component of patient-derived ASPD appears to be Aβ (Ohnishi et al., 2015), ASPD formation should be linked to Aβ production from APP. Full-length APP is synthesized in the endoplasmic reticulum (ER) and transported through the Golgi apparatus to the *trans*-Golgi network (TGN), where the highest concentration of APP is found in neurons in steady state (Greenfield et al., 1999; Hartmann et al., 1997; Xu et al., 1997). From the TGN, a population of APP is further transported in the TGN-derived secretory vesicles to the plasma membrane (PM) where it is either cleaved by α-secretase to produce a soluble molecule, sAPPα, or re-internalized via an endosomal/lysosomal degradation pathway (Haass et al., 2012). Aβ has been reported to be generated from mature APP through β- and γ-secretase cleavages in the above sorting pathways that interconnect the TGN, the cell surface, and the endosomes (Haass et al., 2012). Therefore we hypothesized that ASPD might also be generated in these pathways.

Proteasomes may also be involved in APP/Aβ degradation (Wang and Saunders, 2014). Proteasomes are present mainly in the cytoplasm in mammalian cells, but immune electron microscopy has shown that they can also be associated with the cytoplasmic surface of the ER in mammalian cells (Palmer et al., 1996; Rivett et al., 1992). Membrane proteins like APP are retro-translocated from the ER to the cytoplasm and degraded by the ER-associated proteasomes. This process is termed ER-associated degradation (ERAD) (Vembar and Brodsky, 2008). In general, upward of 30% of newly synthesized proteins are degraded by proteasomes (Schubert et al., 2000), including APP and Aβ (Wang and Saunders, 2014). Proteasome activities are lower in AD brains than in age-matched control brains (Keck et al., 2003; Keller et al., 2000), and proteomic studies have suggested that proteasome impairment might be a risk factor for AD (Manavalan et al., 2013; Tonoki et al., 2009). We report here studies to determine the role of proteasomes in ASPD formation. Our approach was to inhibit the proteasome-mediated degradation of APP and Aβ and determine its effect on ASPD formation in mature neurons. For this purpose, we established an *in vitro* cellular system to monitor ASPD formation in neurons expressing APP-bearing mutations linked to familial early-onset AD. As summarized in the Graphical Abstract, we found that proteasome inhibition dramatically increased intra-neuronal ASPD levels and changed ASPD distribution from the axon to dendrites. ASPD were then secreted and killed neighboring NAKα3 neurons. These findings deepen our understanding of the formation and delivery of toxic Aβ oligomers in AD brains, which in the future may open up the possibility of developing anti-assembly drugs for AD by modifying APP/Aβ degradation.

RESULTS

Introduction of Human APP770 Gene Bearing the Early-Onset Mutations into Mature Hippocampal Neurons by Using an AAV Vector

To establish a mature neuron-based system, we introduced human APP770 gene with a familial AD mutation into rat hippocampal neuronal cultures at 10 days *in vitro* (DIV) using an adeno-associated virus 1-derived (AAV) vector (Li et al., 2006) (Transparent Methods, Figure 1A). Two types of mutations were selected. One was the Swedish mutation (APPswe), which results in the substitution of Lys^{670} and Met^{671}, two amino acids adjacent to the β-secretase cleavage site, into Asn^{670} and Leu^{671}, respectively (Mullan et al., 1992). The other was the Osaka mutation (APPosk), which involves deletion of the entire codon 693 encoding glutamate (corresponding to glutamate at position 22 of Aβ; accordingly designated as E22Δ) (Tomiyama et al., 2008). Western blot and immunocytochemistry confirmed that mature human APP was expressed in neurons transduced with either APPswe or APPosk gene (Figures 1B and 1C). The level of expressed human APP was on average 2.7 times (as to APPswe) or 5.1 times (as to APPosk) as much as that of endogenous rodent APP, based on quantification in western blots (Figure 1B). As reported previously (Powell et al., 2016), the AAV vector showed tropism for neurons over astrocytes. In our study, transduction efficiency of rat hippocampal neurons with the AAV vector was usually >85%. Consistently, in the AAV-infected cultures, the human APP770-specific antibody detected human APP770 protein in almost all the neurons (Figure 1C and enlarged views in insets) and minimal expression in astrocytes (Figure 1C).

Proteasome Inhibition Affects Aβ Metabolism

We first examined the effect of proteasome inhibition on Aβ production by treating the AAV-transduced mature neurons with a proteasome inhibitor, MG132 (IC_{50} of 100 nM; Tsubuki et al., 1996), at 75 nM for 24 h. Because the rate-limiting step in Aβ production is cleavage of APP by BACE-1 (Sinha and Lieberburg, 1999), we monitored cleavage levels using an Aβ N-terminal-end-specific antibody that does not cross-react with full-length APP. As shown in Figure 2A, proteasome inhibition markedly increased Aβ N-terminal-end-specific (N-terAβ) staining in human APP-transduced mature neurons. Although the degree of increase

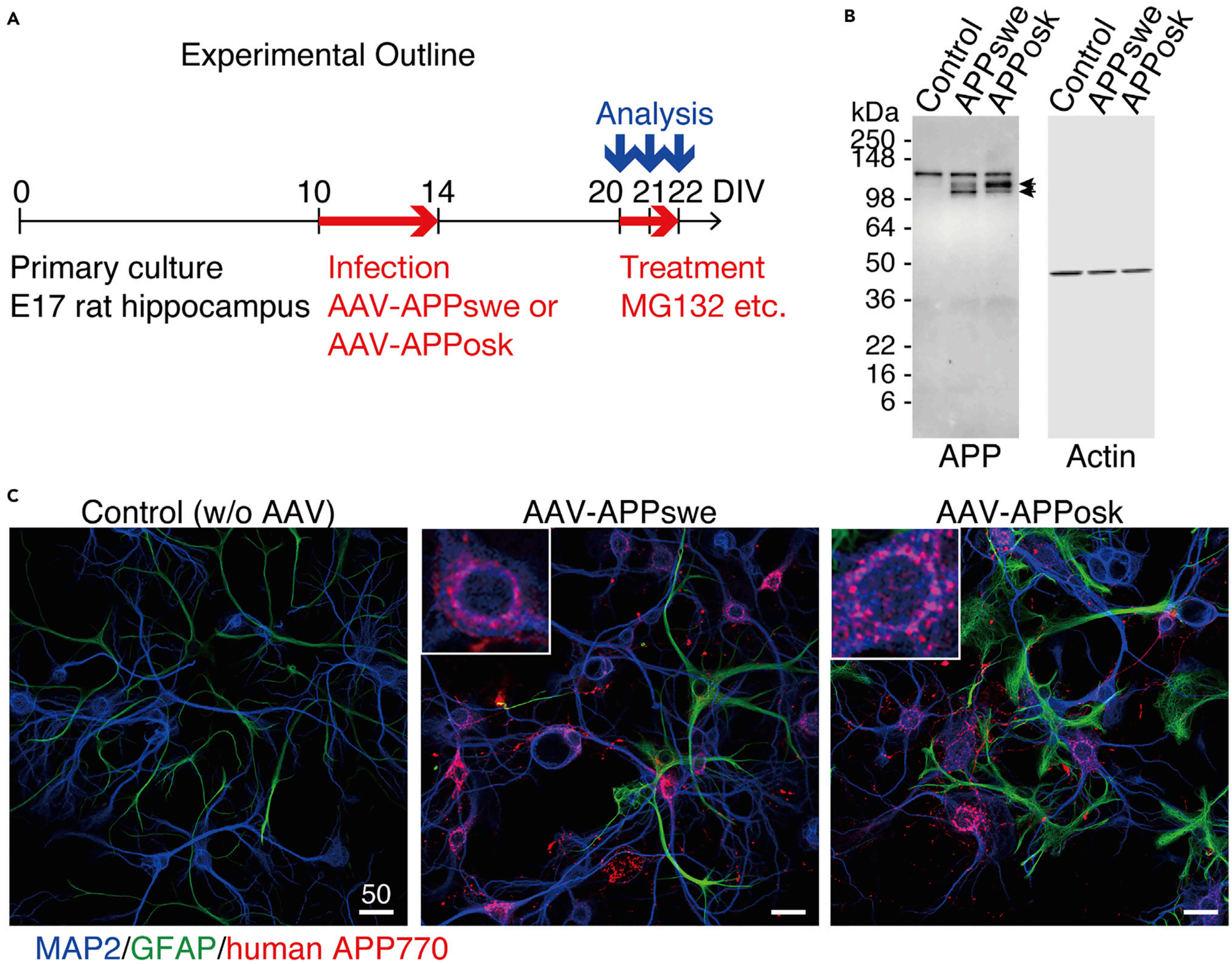

Figure 1. Expression of Human APP in Mature Neurons

(A) Experiments were performed as shown here except for the staining in the upper panels of Figure 5A (performed at 30 DIV).

(B) Representative western blot of whole lysates (10 μg/lane) of primary rat hippocampal neuronal cultures with or without AAV-APP transduction, detected by anti-APP or anti-actin antibody (see Transparent Methods). Arrows show *O*-glycosylated or *N*-glycosylated human APP, above which rat APP was also detected.

(C) Primary rat hippocampal neuronal cultures, with or without AAV-APP transduction, were stained with antibodies against MAP2, GFAP, and human APP at 22 DIV (see Transparent Methods). Representative images are shown. Scale bar, 50 μm. An enlarged view of the field is shown in the insets.

varied widely from neuron to neuron, N-terAβ staining appeared to increase in almost all the neurons (Figures 2A and S1), consistent with human APP expression in almost all the neurons (Figure 1C). Similarly, we found that human APP770-specific staining increased markedly in the neuronal cell body after 24-h MG132 treatment (Figure 2B). At this time, Aβ assemblies were trimeric, as assessed by SDS-PAGE (red arrow in Figure 3 left panel). Western blot showed that Aβ and human APP levels increased approximately 3- and 10-fold, respectively (Figure 3). We confirmed that proteasome inhibition did not accelerate Aβ secretion as the level of secreted Aβ, either $A\beta_{1\text{-}40}$ or $A\beta_{1\text{-}42}$, was not changed or even slightly decreased (*$p = 0.04$ by Scheffé post hoc test; $n = 4$) after 24-h MG132 treatment (Figure S2). Collectively, these data showed that proteasome inhibition led to an increase in the steady-state level of Aβ in our system, either directly by inhibiting ERAD-mediated Aβ degradation or indirectly by increasing the APP available for Aβ production.

Inhibition of Proteasome Activities Increases ASPD Accumulation in Mature Neurons Expressing Human APP Bearing the Early-Onset Swedish Mutation

We next examined the effect of proteasome inhibition on ASPD formation using the APPswe transgene, which increases Aβ production by facilitating APP processing mediated by β-secretase without any change

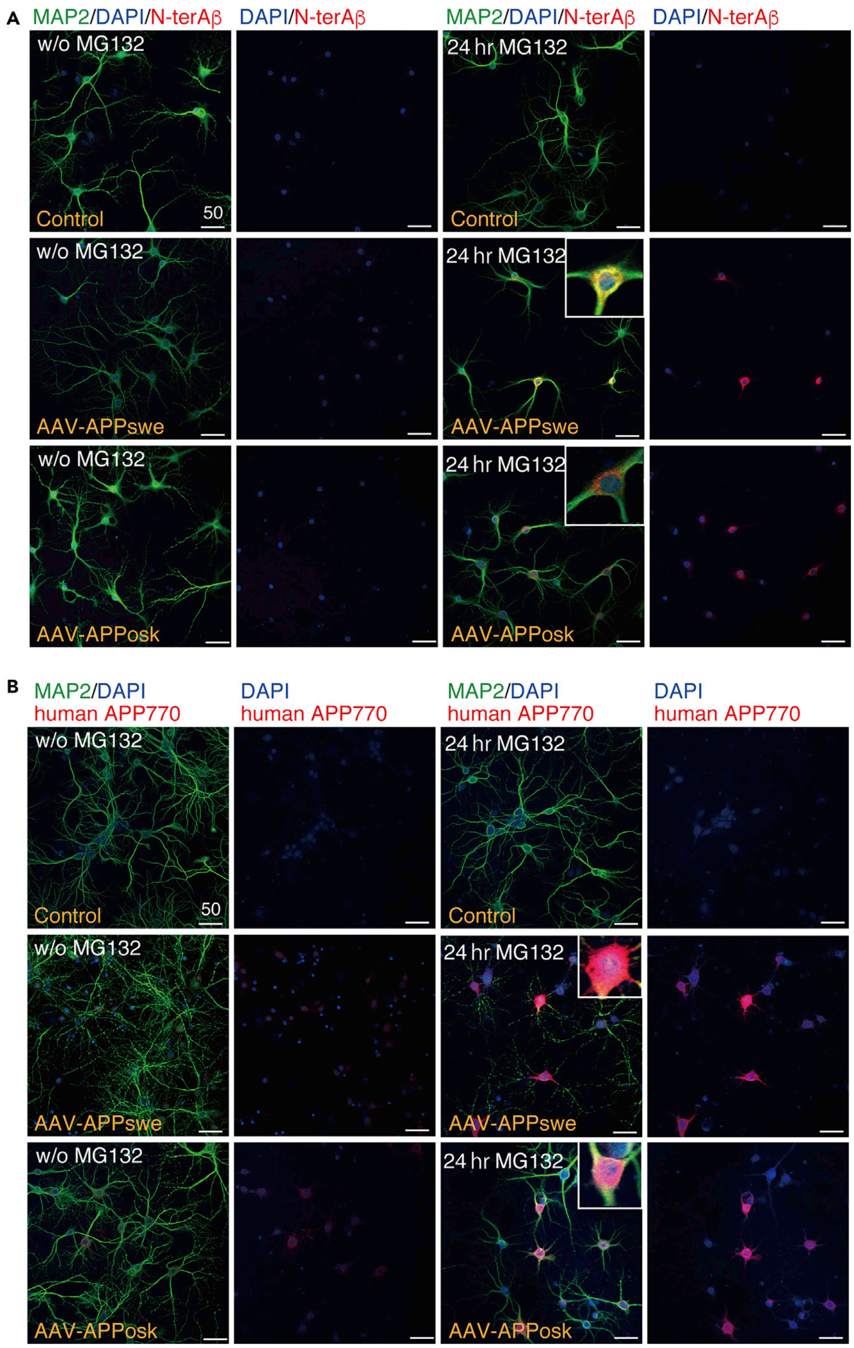

Figure 2. Effect of Proteasome Inhibition on Aβ and APP

(A and B) Primary rat hippocampal neuronal cultures, with or without AAV-APP transduction, were treated with or without 75 nM MG132 for 24 h. The cultures were triple stained with DAPI, anti-MAP2, and anti-Aβ N-terminal end-specific (N-terAβ) antibodies in (A) or stained with DAPI, anti-MAP2, and anti-human APP770-specific antibodies in (B) (Transparent Methods). Representative images are shown. For each condition, left columns show the triple staining, whereas right columns show the corresponding DAPI/N-terAβ staining in (A) or DAPI/human APP770 staining in (B). An enlarged view is shown in the insets. Scale bar, 50 μm.

See Figures 1 and S1.

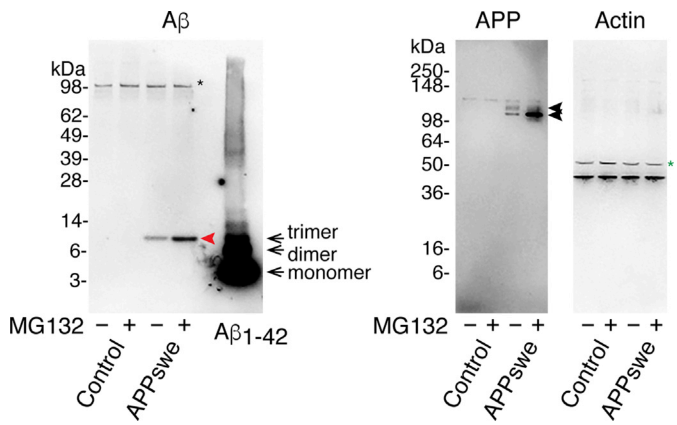

Figure 3. Effect of Proteasome Inhibition on Aβ and APP

Representative western blot of whole lysates (8 μg/lane) of primary rat hippocampal neuronal cultures with or without AAV-APP transduction, treated with or without 75 nM MG132 for 24 h, detected by anti-Aβ N-terminal, anti-APP, or anti-actin antibody (see Transparent Methods). Left panel, Aβ appeared at the position of the trimer in SDS-PAGE (red arrowhead). The right lane represents western blot of synthetic $A\beta_{1-42}$ (4 pmol/lane). Black arrows show monomer, dimer, and trimer positions. The asterisk indicates non-specific bands detected by anti-Aβ N-terminal antibodies. Middle panel, arrows show *O*-glycosylated or *N*-glycosylated human APP, above which rat APP was also detected. Right panel, green asterisk shows non-specific bands detected by an anti-actin antibody. See Figure S2.

in the Aβ sequence (Cai et al., 1993; Citron et al., 1992). As shown in Figures 4A and S3A, after 24-h treatment with MG132, APPswe-transduced neurons showed a marked increase in ASPD staining. Consistent with AAV tropism for neurons (Figure 1C), ASPD staining was increased essentially in microtubule-associated protein 2 (MAP2)-positive neurons, but rarely in glial fibroblast acidic protein (GFAP)-positive astrocytes, after 24-h MG132 treatment (Figure 4A left). However, whereas N-terAβ antibody staining was observed in some degree in almost all the neurons, only a limited population of the APPswe-transduced neurons showed an increased ASPD staining (arrowheads in Figure S1). The level of ASPD staining thus does not simply correlate with N-terAβ staining. In contrast with APPswe-transduced neurons, untransduced neurons (without human APP) that produce only endogenous rodent Aβ rarely accumulate ASPD. This is reasonable because, owing to the three amino acid substitutions, Arg5Gly, His13Arg, and Tyr10Phe, rodent Aβ is less prone to form toxic, smaller aggregates when compared with human Aβ, resulting in higher resistance to the development of AD-like neuropathology (Roychaudhuri et al., 2015).

To confirm that proteasomal dysfunction caused the ASPD formation, we examined the concentration-dependent effects of various pharmacologically unrelated inhibitors on ASPD formation. In addition to a reversible inhibitor, MG132 (Figure S3A), we examined an irreversible inhibitor, epoxomicin, (IC_{50} of ~4 nM; Kim et al., 1999; Figure S3B), and an irreversible inhibitor, lactacystin, (IC_{50} of 4.8 μM; Csizmadia et al., 2010; Figure S3C). All these proteasome inhibitors increased the neuronal ASPD staining at 24 h in a dose-dependent fashion (Figures 4A and S3). Based on these observations, further experiments were performed using MG132 at 75 nM.

We next examined spatiotemporal change in ASPD staining after 75 nM MG132 treatment. As shown in Figure 4B, left columns, baseline levels of ASPD staining were detected in untransduced control cultures, which did not change after 24-h MG132 treatment (see quantification in Figure 4B right). In contrast with control cultures, MG132 treatment increased the ASPD levels substantially and significantly with time in APPswe-transduced neurons (see quantification in Figure 4B right). Initially, very diffuse ASPD staining was consistently detected in the APPswe-transduced neurons before proteasome inhibition (see images of AAV-APPswe at 0 h in Figures 4B and S3A–S3C). This diffuse ASPD staining in neuronal cell bodies was usually accompanied with axonal ASPD staining that was co-stained by an axonal marker, an antibody against neurofilament heavy chain (arrows at 0 h in Figure 4B right and orange arrows in upper panels of Figure 5A). MG132 treatment for 6 h markedly increased the ASPD staining in neuronal cell bodies (representative image of the 6-h MG132 treatment: Figure 4B middle and right). At this time point, in addition to the axonal ASPD staining, dendritic ASPD staining appeared (arrowheads at 6 h in Figure 4B right). MG132 treatment for 24 h dramatically increased both the number of neurons that contained ASPD and the

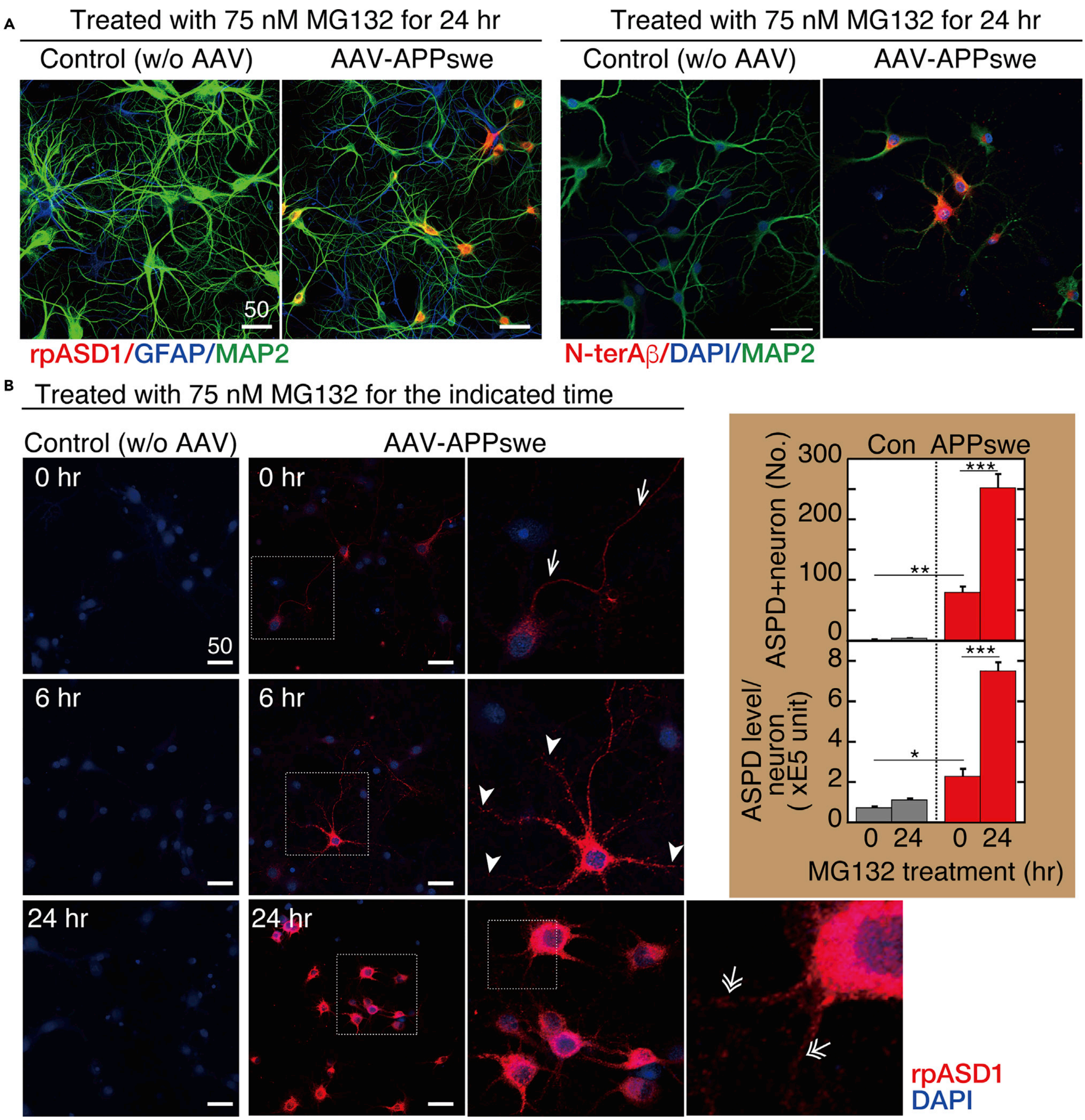

Figure 4. Proteasome Inhibition Increases Intra-neuronal ASPD Accumulation

(A) Primary rat hippocampal neuronal cultures, with or without AAV-APPswe transduction, were treated with 75 nM MG132 for 24 h. The cultures were triple stained with antibodies against N-terAβ, MAP2, and DAPI on the right side, or against MAP2, GFAP, and ASPD (rpASD1) on the left side. Representative images are shown. Scale bar, 50 μm. In this work, ASPD were detected by immunohistochemical staining with ASPD-specific rpASD1 antibody or mASD3 antibody (Noguchi et al., 2009), both of which have been used to detect ASPD in immunopathological studies of human brains (Noguchi et al., 2009; Ohnishi et al., 2015).

(B) Primary rat hippocampal neuronal cultures, with or without AAV-APPswe transduction, were treated with 75 nM MG132 for the indicated time. The cultures were double stained with anti-ASPD rpASD1 antibody and DAPI. An enlarged view of the field enclosed by a hatched line is shown immediately on the right. Representative images are shown. Scale bar, 50 μm. The number of ASPD and MAP2 double-positive cells was counted by using a GE Healthcare Life Sciences "IN Cell Analyzer" system and is shown as "ASPD + neuron" in the inset upper panel. Then the total amount of rpASD1-immunostained ASPD that was detected in MAP2-positive cells was determined by using an IN Cell Analyzer and was divided by the number of ASPD and MAP2 double-positive cells, which is shown as "ASPD level/neuron" in the inset lower panel (mean ± SD, n = 3; Scheffé post hoc test; ***$p < 0.0001$, **$p = 0.0006$, *$p = 0.0176$).
See Figures 1, S1, S3, and 5.

ASPD level in each neuron (an image of the 24-h MG132 treatment is shown in Figure 4B, middle and right; quantification on the right). Interestingly, at this stage, the axonal ASPD staining disappeared (orange arrows in lower panels of Figure 5A). Conversely, the dendritic ASPD staining became stronger, and its distribution changed (double-lined white arrows in lower panels of Figure 5A). At 6-h MG132 treatment, the dendritic ASPD staining was distributed along the entire length of the dendrite, all the way to its tip (arrowhead at 6 h in Figure 4B right). However, at 24-h treatment, the dendritic ASPD staining reached the dendritic branch points, but the staining at the tip had weakened and become patchy (double-lined arrows at 24 h in Figure 4B rightmost panel and double-lined white arrows in lower panels of Figure 5A). High-power images showed that ASPD mostly appeared to stay inside of the dendrites (orange arrows in Figure 5B), but some dendritic ASPD signals on MAP2-labeled dendrites (39.6% $\pm$ 4.7%; n = 7 and total count = 1,614) appeared on the surface proximal to the Bassoon staining (double-lined white arrows in Figure 5B). The spatiotemporal change in ASPD staining is schematically illustrated in Figure 5C. Thus proteasome inhibition markedly increased the intra-neuronal ASPD level in steady state and led to changes in its intra-neuronal distribution.

ASPD Accumulate in the *Trans*-Golgi Network

Next, we examined the subcellular location of ASPD in the APPswe-transduced neurons by double labeling neurons with an ASPD-specific rpASD1 antibody and organelle-specific antibodies. Representative images and their single-channel images are shown in Figures 6 and S4, respectively. Before MG132 treatment, the number of ASPD signals was small, but they were present mainly where the *trans*-Golgi network-38 (TGN38) signal (Humphrey et al., 1993) was found (see arrowheads in enlarged views of TGN38/rpASD1 staining of Figure 6, and their line scans in Figure 7). With longer MG132 treatment, more ASPD accumulated at the TGN (compare 0-, 6-, and 24-h MG132 treatment in enlarged views of Figures 6 and 7). In contrast, ASPD staining was not co-localized with the ER marker, protein disulfide isomerase (PDI) (Wilkinson and Gilbert, 2004), or a *cis*-Golgi marker, GM130 (Nakamura et al., 1995), without proteasome inhibition and only rarely co-stained with them at 6-h MG132 treatment (see arrowhead in lower part of Figure 6; their line scans in Figure 7). After 24-h MG132 treatment, more ASPD signals were found together with PDI and GM130 signals, but the coexistence rate in TGN38/ASPD appeared to be higher than that in PDI/ASPD or GM130/ASPD (compare staining of TGN38/ASPD with that of PDI or GM130/ASPD in Figures 6 and S4). ASPD staining in mature neurons was also rarely co-localized with early endosome antigen 1 (EEA1) (Barysch et al., 2009) or lysosomal-associated membrane protein-1 (LAMP1) (Carlsson and Fukuda, 1989) at 6-h MG132 treatment (Figures 6, single channel images in S4, and line scans in Figure 7). This basically remained the case at 24-h MG132 treatment, at which time the vast majority of ASPD staining did not overlap with EEA1 or LAMP1 staining, although some overlap of the ASPD signal with them was seen (see arrowheads in lower part of Figure 6). ASPD staining was rarely observed in untransduced neurons with or without MG132 treatment (Figure S5).

Although the TGN has been presumed to be a sorting site for newly synthesized membrane and secretory proteins, recent studies suggested that the recycling endosomes (REs), detected by an antibody either against the transferrin receptor (TfR) or Rab11 (Kobayashi and Fukuda, 2013), may serve as a sorting hub to direct proteins to the PM (Lasiecka and Winckler, 2011). Interestingly, we found that ASPD were present in the REs of APPswe-transduced neurons at 24-h MG132 treatment (Figures 8 and S6), which is not surprising, given the close and dynamic cross-talk between the TGN and the REs in neurons (Schmidt and Haucke, 2007). However, whereas ASPD always appears to co-localize with the TGN, ASPD co-localization with the REs was rarely detected up to 6-h MG132 treatment. The results strongly support the idea that the TGN is the major and initial site of ASPD localization in mature neurons.

To further elucidate ASPD localization in the TGN, we used brefeldin A (BFA), a lactone antibiotic and ATPase inhibitor for protein transport (IC_{50} of 0.06 μg/mL in HCT116 cells; Zhu et al., 2000), which rapidly collapses the Golgi apparatus into the ER by inhibiting protein transport from the ER to the Golgi apparatus (Nebenfuhr et al., 2002; Sciaky et al., 1997). In our system, BFA treatment at 0.6 μg/mL was enough to destroy the Golgi structure without affecting the cell viability in untransduced neurons (compare neurons with the preserved Golgi structure [orange arrow] and those with BFA-destroyed Golgi structure [green arrow] in Figure S7). When MG132-treated APPswe-transduced mature neurons were treated with 0.6 μg/mL BFA for 24 h, the level of ASPD staining was markedly reduced to 36% $\pm$ 13% (n = 3) of that without BFA treatment (see high-power images in the right, quantification results below in Figure 9). We also found that BFA treatment of MG132-treated APPswe-transduced neurons substantially decreased

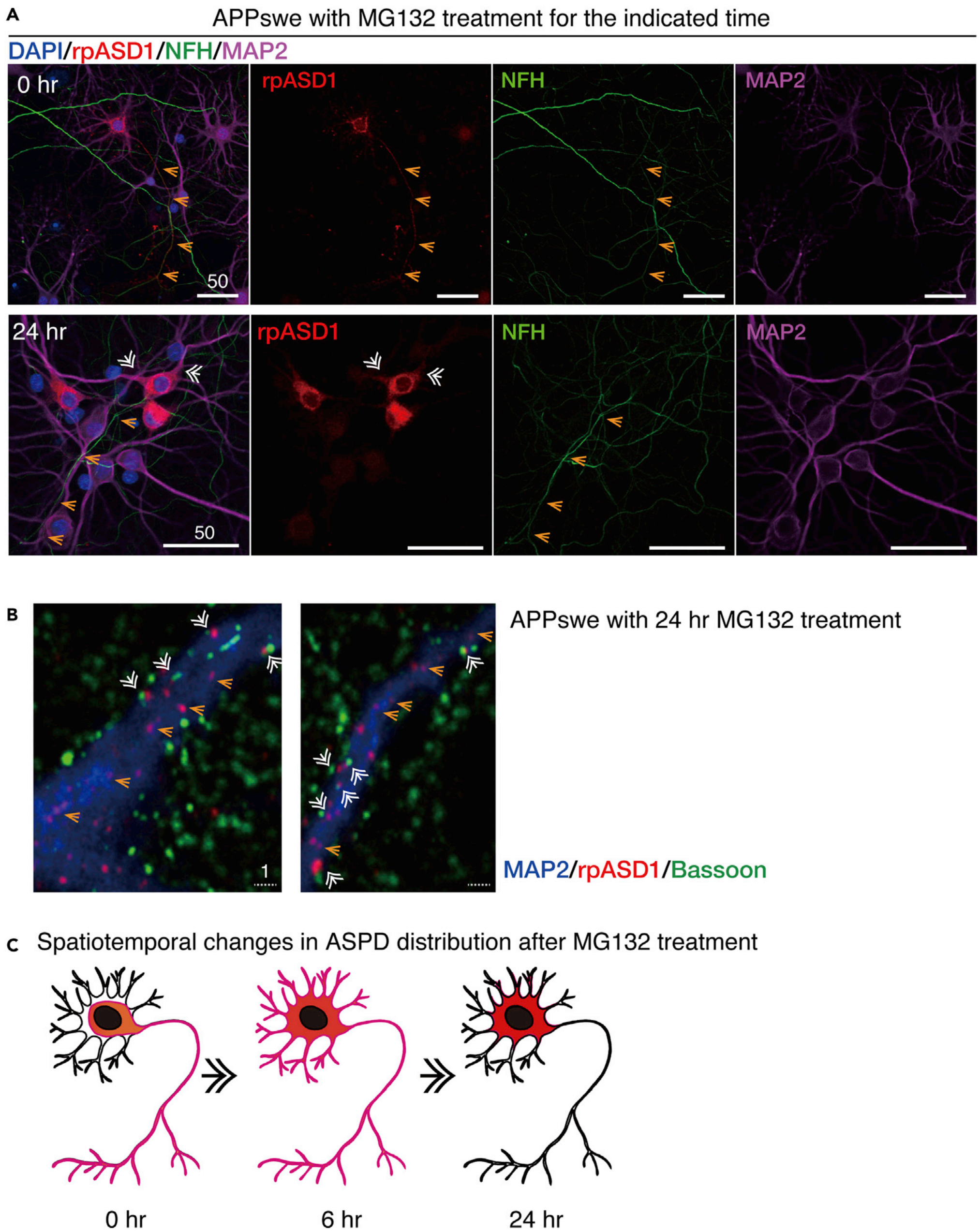

Figure 5. Proteasome Inhibition Changes ASPD Distribution from Axon to Dendrites

(A) Upper panels: primary rat hippocampal neuronal cultures with AAV-APPswe transduction were quadruple stained at 30 DIV with the anti-ASPD rpASD1 antibody, anti-NFH antibody, anti-MAP2 antibody, and DAPI (see Transparent Methods). Lower panels: primary rat hippocampal neuronal cultures with AAV-APPswe transduction were treated with 75 nM MG132 for 24 h and quadruple stained at 22 DIV as in the upper panels. A representative image, along with the corresponding single red, green, or magenta image, is shown with 50-μm scale bars. Orange arrows mark the axon, whereas white double-lined arrows mark dendrites. ASPD were co-localized with NFH (orange arrows) in the upper panels, but co-localized with MAP2 (white double-lined arrows) in the lower panels.

(B) APPswe-transduced primary rat hippocampal neuronal cultures were treated with 75 nM MG132 for 24 h. The cultures were triple stained with antibodies against MAP2, Bassoon, and ASPD (rpASD1) on the left side. Representative images are shown. Scale bar, 1 μm.

(C) Spatiotemporal changes in the ASPD distribution observed in Figures 3B and 4A are schematically shown in red. See Figures 4 and S19.

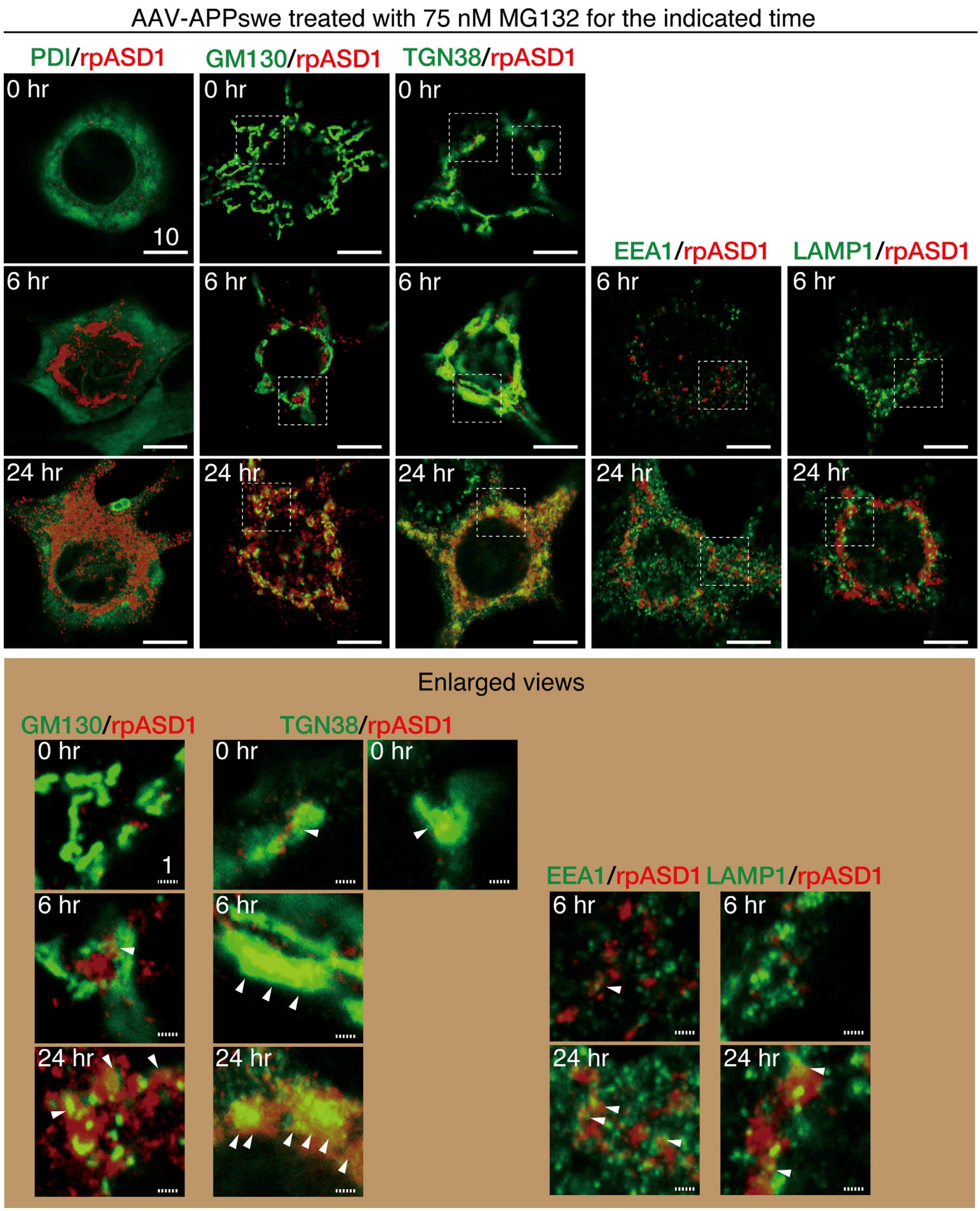
AAV-APPswe treated with 75 nM MG132 for the indicated time
PDI/rpASD1
GM130/rpASD1
TGN38/rpASD1
EEA1/rpASD1
LAMP1/rpASD1
0 hr
6 hr
24 hr
10
Enlarged views
1

Figure 6. ASPD Accumulate in the *Trans*-Golgi of Mature Neurons

Primary rat hippocampal neuronal cultures, with or without AAV-APPswe transduction, were treated with 75 nM MG132 for the indicated time. The cultures were double-stained with anti-ASPD rpASD1 antibody and antibody against organelle marker protein (see Transparent Methods). A highly sensitive, quantitative single-photon-counting system employing avalanche photodiodes on a Zeiss LSM710 microscope was used to perform detailed analyses along the z axis in high-power views of each neuronal cell body doubly-stained with ASPD-specific rpASD1 antibody and an antibody against an organelle marker. Representative images obtained with a 100X oil objective lens are shown. An enlarged view of the field enclosed by a hatched line is shown below. Solid and hatched scale bars, 10 and 1 μm, respectively. Single red and green images for each time point are shown in Figure S4. See also representative images of control cultures without AAV transduction in Figure S5. See Figures 7, S4, and S5.

the ASPD and TGN38 signals in a time-dependent manner (Figure S8). These results further support the idea that ASPD are mainly present in the TGN under steady-state conditions.

We then examined the steady-state distribution of human APP770 and N-terAβ in APPswe-transduced mature neurons treated with MG132 for 24 h. As shown in Figure S9, human APP770-specific signals increased most intensely in the TGN and also in the ER in APPswe-transduced neurons with MG132 treatment. In the case of N-terAβ staining, the signal was increased mainly in the *cis*-Golgi, and also on the TGN, the REs, and the ER surface, but was rarely observed in the early endosomes (EEs) or the Lys in our system (Figures S10 and S11). In contrast, without MG132 treatment, the signal intensity of either human APP770 or N-terAβ was too weak to determine its subcellular distribution (representative images in Figures S9–S11).

Finally, we performed a quantitative co-localization analysis of N-terAβ staining and ASPD staining with organelle markers in MG132-treated APPswe-transduced cells. As shown in Figure 10, although N-terAβ and ASPD co-localized to some extent with EEA1 and LAMP1-stained areas, the levels of co-localization in PDI-, GM130-, TGN38-, and TfR-stained areas were always substantially and significantly ($p < 0.0001$ by Scheffé post hoc test, see legend in Figure 10) higher than those in EEA1- and LAMP1-stained areas. Interestingly, among PDI-, GM130-, TGN38-, and TfR-stained areas, the co-localization coefficients for N-terAβ were consistently significantly higher in GM130-stained areas, whereas the coefficients for ASPD were always significantly higher in TGN38-stained areas ($p < 0.0001$ by Scheffé post hoc test, see the legend in Figure 10) in steady state.

ASPD Accumulate in the *Trans*-Golgi Network and the Recycling Endosomes of Mature Neurons Expressing APP Bearing the Osaka Mutation

The Osaka mutation causes the deletion of a single amino acid, residue E693 (corresponding to E22 of Aβ). Because Aβ fibrils appeared to be absent in the brains of patients and mice carrying this mutation (Tomiyama et al., 2008, 2010), the mutation was believed to accelerate only the formation of Aβ oligomers. However, precise conformational and assembly kinetic studies of the mutant peptides *in vitro* revealed that the primary biophysical effect of this mutant is to accelerate conformational changes in the monomer that facilitate oligomerization and fibril formation (Inayathullah and Teplow, 2011). To address whether this mutation facilitates ASPD formation in mature neurons, we first examined whether E22Δ-$A\beta_{1-42}$ ($A\beta_{1-42}$-osk) formed neurotoxic ASPD by using a toxicity assay, transmission electron microscopic analysis, and dot blotting with anti-ASPD antibody rpASD1 (Figure 11A). Interestingly, ASPD derived from $A\beta_{1-42}$-osk were more toxic to mature hippocampal neurons than ASPD from wild-type $A\beta_{1-42}$ (compare viability data at 18 nM in Figure 11A). Treatment of the APPosk-transduced neurons with 75 nM MG132 for 24 h led to a marked increase in both the number of the ASPD-containing neurons and the ASPD levels in each neuron (see Figure 11B), as observed in the case of the APPswe transduction, except that the ASPD level in each neuron was significantly lower in the case of APPosk transduction, compared with APPswe transduction ($n = 3$, $p < 0.0001$ by Scheffé post hoc test, Figure 11B below). As observed in APPswe-transduced neurons, proteasome inhibition increased N-terAβ and human APP770 staining in almost all APPosk-expressing neurons (Figures 2), whereas ASPD accumulation was detected only in some of the N-terAβ-labeled neurons (Figure S1). High-power images of these ASPD-containing APPosk-expressing neurons showed that ASPD staining was co-localized mainly with TGN38 and also with the cis-Golgi GM130 and the RE marker, TfR, as observed in the APPswe-expressing neurons, at 24-h MG132 treatment (Figure 11C). Finally, the Golgi-destroying BFA treatment confirmed that ASPD accumulated in the Golgi apparatus of the APPosk-transduced neurons (Figure S12). Thus based on the findings in neurons expressing the two different APP transgenes, we conclude that the TGN is the primary site of ASPD accumulation in steady state in APP-expressing mature neurons.

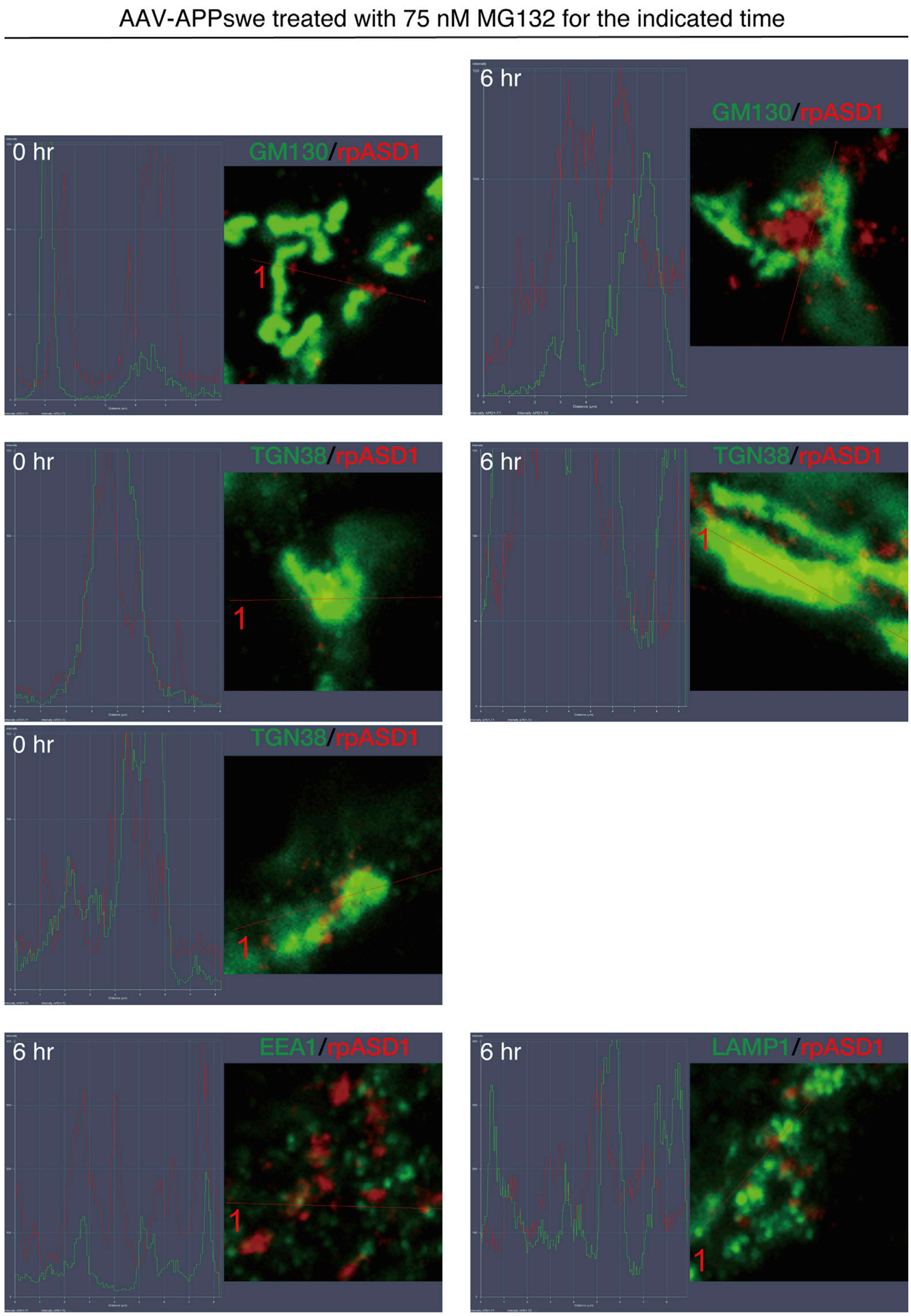

Figure 7. Line scans of ASPD Accumulate in the *Trans*-Golgi of Mature Neurons

Primary rat hippocampal neuronal cultures, with or without AAV-APPswe transduction, were treated with 75 nM MG132 for the indicated time. The cultures were double stained with anti-ASPD rpASD1 antibody and antibody against organelle marker protein as in Figure 6 (see Transparent Methods). Representative line scans of enlarged views shown in Figure 6 are included. See Figure 6

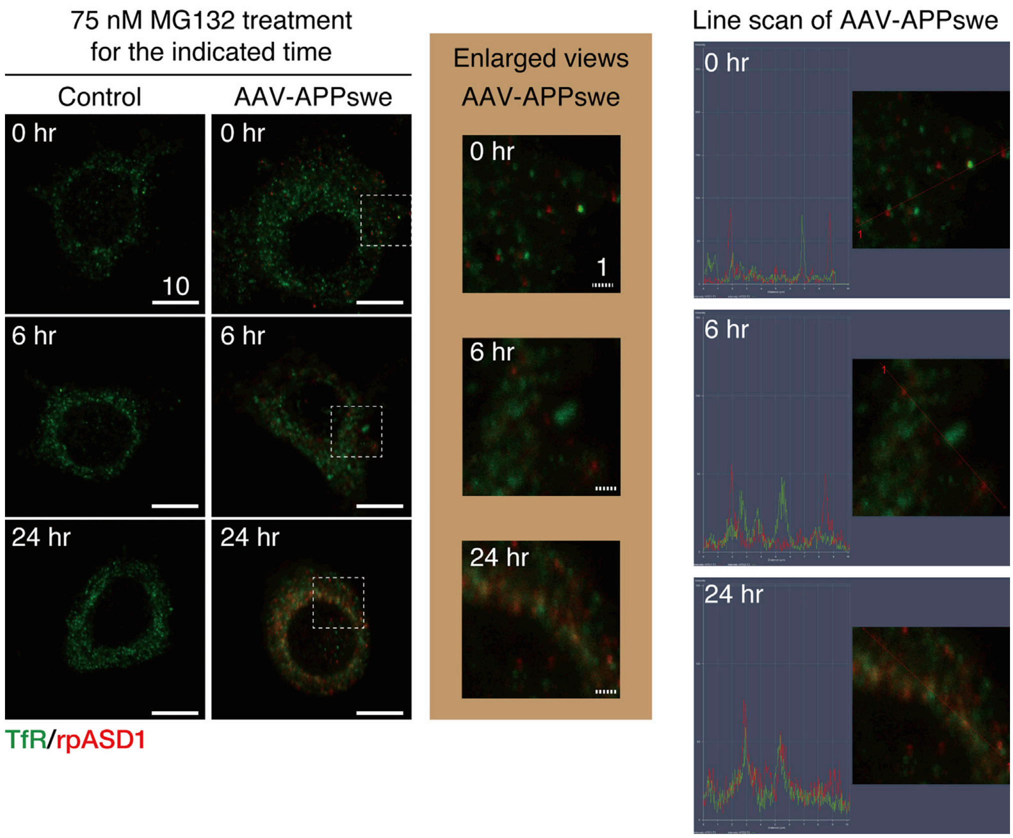

Figure 8. ASPD Are Also Present in the Recycling Endosomes of Mature Neurons

Primary rat hippocampal neuronal cultures, with or without AAV-APPswe transduction, were treated with 75 nM MG132 for the indicated time. The cultures were double-stained with anti-ASPD rpASD1 antibody and anti-transferrin receptor (TfR) antibody (see Transparent Methods). Representative images obtained with a highly sensitive, direct photon-counting system with a 100X oil objective lens are shown. An enlarged view of the field enclosed by a hatched line is shown below. Solid and hatched scale bars, 10 and 1 μm, respectively. Single red and green images for each time point are shown in Figure S6. See Figure S6.

Intra-neuronal ASPD Are Secreted and Are Toxic to NAKα3-Expressing Neurons

Our previous studies have shown that NAKα3 is the only ASPD-binding protein that is directly linked to ASPD neurotoxicity (Ohnishi et al., 2015). ASPD bind to the extracellular region of NAKα3 located in the L7/8 extracellular loop encompassing Asn^{879} and Trp^{880} and induce neurodegeneration by inhibiting NAKα3 pump activity (Ohnishi et al., 2015). Accordingly, ASPD that form inside neurons should be secreted to be neurotoxic. We therefore examined whether intra-neuronal ASPD were secreted and exerted neurotoxicity against NAKα3-expressing neurons. To this end, we developed a chemiluminescent enzyme immunoassay (CLEIA) that selectively detects ASPD with two ASPD-specific antibodies (see scheme in Figure 12A). This ASPD-specific CLEIA system enabled us to detect ASPD in the picomolar range. It did not detect low-molecular-weight Aβ, mostly monomers and dimers, which passed through a 50-kDa molecular weight cutoff filter (Xiao et al., 2015) (Figure 12A). Note that in Figures 12A, 12B, and S13, to enable easier comparison between ASPD and Aβ, the concentration of ASPD (128 kDa average mass; Matsumura et al., 2011) is expressed in terms of $A\beta_{1-42}$ monomer (4.53 kDa mass). We found that ASPD were recovered in the 10× concentrated 100-kDa retentate fraction of the culture supernate of the MG132-treated APPswe-transduced neurons at a concentration of 12.8 ± 4.8 pM (n = 3) (Figure 12B). ASPD were not detected in the 100-kDa flow-through fraction (Figure S13 left). The culture supernates of the MG132-treated APPswe-expressing neurons also contained $A\beta_{1-40}$ and $A\beta_{1-42}$ at 237.5 ± 53.7 pM and 39.9 ± 9.4 pM (n = 3), respectively, which were mostly recovered in the 100-kDa flow-through fraction (Figure S13 right). The ASPD level was below the detection limit in the 10× concentrated 100-kDa retentate fraction of the culture supernate of untransduced neurons (Figure 12B), which is in line with the quantification showing

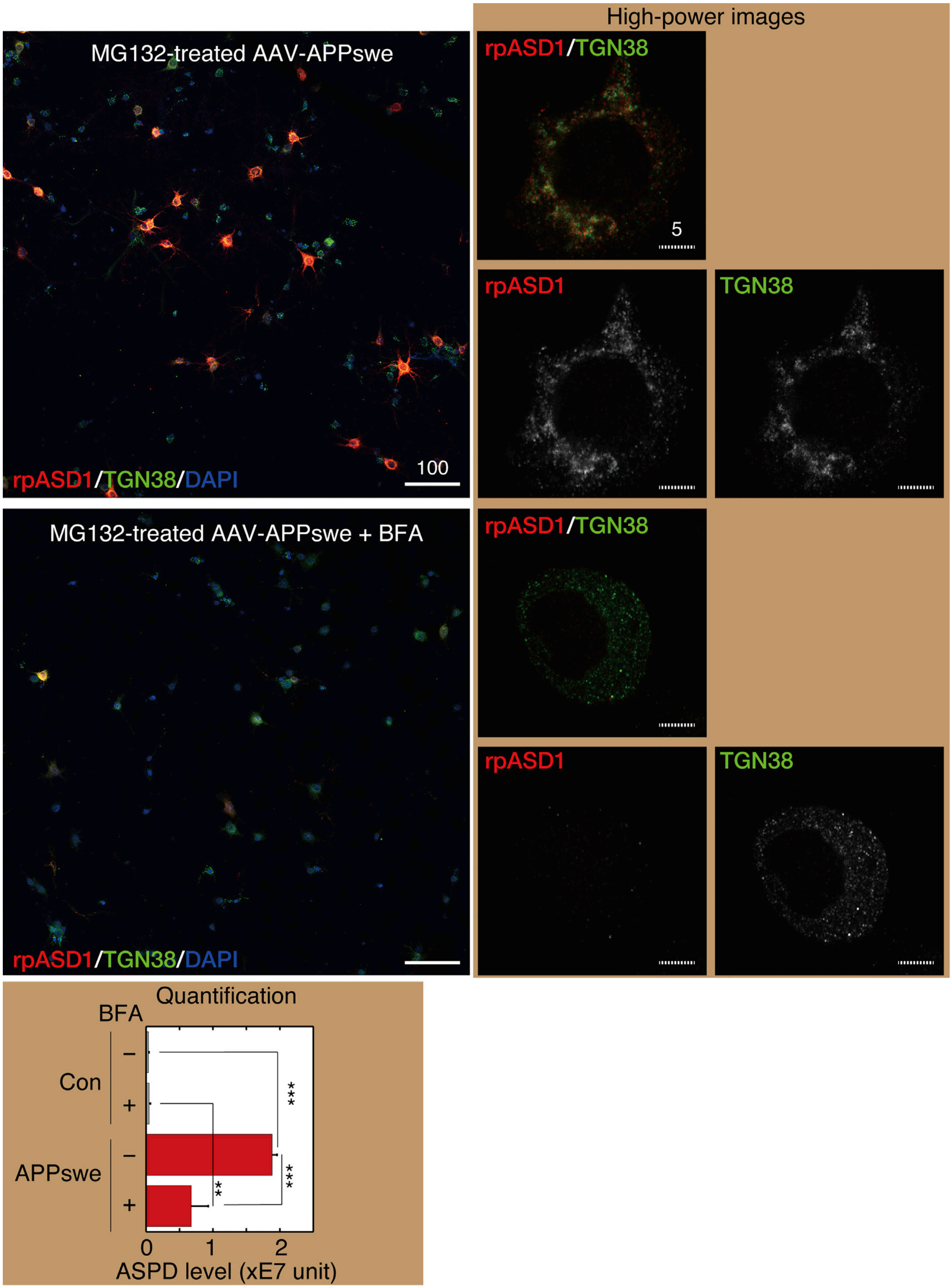
MG132-treated AAV-APPswe
rpASD1/TGN38/DAPI
100
MG132-treated AAV-APPswe + BFA
rpASD1/TGN38/DAPI
High-power images
rpASD1/TGN38
5
rpASD1
TGN38
rpASD1/TGN38
rpASD1
TGN38
Quantification
BFA
Con
APPswe
−
+
−
+
***
***
**
0
1
2
ASPD level (xE7 unit)

Figure 9. BFA Markedly Reduced ASPD Accumulation

Primary rat hippocampal neuronal cultures, with or without AAV-APPswe transduction, were treated with 75 nM MG132 for 24 h in the absence or presence of 0.6 μg/mL BFA. We determined this concentration by examining BFA concentrations from 0.6 to 10 μg/mL in our system and found that 0.6 μg/mL BFA treatment was enough to destroy the Golgi structure without affecting the cell viability. The cultures were triple-stained with rpASD1, anti-TGN38 antibody (TGN marker), and DAPI. Representative images are shown. High-power images on the right were obtained with a highly sensitive, direct photon-counting system with a 100X oil objective lens. Solid and hatched scale bars, 10 and 1 μm, respectively. See also representative images of control cultures without AAV transduction in Figure S7. The total amount of rpASD1-immunostained ASPD detected in MAP2-positive neurons was determined by using an IN Cell Analyzer as in Figure 4B, right, and is shown as "ASPD level" below (mean ± SD, n = 3; Scheffé post hoc test, ***p < 0.0001, **p = 0.001).

See Figures S7 and S8.

only a trace amount of ASPD formed in untransduced neurons (Figure 4B right). Before MG132 treatment, the ASPD levels were approximately 5.7 pM in the 10× concentrated 100-kDa retentates, suggesting that ASPD secretion increased after MG132 treatment.

We next examined whether NAKα3-expressing neurons degenerated in the MG132-treated AAV-APPswe-transduced cells. The level of NAKα3-expressing neurons in MG132-treated AAV-APPswe-transduced cultures significantly decreased to 72.9% ± 23.9% (n = 52) of that in MG132-treated untransduced cultures (***p < 0.0001 by Scheffé post hoc test), which correlated with the ASPD amounts in culture supernates. Previously, we showed that pretreatment of mASD3 antibody (with a K_d of 0.003 nM for ASPD) specifically blocked ASPD neurotoxicity against mature neurons (Noguchi et al., 2009). Consistent with this observation, the addition of an excess amount of mASD3 antibody in culture media of MG132-treated AAV-APPswe-transduced mature neurons completely blocked the decrease in NAKα3-expressing neurons (Figure 12C). We confirmed that incubation of MG132-treated untransduced mature neurons with mASD3 antibody did not affect the level of NAKα3-expressing neurons (Figure 12C). Given that antibodies usually do not cross the cell membrane, these results demonstrate that secreted ASPD caused the neurodegeneration observed in the MG132-treated AAV-APPswe-transduced mature neurons.

To further test our claim, we collected culture media from MG132-treated APPswe-transduced or untransduced cultures and applied them to untransduced mature neurons. Before application, ASPD were immunodepleted from the collected media by 1-h incubation with mASD3-antibody-covered magnetic beads. As a control, the collected media were separately incubated with normal mouse-IgG-covered magnetic beads. As clearly shown in Figure 12D, the collected media that were incubated with normal IgG induced degeneration in NAKα3-expressing neurons. This neurodegeneration was not observed when ASPD in the media were immunodepleted by prior incubation with mASD3-antibody-covered magnetic beads (Figure 12D). These results collectively demonstrate that ASPD were secreted and were toxic to NAKα3-expressing neurons.

We next performed detailed viability analyses of the ASPD-producing neurons. WST-8 assay (Figure 13A) showed that the viability of the APPswe-transduced mature hippocampal neurons at 21 DIV was lower than that of the untransduced neurons before the MG132 treatment (p = 0.089 by Scheffé post hoc test; n = 3). The 24-h MG132 treatment further reduced the viability of the APPswe-transduced mature hippocampal neurons (Figure 13A). Similar results were obtained with APPosk-transduced neurons (Figure 13A). The viability of the APPosk-transduced mature hippocampal neurons was significantly lower than that of the untransduced neurons before the MG132 treatment (**p = 0.0268 by Scheffé post hoc test; n = 3), and the 24-h MG132 treatment further reduced the viability of the APPosk-transduced neurons (Figure 13A). We confirmed that neither 24-h MG132 treatment nor AAV transduction of GFP itself affected cell viability (Figure 13A). Taken together, the viability of the neurons declined concomitantly with the accumulation of ASPD.

We next examined whether apoptotic cell death occurred in these neurons by detecting DNA fragmentation using TUNEL staining. To our surprise, TUNEL-positive apoptosis did not occur in the ASPD-producing neurons but did occur in the neurons surrounding these ASPD-positive neurons (arrowhead in Figure 13B, left and middle columns, and S14). MAP2 immunostaining showed a marked reduction of neurons in the APPswe- and APPosk-transduced mature neuronal cultures treated with 75 nM MG132 for 24 h (Figures 13B right and S14). We counted the number of MAP2- or GFAP-positive cells in MG132-treated AAV-APPswe-transduced cultures that were double stained with TUNEL and MAP2/GFAP and found

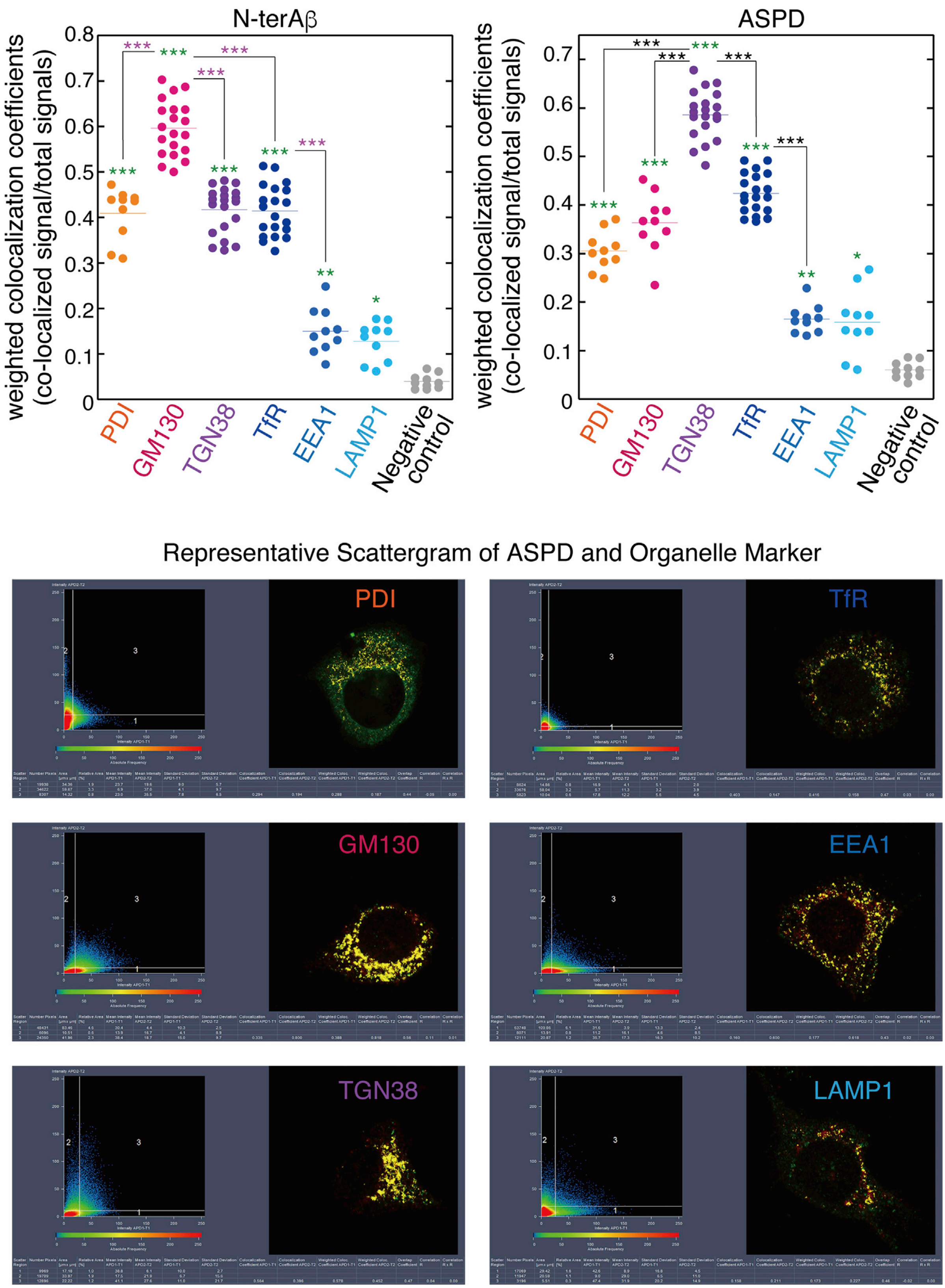
N-terAβ
ASPD
weighted colocalization coefficients
(co-localized signal/total signals)
0.8
0.7
0.6
0.5
0.4
0.3
0.2
0.1
0
PDI
GM130
TGN38
TfR
EEA1
LAMP1
Negative control
***
**
*
Representative Scattergram of ASPD and Organelle Marker
PDI
TfR
GM130
EEA1
TGN38
LAMP1

Figure 10. Quantitative Co-localization Analyses

The weighted colocalization coefficients were obtained using ZEN 2009 software (Zeiss) exactly according to the manufacturer's instructions (see Transparent Methods). The weighted colocalization coefficients represent the number of red pixels (rpASD1 or N-terAβ) that co-localize with green pixels (organelle markers) divided by the total number of red pixels. Analyses were performed using different sets of MG132-treated APP-expressing neurons. A representative scattergram is shown below. Statistical significance was calculated using Scheffé post hoc test (green asterisks: ***$p < 0.0001$, **$p = 0.0008$ [for ASPD] and 0.0019 [for N-ter Aβ], *$p = 0.021$ [for ASPD] and 0.0316 [for N-ter Aβ], compared with negative control using DAPI staining; pink asterisks and black asterisks ***$p < 0.0001$). See Figures S9–S11.

that, after 24-h MG132 treatment, on an average 54% of MAP2-positive neurons was lost in APPswe-transduced cells (n = 7), whereas the number of GFAP-positive astrocytes was not changed (Figures 13C and S14). Following apoptotic cell death in the surrounding neurons, the ASPD-producing neurons themselves degenerated after 48 h of 75 nM MG132 treatment, as indicated by propidium iodide (PI) staining (Figure 13D, see also arrowheads in Figure S15). PI-detectable, non-apoptotic neurodegeneration was rarely observed until 24-h MG132 treatment (Figures 13D and S15). This suggests that the ASPD-producing neurons either die very slowly or degenerate due to the lack of synaptic inputs from the surrounding neurons.

ASPD Appear to Primarily Form in Excitatory Neurons

In Figures 4A and S1, we showed that ASPD increased in only a limited population of neurons. Therefore we examined in which type of neurons the intra-neuronal ASPD increase. We first showed that the AAV transduction ratio did not vary according to the neuronal subtype by introducing non-toxic GFP (as shown in Figure 13A) by AAV. As shown in Figure S16, GFP was transduced to almost all neurons, irrespective of Math2-positive excitatory neurons (Schwab et al., 2000) (99.1% ± 1.4%, n = 30) or parvalbumin (PV)-positive GABAergic interneurons (97.0% ± 3.7%, n = 30; see representative images of Figure S16). Although APPswe transduction itself does not seem to affect the ratio between Math2-positive excitatory neurons and PV-labeled interneurons (Figure S17), interestingly, most of the Math2-positive excitatory neurons accumulated ASPD (84% ± 14%, n = 6), whereas most of the PV-labeled interneurons did not accumulate ASPD (8.7% ± 10.0%, n = 24) (Figure 14). We also examined calbindin-labeled neurons, which are mostly inhibitory neurons (McDonald and Mascagni, 2001) and found that most of the calbindin-positive inhibitory neurons did not accumulate ASPD (9.0% ± 3.2%, n = 5) (Figure S18). Thus it appears that ASPD primarily form in the excitatory neurons and are secreted from these neurons, exhibiting neurotoxicity toward the surrounding NAKα3-expressing neurons (Graphical Abstract; see Discussion).

DISCUSSION

In AD, Aβ oligomers accumulate in the brain. This accumulation might arise because of defects in APP processing or Aβ degradation, a shift in Aβ profiles to longer Aβs, or a change in Aβ assembly propensity caused by biological or chemical factors (Haass et al., 2012). Here we studied how impairment of the proteasome function affected APP/Aβ turnover and oligomer formation. We found that the inhibition of proteasomes by a variety of inhibitors led to higher levels of ASPD in steady state by increasing Aβ levels in APP-expressing neurons and triggered changes in the subcellular distribution of ASPD from the axon to dendrites. Interestingly, ASPD appeared to form primarily in excitatory neurons and were secreted into the medium, leading to apoptotic death of surrounding NAKα3-expressing neurons (Figure 12). This is consistent with our previous finding that ASPD bind to NAKα3 on synapses and cause neuronal degeneration by inactivating NAKα3 pump activity (Ohnishi et al., 2015). NAKα3 neurons died apoptotically due to secreted ASPD, whereas ASPD-producing neurons that killed NAKα3 neurons died slowly and non-apoptotically (Figures 13, S14, and S15).

In using APP-overexpressing neurons as a model, we are aware that some phenotypes of APP-overexpressing mice models, such as sudden death, may be the result of APP overexpression per se and thus may not be reflective of the disease process in humans (Sasaguri et al., 2017). Nevertheless, these mouse APP overexpression model systems have proved to be useful and relevant in numerous studies of the production or deposition of Aβ (Sasaguri et al., 2017). In our system, as shown in Figure 11B, MG132 treatment substantially and significantly ($p < 0.0001$ by Scheffé post hoc test) increased the levels of ASPD and the number of ASPD-containing neurons, relative to control neurons, suggesting that the effects we observed were not merely due to APP overexpression. More importantly, intra-neuronal accumulation of ASPD is indeed present in the brains of patients with AD (Noguchi et al., 2009). The AAV-APP system used

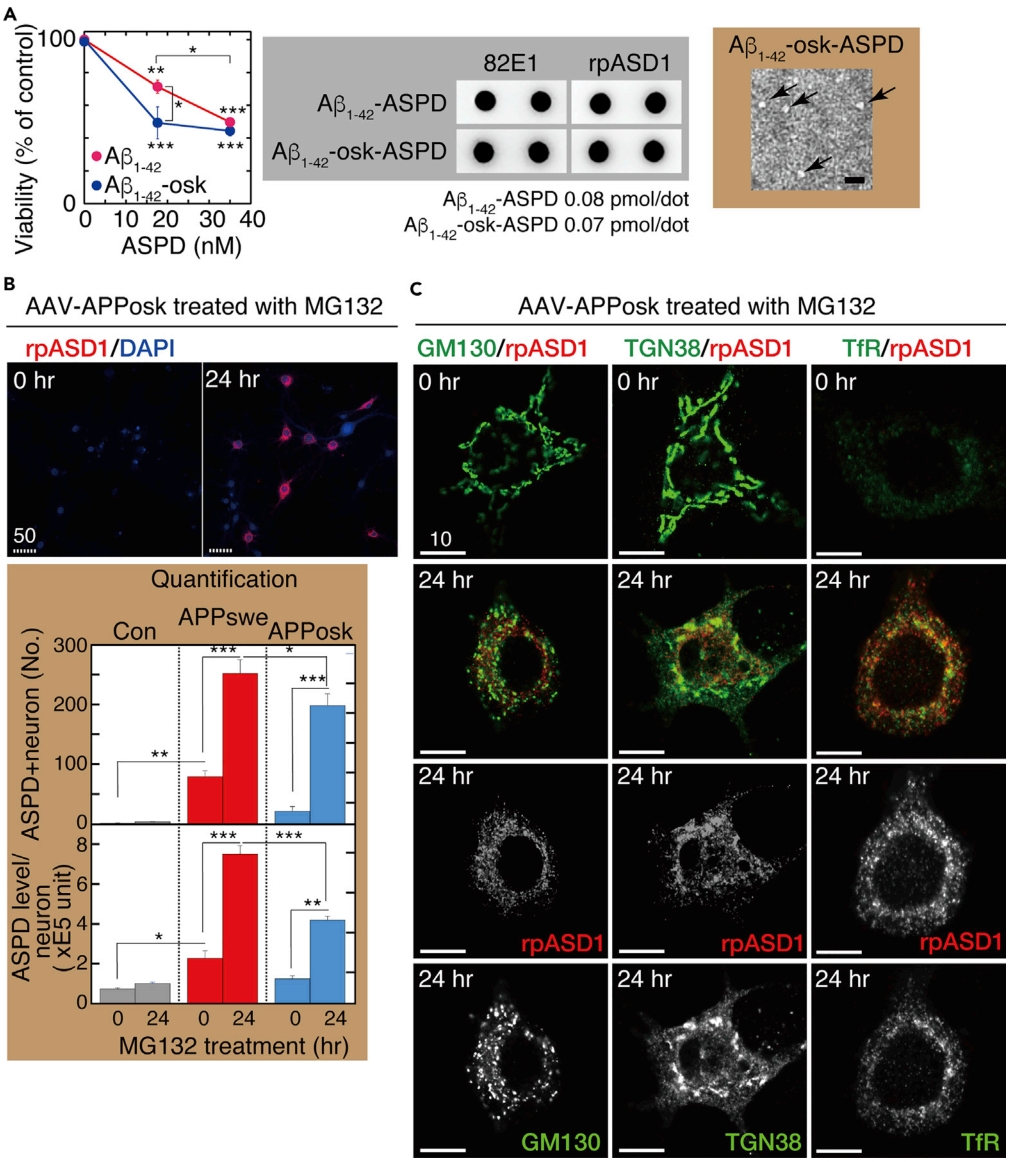

Figure 11. ASPD Form from $A\beta_{1-42}$-osk

(A) Primary rat hippocampal neuronal cultures at 21 DIV were treated with synthetic ASPD produced either from $A\beta_{1-42}$ or $A\beta_{1-42}$-osk (E22Δ) at the indicated concentration for 24 h. Viability of each culture was determined by using highly water-soluble tetrazolium salt, WST-8, (Transparent Methods; mean ± SD, n = 3; Scheffé post hoc test, ***$p < 0.0001$ and **$p = 0.0007$ compared with ASPD-untreated neurons; *$p = 0.0048$ compared with $A\beta_{1-42}$-osk-derived ASPD). Representative dot blotting (using anti-Aβ N-terminal 82E1 and ASPD-specific rpASD1 antibodies) and a representative transmission electron microscopic image of the negatively stained $A\beta_{1-42}$-osk-derived ASPD (arrows) are shown on the right.

(B) Primary rat hippocampal neuronal cultures with AAV-APPosk transduction were treated with 75 nM MG132 for the indicated time, stained, and photographed as in Figure 4B (left column). Representative images are shown. Scale bar, 50 μm. The ASPD staining of each culture was quantified using the In Cell Analyzer (GE Healthcare Lifesciences) as in Figure 4B (mean ± SD, n = 3; Scheffé post hoc test; ***$p < 0.0001$, **$p < 0.0005$, *$p = 0.01$).

(C) Primary rat hippocampal neuronal cultures with AAV-APPosk transduction were treated with 75 nM MG132 for the indicated time, stained, and photographed as in Figures 6 and 8. High-power images were obtained with a highly sensitive, direct photon-counting system with a 100X oil objective lens. For the 24-h MG132 treatment, the single red or green image is also shown. Representative images are shown. Scale bar, 10 μm.

See Figures 2, S1, and S12.

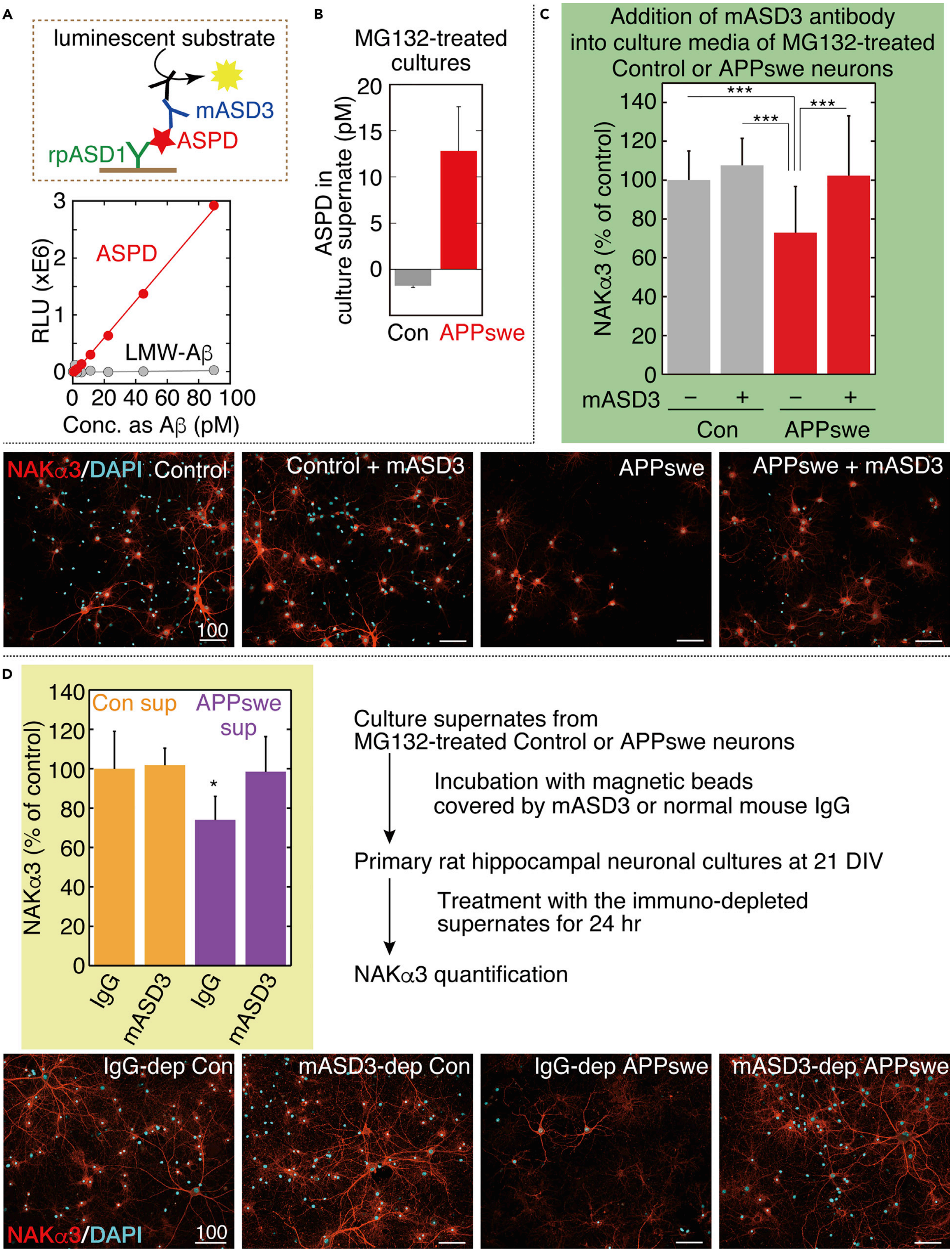
A
luminescent substrate
mASD3
ASPD
rpASD1
RLU (xE6)
ASPD
LMW-Aβ
Conc. as Aβ (pM)
B
MG132-treated cultures
ASPD in culture supernate (pM)
Con APPswe
C
Addition of mASD3 antibody into culture media of MG132-treated Control or APPswe neurons
NAKα3 (% of control)
mASD3 – + – +
Con APPswe
NAKα3/DAPI Control
Control + mASD3
APPswe
APPswe + mASD3
100
D
Con sup
APPswe sup
NAKα3 (% of control)
IgG mASD3 IgG mASD3
Culture supernates from MG132-treated Control or APPswe neurons
Incubation with magnetic beads covered by mASD3 or normal mouse IgG
Primary rat hippocampal neuronal cultures at 21 DIV
Treatment with the immuno-depleted supernates for 24 hr
NAKα3 quantification
IgG-dep Con
mASD3-dep Con
IgG-dep APPswe
mASD3-dep APPswe
NAKα3/DAPI
100

Figure 12. Intra-neuronal ASPD Were Secreted and Kill NAKα3 Neurons

(A) The CLEIA system was developed based on our previous enzyme-linked immunosorbent assay (ELISA) that selectively detected ASPD with two ASPD-specific antibodies (Noguchi et al., 2009). The newly established ASPD-specific CLEIA (see a schematic image in upper panel and details in Transparent Methods) detects picomolar levels of ASPD (expressed as Aβ monomer concentration) but does not respond to low-molecular-weight (LMW)-Aβ in the 50-kDa flow-through fraction. R^2 = 0.99891 for ASPD and 0.01162 for LMW-Aβ.

(B) ASPD level in culture supernates detected by ASPD-specific CLEIA in (A). A 10× concentrated culture supernate was obtained using 100-kDa filters from the neuronal cultures (with or without AAV-APPswe) treated with 75 nM MG132 for 24 h (see Methods). $A\beta_{1\text{-}40}$ and $A\beta_{1\text{-}42}$ were also quantified (see Figure S13). Mean ± SD, n = 3.

(C) APPswe-transduced or untransduced control neuronal cultures were treated with 75 nM MG132 for 24 h in the presence or absence of mASD3 antibody (1 ng/mL) that can block ASPD neurotoxicity (Noguchi et al., 2009) and stained with anti-NAKα3 antibody and DAPI (Transparent Methods). The NAKα3 level was quantified using a Yokogawa CQ1 (see Transparent Methods; mean ± SD, n = 28 for MG132-treated control, 19 for mASD3-treated MG132-treated control, 52 for MG132-treated APPswe, or 31 for mASD3-treated MG132-treated APPswe; Scheffé post hoc test; ***p < 0.0001). Representative images, used for the quantification, are shown with 100-μm scale bars. Note that NAKα3 was detected by an antibody that specifically recognizes an internal region of NAKα3 (SANTA CRUZ sc-16051-R). Therefore, ASPD binding to the extracellular region of NAKα3 does not interfere with the binding of the anti-NAKα3 antibody to NAKα3 (Ohnishi et al., 2015).

(D) Culture supernates were collected from 24-h MG132-treated APPswe-transduced or untransduced control neuronal cultures. From the collected culture supernates, ASPD were immunodepleted by mASD3-covered magnetic beads, and another 22 DIV primary rat hippocampal neuronal culture was treated with the resulting immunodepleted culture supernates. As a control, the collected culture supernates were also incubated with normal mouse IgG-covered magnetic beads (see Transparent Methods). The NAKα3 level was quantified as in (C) after 24 h. Mean ± SD, n = 8, Scheffé post hoc test; *p = 0.0172 compared with IgG-treated control supernate. Representative images, used for the quantification, are shown with 100-μm scale bars.

See Figure S13

in this work thus appears capable of revealing how ASPD may form in neurons in the human brain and affect disease pathology.

We showed that proteasome inhibition led to an increase in Aβ in steady state, by inhibiting ERAD-mediated degradation of Aβ or APP, without affecting its secretion (Figures 2, 3, and S2). The rate-limiting step in ERAD is ubiquitination performed by ER-membrane-anchored E3 ubiquitin ligases, which seem to target only a small number of proteins. Recent studies have identified several E3 ubiquitin ligases for APP that directly interact with APP and mediate APP degradation by proteasomes (Kaneko et al., 2010; Kumar et al., 2007; Wang and Saunders, 2014; Watanabe et al., 2012). Notably, gene suppression of one of the E3 ubiquitin ligases for APP, hydroxymethylglutaryl-coenzyme A reductase degradation protein 1 (HRD1), leads to APP accumulation and an increase in Aβ production, and vice versa (Kaneko et al., 2010). MG132 inhibits APP degradation induced by increased HRD1 expression (Kaneko et al., 2010). In the case of Aβ, another E3 ubiquitin ligase, parkin, promotes proteasome-mediated clearance of $A\beta_{1\text{-}42}$ in neurons (Burns et al., 2009). This is consistent with findings in a parkin-null mouse model, where the accumulation of Aβ deposits was observed in the brain even without modification of APP, presenilins, or secretases (Rodriguez-Navarro et al., 2008). These findings support the notion that proteasomes may play a role in regulating APP/Aβ metabolism. Our findings demonstrate a link between ASPD levels and proteasome function, which may have important implications for AD pathophysiology. It will be interesting in the future to determine which E3 ubiquitin ligases or other regulators of APP/Aβ degradation are indeed involved in increasing ASPD formation.

Previous reports have shown that Aβ can be generated in all possible compartments of the secretory pathways, including the ER (Cook et al., 1997; Greenfield et al., 1999; Hartmann et al., 1997), the TGN (Greenfield et al., 1999; Xu et al., 1997), the PM (Chyung and Selkoe, 2003; Tarassishin et al., 2004), the endosomes (Grbovic et al., 2003; Koo and Squazzo, 1994; Perez et al., 1999), and the lysosomes (Yu et al., 2004). We consistently detected the N-terminal end of Aβ (N-terAβ) in steady state in compartments ranging from the ER to the lysosomes (Figure 10). Among the possible compartments, the subcellular localization of BACE suggested that either the TGN or endosomes would serve as the locus of Aβ production. Recent studies have emphasized the role of EEs in Aβ production, because blocking endocytosis reduces Aβ production (Carey et al., 2005; Perez et al., 1999), whereas enhancing endocytosis increases it (Grbovic et al., 2003). Proteins related to endocytosis have been reported to be involved in APP processing (Sannerud et al., 2011; Schneider et al., 2008; Ubelmann et al., 2017) (see also review Rajendran and Annaert, 2012). However, these studies do not rule out a role for the TGN in β-cleavage. For example, fluorescence resonance energy transfer analyses have shown that APP and BACE interact at

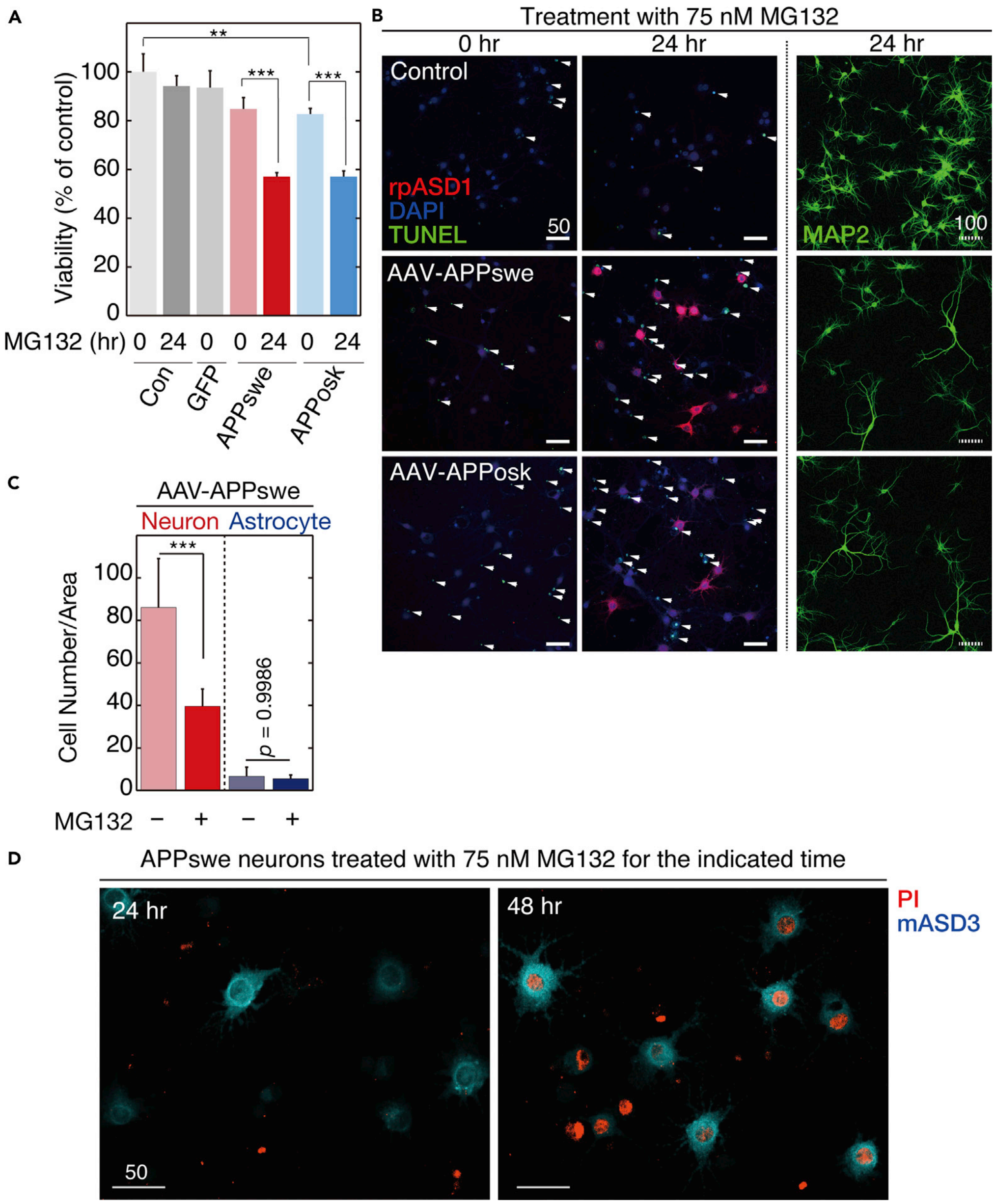

Figure 13. Secreted ASPD Induced Apoptotic Degeneration of Surrounding Neurons

(A) APP- or GFP-transduced or untransduced control neuronal cultures were treated with 75 nM MG132 for the indicated time. Viability was determined with a Cell Counting Kit-8 (see Transparent Methods; mean ± SD, n = 3; Scheffé post hoc test, ***p < 0.0001, **p = 0.0268). The viability of GFP-transduced cultures was 93.5% ± 7.0% of that of the untransduced control cultures (n = 3, p = 0.1854 by Scheffé posy hoc test), indicating that AAV transduction itself does not affect cell viability.

(B) APP-transduced or untransduced control cultures were treated with 75 nM MG132 for the indicated time and stained with the anti-ASPD rpASD1 antibody, DAPI, and TUNEL (arrowhead) or with the anti-MAP2 antibody (Transparent Methods). Solid and hatched scale bars, 50 and 100 μm, respectively.

(C) APP-transduced or untransduced control cultures were treated with or without 75 nM MG132 for 24 h and quadruple-stained with rpASD1, DAPI, TUNEL, and MAP2/GFAP. The number of MAP2-labeled neurons or GFAP-labeled astrocytes in APPswe-transduced cultures was counted and is shown (n = 7, Scheffé post hoc test, ***p < 0.0001). Representative images are shown in Figure S14.

(D) APPswe-transduced primary rat hippocampal neuronal cultures were treated with 75 nM MG132 for the indicated time; triple-stained with propidium iodide (PI), calcein-AM, and anti-ASPD mASD3 antibody

Figure 13. *Continued*

(see Transparent Methods); and photographed (see Figure S15). Representative images of the corresponding PI/mASD3 staining are shown with 50-μm scale bars. PI-detectable non-apoptotic death was detected in ASPD-producing neurons at 48-h MG132 treatment.

See Figures S14 and S15.

least in the GM130-detected *cis*-Golgi, in addition to at the cell surface and in the EEs (Kinoshita et al., 2003). Aβ40 has been reported to be generated in the TGN depending on retromer-mediated APP recycling from the EEs to the TGN (Choy et al., 2012). Accumulating data support the importance of the sorting mechanisms that transport APP and BACE from the cell surface to the endosomes and from the endosomes to the TGN. The exact location of APP processing will depend on the balance of traffic of APP and secretases. Therefore some discrepancies in existing data may derive from the use of different cell types and conditions. In particular, to establish and maintain functionally distinct domains in membranes, neurons have developed trafficking systems to deliver transmembrane proteins to the correct compartments (Lasiecka and Winckler, 2011). Accordingly, the trafficking and processing of APP in highly polarized neurons might well be different from the processes in non-neuronal cells. For example, the sorting signal(s) mediating transport of APP to the axon or dendrites in neurons is completely different from that mediating the basolateral transport in MDCK cells (Back et al., 2007; Szodorai et al., 2009). In our system, ASPD signals were broadly distributed in steady state, but the TGN was shown to be the initial and highest localization site of ASPD in APP-expressing neurons (Figures 6 and 10). This suggests the possibility that ASPD may form mainly in the TGN. However, other possibilities cannot be excluded given the close and dynamic cross talk between TGN and endosomes (Schmidt and Haucke, 2007). Real-time imaging that enables detection of ASPD separately from Aβ monomers in mature neurons is needed to give a more definitive answer as to the exact location of ASPD formation in mature neurons. Interestingly, ASPD are present not only in the TGN, but also in the REs, which lie between the ER-TGN system and the endosome system. Because the RE serves as a hub to direct proteins to the PM, it is possible that the REs serve as a port for ASPD to be secreted. The REs, which are clustered tightly near the nucleus in close proximity to the TGN in non-neuronal cells, are spread almost evenly throughout the cell body, dendrites, and the axons in neurons (Wang et al., 2008). One may speculate that axon-directed REs or dendrite-directed REs separately serve as hubs to direct ASPD to the axons or dendrites. We showed in Figure 5B that some population of dendritic ASPD co-localizes with Bassoon, suggesting that ASPD could be released at synapses. This observation is consistent with our previous study showing that ASPD bind to the pre-synaptic side of the neuron to induce neurodegeneration (Noguchi et al., 2009). Scheme 1 integrates our results with those extant.

Previously, we observed substantial accumulation of ASPD in the cerebral cortex and little accumulation in the cerebellum (Ohnishi et al., 2015). These findings strongly suggest that there exist regional or cell-type differences in ASPD accumulation. Consistently, we found that only excitatory neurons appear to form ASPD (Figure 14). This may be due to factors intrinsic to these cells that affect assembly propensity or it may be that only inhibitory neurons have a degradation system for ASPD, about which we do not know anything. Interestingly, proteasome inhibition led to a distribution change of both ASPD and Aβ from axons to dendrites (Figures 5 and S19), suggesting the presence of a common mechanism underlying this distribution change. The reason why such a change in ASPD delivery occurs remains to be established, as do the molecular mechanisms of ASPD secretion. Neurons have specialized Golgi compartments called "Golgi outposts" within dendritic arbors, which are essential for the proper elaboration of dendrites and neuronal polarity (Lasiecka and Winckler, 2011). Golgi outposts are discontinuous from the somatic Golgi and are frequently localized at dendritic branch points (Lasiecka and Winckler, 2011). Aβ and ASPD might use this system to be delivered to dendrites. We found that after 24 h of MG132 treatment the Golgi structure appeared to be fragmented in most of the APPswe-transduced neurons. Because the Golgi did not appear to be fragmented and ASPD had already accumulated at the TGN at 6-h MG132 treatment (Figure 6), it is unlikely that Golgi fragmentation causes ASPD accumulation at the TGN. Golgi fragmentation enhances vesicle budding and accelerates protein trafficking (Wang et al., 2008), and reversible fragmentation has been detected in hyperactive neurons (Thayer et al., 2013). We therefore speculate that Golgi fragmentation at 24-h MG132 treatment might be a compensatory reaction to allow faster protein trafficking when the cells are under stress.

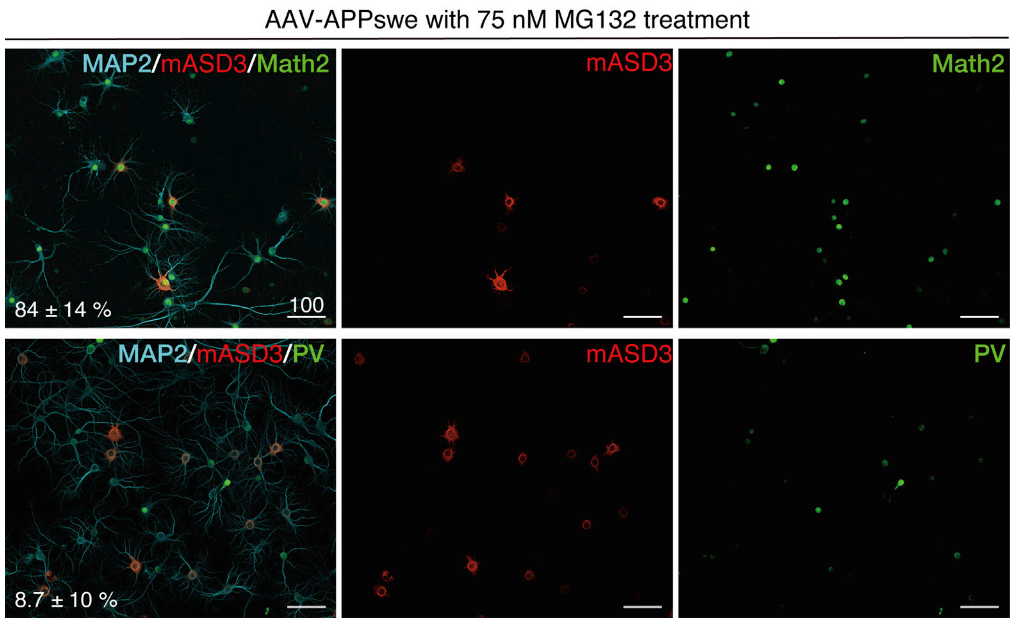

Figure 14. ASPD Accumulate Only in Excitatory Neurons

APPswe-transduced neuronal cultures were treated with 75 nM MG132 for 24 h and stained with the indicated antibodies. The ratio of the ASPD-containing neurons among either MAP2/PV or MAP2/Math2 double-positive neurons was quantified using a Yokogawa CQ1 (see Transparent Methods; inset, mean $\pm$ SD, n = 6 for MAP2/Math, 24 for MAP2/PV). ASPD were detected by anti-ASPD rpASD1 or mASD3 antibody. GABAergic interneurons are composed of a highly diverse population of inhibitory neurons, which represent about 20% of cortical/hippocampal neurons (Amaral, 1978). For quantification purposes, we used an antibody against PV, because PV-labeled interneurons represent ~40% of the total number of GABAergic interneurons in the CA1 and CA3 of hippocampus (Ribak et al., 1990) and the PV antibody clearly stains the neuronal cell body. Representative images, used for the quantification, are shown with 100 μm scale bars. See control data in Figures S16 and S17 and calbindin data in Figure S18.
See Figures S16–18.

In this work, we found that $A\beta_{1\text{-}42}$-osk (E22Δ-$A\beta_{1\text{-}42}$) forms ASPD. As shown in quantification in Figure 11, the formation ratio of ASPD from $A\beta_{1\text{-}42}$-osk was lower than that of ASPD from wild-type $A\beta_{1\text{-}42}$ in APPswe-transduced neurons. Nevertheless, the total cell death level of the APPosk-transduced cultures was equivalent to that of the APPswe-transduced cultures, as shown by viability assay, MAP2 staining, and TUNEL staining (Figures 13A, 13B, and S14). This could be due to increased toxicity of the ASPD derived from $A\beta_{1\text{-}42}$-osk compared with that of ASPD derived from wild-type $A\beta_{1\text{-}42}$. Our previous solution nuclear magnetic resonance (NMR) analysis of ASPD showed that the E22 residue resides in a core region of ASPD (Ohnishi et al., 2015). Therefore it is unlikely that E22 directly affects ASPD binding to NAKα3. It is more likely that the E22Δ mutation alters the conformation of the Aβ monomer (Inayathullah and Teplow, 2011), which leads to differences in the structure of ASPD. Further solution NMR studies will be needed to determine at the atomic level precisely how the deletion of E22 changes the structure of ASPD and thus their toxicity.

Biomarker studies on humans indicate that accumulation of Aβ precedes the clinical onset of AD by more than a decade (Weiner et al., 2012). Notably, western blot analyses of human brains obtained from the Nun study showed distinct trends in levels of dimers, trimers, and dodecamers, according to the disease stage, suggesting that dodecamers might form earlier than trimers or dimers (Lesné et al., 2013). However, the lack of specific antibodies makes it difficult to monitor their actual formation. We have identified ASPD from brains of patients with AD as the key species responsible for neurodegeneration and also obtained ASPD-specific antibodies that could specifically detect the native tertiary structure of ASPD (Noguchi et al., 2009; Ohnishi et al., 2015). Building on that work, we established a mature neuron-derived system that was usable to monitor where ASPD form. As described above, the sorting and processing mechanisms of APP in neurons are expected to be more complicated than those in non-neuronal cells owing to dynamic cross talk between the TGN and the endosome system.

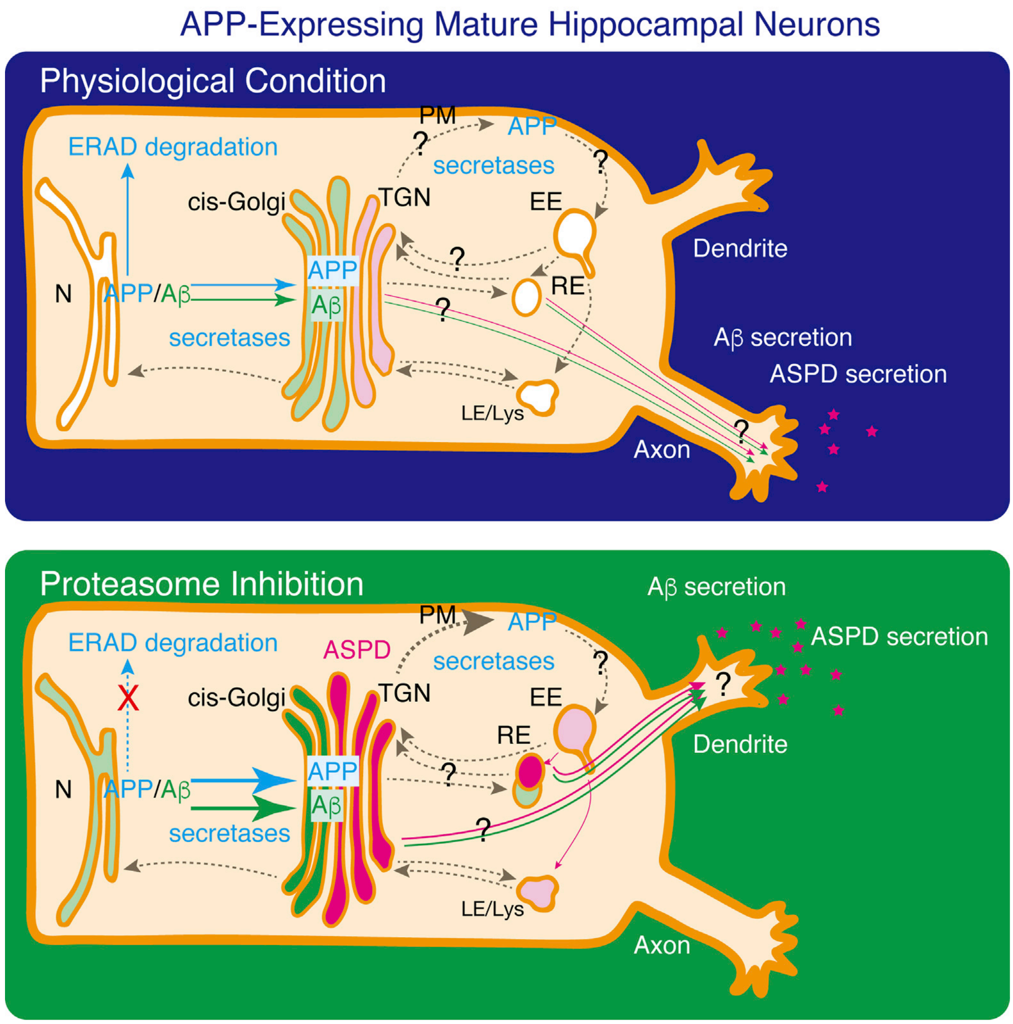

Scheme 1. Steady-State Distribution of APP, N-terminal end of Aβ, and ASPD, Detected in This Work under Physiological Conditions without Proteasome Inhibition and with Proteasome Inhibition, Integrated with Previous Findings as to APP Degradation and Trafficking

In mature neurons, APP was widely detected in the ER-TGN as reported previously (Greenfield et al., 1999; Hartmann et al., 1997; Xu et al., 1997). Proteasome inhibition leads to a higher steady-state level of APP and N-terAβ in APP-expressing neurons, possibly by inhibiting ERAD (see text). Under physiological conditions without proteasome inhibition, N-terAβ staining is too weak to allow its subcellular distribution to be determined (representative images in Figures S10 and S11). From the red enhanced images, it appears that the weak N-terAβ signal is co-localized with the ER or the *cis*-Golgi, but not with the TGN, the EE, the RE, or the Lys (Figures S10 and S11). After 24-h MG132 treatment, N-terAβ staining was detected mainly in the *cis*-Golgi, and also on the TGN, the RE, and the ER surface, but was rarely observed in the EE or the Lys in our system (Figures 10, S10, and S11). In the case of ASPD, a limited amount of ASPD was detected mainly in the TGN under physiological conditions (Figures 6 and 7). With proteasome inhibition, the steady-state level of ASPD increased markedly, in particular, in the TGN, and also in the *cis*-Golgi and the RE. ASPD were also detected to some extent in the ER, and a very few were present in the EE and the Lys. Proteasome inhibition changes both N-terAβ and ASPD distribution from axons to dendrites (Figures 5 and S19). Blue arrows, APP; green arrows, N-terAβ; pink arrows, ASPD. Higher levels of APP and N-terAβ were detected after inhibiting ERAD (see text). Hatched brown arrows show possible cross-talk reported previously. N, nucleus; ER, endoplasmic reticulum; TGN, *trans*-Golgi network; PM, plasma membrane; EE, early endosome; RE, recycling endosome; LE/Lys, late endosome and lysosome.

Disturbances in these complex sorting and processing systems in neurons could affect Aβ production and have been linked to AD pathogenesis. Thus the mature neuron-based system established in the present work, and the findings resulting from its use, should further deepen our understanding of how Aβ assemblies may form in the human brain.

METHODS

All methods can be found in the accompanying Transparent Methods supplemental file.

SUPPLEMENTAL INFORMATION

Supplemental Information includes Transparent Methods and 19 figures and can be found with this article online at https://doi.org/10.1016/j.isci.2019.01.018.

ACKNOWLEDGMENTS

We thank Manami Akioka, Masafumi Inoue, Yoshitaka Matsumura, and Takashi Nishiyama for technical help; Masatoshi Takeichi and Shigenobu Yonemoto for help in using the TEM instrument; and David B. Teplow, Koshi Murata, Yugo Fukazawa, and Masatoshi Hagiwara for helpful discussion. M.H. thanks the Ministry of Education, Culture, Sports, Science and Technology (Grant-in-Aid for Scientific Research B), Niigata University (the Collaborative Research Project of the Brain Research Institute), and Takeda Science Foundation (Life Science Research Grant) for support.

AUTHOR CONTRIBUTIONS

Conceptualization, M.H.; Methodology, H.K., S.K., T.S., Y.A., N.T., Y.-I.N., S.-I.M., I.K., and M.H.; Investigation, H.K., S.K., T.S., Y.A., K.S., N.T., M.S., T.O., and M.H.; Writing – Original Draft, H.K., S.K., T.S., S.-I.M., I.K., and M.H.; Writing – Review & Editing, all authors; Visualization, H.K., S.K., T.S., and M.H.; Supervision, M.H.; Funding Acquisition, M.H.

DECLARATION OF INTERESTS

M.H. has served as a technical advisor to TAO Health Life Pharma Co. Ltd., a Kyoto University-derived bioventure, with the permission of the Conflict of Interest Committee of Kyoto University and the Foundation for Biomedical Research and Innovation at Kobe; H.K., Y.A., S.K., T.S., K.S., and T.O. are employees of TAO Health Life Pharma Co. Ltd.

Received: April 25, 2018
Revised: November 14, 2018
Accepted: January 11, 2019
Published: February 28, 2019

REFERENCES

Amaral, D.G. (1978). A Golgi study of cell types in the hilar region of the hippocampus in the rat. J. Comp. Neurol. *182*, 851–914.

Back, S., Haas, P., Tschape, J.A., Gruebl, T., Kirsch, J., Muller, U., Beyreuther, K., and Kins, S. (2007). β-amyloid precursor protein can be transported independent of any sorting signal to the axonal and dendritic compartment. J. Neurosci. Res. *85*, 2580–2590.

Barysch, S.V., Aggarwal, S., Jahn, R., and Rizzoli, S.O. (2009). Sorting in early endosomes reveals connections to docking- and fusion-associated factors. Proc. Natl. Acad. Sci. U S A *106*, 9697–9702.

Benilova, I., Karran, E., and De Strooper, B. (2012). The toxic Aβ oligomer and Alzheimer's disease: an emperor in need of clothes. Nat. Neurosci. *15*, 349–357.

Burns, M.P., Zhang, L., Rebeck, G.W., Querfurth, H.W., and Moussa, C.E. (2009). Parkin promotes intracellular $A\beta_{1-42}$ clearance. Hum. Mol. Genet. *18*, 3206–3216.

Cai, X.D., Golde, T.E., and Younkin, S.G. (1993). Release of excess amyloid beta protein from a mutant amyloid beta protein precursor. Science *259*, 514–516.

Carey, R.M., Balcz, B.A., Lopez-Coviella, I., and Slack, B.E. (2005). Inhibition of dynamin-dependent endocytosis increases shedding of the amyloid precursor protein ectodomain and reduces generation of amyloid β protein. BMC Cell Biol. *6*, 30.

Carlsson, S.R., and Fukuda, M. (1989). Structure of human lysosomal membrane glycoprotein 1. assignment of disulfide bonds and visualization of its domain arrangement. J. Biol. Chem. *264*, 20526–20531.

Chiti, F., and Dobson, C.M. (2009). Amyloid formation by globular proteins under native conditions. Nat. Chem. Biol. *5*, 15–22.

Choy, R.W.Y., Cheng, Z.L., and Schekman, R. (2012). Amyloid precursor protein (APP) traffics from the cell surface via endosomes for amyloid β (Aβ) production in the *trans*-Golgi network. Proc. Natl. Acad. Sci. U S A *109*, E2077–E2082.

Chyung, J.H., and Selkoe, D.J. (2003). Inhibition of receptor-mediated endocytosis demonstrates generation of amyloid β-protein at the cell surface. J. Biol. Chem. *278*, 51035–51043.

Citron, M., Oltersdorf, T., Haass, C., McConlogue, L., Hung, A.Y., Seubert, P., Vigo-Pelfrey, C., Lieberburg, I., and Selkoe, D.J. (1992). Mutation of the β-amyloid precursor protein in familial Alzheimer's disease increases β-protein production. Nature *360*, 672–674.

Cook, D.G., Forman, M.S., Sung, J.C., Leight, S., Kolson, D.L., Iwatsubo, T., Lee, V.M.Y., and Doms, R.W. (1997). Alzheimer's Aβ(1-42) is generated in the endoplasmic reticulum/intermediate compartment of NT2N cells. Nat. Med. *3*, 1021–1023.

Csizmadia, V., Csizmadia, E., Silverman, L., Simpson, C., Raczynski, A., O'Brien, L., Gallacher, M., Cardoza, K., Kadambi, V.J., Fedyk, E.R., et al. (2010). Effect of proteasome inhibitors with different chemical structures on the ubiquitin-proteasome system in vitro. Vet. Pathol. *47*, 358–367.

Glabe, C.G. (2008). Structural classification of toxic amyloid oligomers. J. Biol. Chem. *283*, 29639–29643.

Grbovic, O.M., Mathews, P.M., Jiang, Y., Schmidt, S.D., Dinakar, R., Summers-Terio, N.B., Ceresa, B.P., Nixon, R.A., and Cataldo, A.M. (2003). Rab5-stimulated Up-regulation of the endocytic pathway increases intracellular β-cleaved amyloid precursor protein carboxyl-terminal fragment levels and Aβ production. J. Biol. Chem. *278*, 31261–31268.

Greenfield, J.P., Tsai, J., Gouras, G.K., Hai, B., Thinakaran, G., Checler, F., Sisodia, S.S., Greengard, P., and Xu, H. (1999). Endoplasmic reticulum and *trans*-Golgi network generate distinct populations of Alzheimer β-amyloid peptides. Proc. Natl. Acad. Sci. U S A *96*, 742–747.

Haass, C., Kaether, C., Thinakaran, G., and Sisodia, S. (2012). Trafficking and proteolytic processing of APP. Cold Spring Harb. Perspect. Med. *2*, a006270.

Hardy, J., and Selkoe, D.J. (2002). The Amyloid hypothesis of alzheimer's disease: progress and problems on the road to therapeutics. Science *297*, 353–356.

Hartmann, T., Bieger, S.C., Bruhl, B., Tienari, P.J., Ida, N., Allsop, D., Roberts, G.W., Masters, C.L., Dotti, C.G., Unsicker, K., et al. (1997). Distinct sites of intracellular production for Alzheimer's disease Aβ40/42 amyloid peptides. Nat. Med. *3*, 1016–1020.

Hoshi, M., Sato, M., Matsumoto, S., Noguchi, A., Yasutake, K., Yoshida, N., and Sato, K. (2003). Spherical aggregates of β-amyloid (amylospheroid) show high neurotoxicity and activate tau protein kinase I/glycogen synthase kinase-3β. Proc. Natl. Acad. Sci. U S A *100*, 6370–6375.

Humphrey, J.S., Peters, P.J., Yuan, L.C., and Bonifacino, J.S. (1993). Localization of TGN38 to the *trans*-Golgi network: involvement of a cytoplasmic tyrosine-containing sequence. J. Cell. Biol. *120*, 1123–1135.

Inayathullah, M., and Teplow, D.B. (2011). Structural dynamics of the ΔE22 (Osaka) familial Alzheimer's disease-linked amyloid β-protein. Amyloid *18*, 98–107.

Jarosz-Griffiths, H.H., Noble, E., Rushworth, J.V., and Hooper, N.M. (2016). Amyloid-β receptors: the good, the bad, and the prion protein. J. Biol. Chem. *291*, 3174–3183.

Kaneko, M., Koike, H., Saito, R., Kitamura, Y., Okuma, Y., and Nomura, Y. (2010). Loss of HRD1-mediated protein degradation causes amyloid precursor protein accumulation and amyloid-β generation. J. Neurosci. *30*, 3924–3932.

Keck, S., Nitsch, R., Grune, T., and Ullrich, O. (2003). Proteasome inhibition by paired helical filament-tau in brains of patients with Alzheimer's disease. J. Neurochem. *85*, 115–122.

Keller, J.N., Hanni, K.B., and Markesbery, W.R. (2000). Impaired proteasome function in alzheimer's disease. J. Neurochem. *75*, 436–439.

Kim, K.B., Myung, J., Sin, N., and Crews, C.M. (1999). Proteasome inhibition by the natural products epoxomicin and dihydroeponemycin: insights into specificity and potency. Bioorg. Med. Chem. Lett. *9*, 3335–3340.

Kinoshita, A., Fukumoto, H., Shah, T., Whelan, C.M., Irizarry, M.C., and Hyman, B.T. (2003). Demonstration by FRET of BACE interaction with the amyloid precursor protein at the cell surface and in early endosomes. J. Cell. Sci. *116*, 3339–3346.

Klein, W.L., Krafft, G.A., and Finch, C.E. (2001). Targeting small Aβ oligomers: the solution to an Alzheimer's disease conundrum? Trends Neurosci. *24*, 219–224.

Kobayashi, H., and Fukuda, M. (2013). Arf6, Rab11 and transferrin receptor define distinct populations of recycling endosomes. Commun. Integr. Biol. *6*, e25036.

Koo, E.H., and Squazzo, S.L. (1994). Evidence that production and release of amyloid β-protein involves the endocytic pathway. J. Biol. Chem. *269*, 17386–17389.

Kouchi, Z., Kinouchi, T., Sorimachi, H., Ishiura, S., and Suzuki, K. (1998). The deletion of the C-terminal tail and addition of an endoplasmic reticulum targeting signal to Alzheimer's amyloid precursor protein change its localization, secretion, and intracellular proteolysis. Eur. J. Biochem. *258*, 291–300.

Kumar, P., Ambasta, R.K., Veereshwarayya, V., Rosen, K.M., Kosik, K.S., Band, H., Mestril, R., Patterson, C., and Querfurth, H.W. (2007). CHIP and HSPs interact with β-APP in a proteasome-dependent manner and influence Aβ metabolism. Hum. Mol. Genet. *16*, 848–864.

Lasiecka, Z.M., and Winckler, B. (2011). Mechanisms of polarized membrane trafficking in neurons – focusing in on endosomes. Mol. Cell. Neurosci. *48*, 278–287.

Lesné, S.E., Sherman, M.A., Grant, M., Kuskowski, M., Schneider, J.A., Bennett, D.A., and Ashe, K.H. (2013). Brain amyloid-β oligomers in ageing and Alzheimer's disease. Brain *136*, 1383–1398.

Li, X.G., Okada, T., Kodera, M., Nara, Y., Takino, N., Muramatsu, C., Ikeguchi, K., Urano, F., Ichinose, H., Metzger, D., et al. (2006). Viral-mediated temporally controlled dopamine production in a rat model of Parkinson disease. Mol. Ther. *13*, 160–166.

Manavalan, A., Mishra, M., Feng, L., Sze, S.K., Akatsu, H., and Heese, K. (2013). Brain site-specific proteome changes in aging-related dementia. Exp. Mol. Med. *45*, e39.

Matsumura, S., Shinoda, K., Yamada, M., Yokojima, S., Inoue, M., Ohnishi, T., Shimada, T., Kikuchi, K., Masui, D., Hashimoto, S., et al. (2011). Two distinct amyloid β-protein (Aβ) assembly pathways leading to oligomers and fibrils identified by combined fluorescence correlation spectroscopy, morphology, and toxicity analyses. J. Biol. Chem. *286*, 11555–11562.

McDonald, A.J., and Mascagni, F. (2001). Colocalization of calcium-binding proteins and GABA in neurons of the rat basolateral amygdala. Neuroscience *105*, 681–693.

Mullan, M., Crawford, F., Axelman, K., Houlden, H., Lilius, L., Winblad, B., and Lannfelt, L. (1992). A pathogenic mutation for probable Alzheimer's disease in the APP gene at the N-terminus of β-amyloid. Nat. Genet. *1*, 345–347.

Nakamura, N., Rabouille, C., Watson, R., Nilsson, T., Hui, N., Slusarewicz, P., Kreis, T.E., and Warren, G. (1995). Characterization of a *cis*-golgi matrix protein, GM130. J. Cell Biol. *131*, 1715–1726.

Nebenfuhr, A., Ritzenthaler, C., and Robinson, D.G. (2002). Brefeldin a: deciphering an enigmatic inhibitor of secretion. Plant Physiol. *130*, 1102–1108.

Noguchi, A., Matsumura, S., Dezawa, M., Tada, M., Yanazawa, M., Ito, A., Akioka, M., Kikuchi, S., Sato, M., Ideno, S., et al. (2009). Isolation and characterization of patient-derived, toxic, high mass amyloid β-protein (Aβ) assembly from alzheimer disease brains. J. Biol. Chem. *284*, 32895–32905.

Ohnishi, T., Yanazawa, M., Sasahara, T., Kitamura, Y., Hiroaki, H., Fukazawa, Y., Kii, I., Nishiyama, T., Kakita, A., Takeda, H., et al. (2015). Na, K-ATPase α3 is a death target of Alzheimer patient amyloid-β assembly. Proc. Natl. Acad. Sci. U S A *112*, E4465–E4474.

Palmer, A., Rivett, A.J., Thomson, S., Hendil, K.B., Butcher, G.W., Fuertes, G., and Knecht, E. (1996). Subpopulations of proteasomes in rat liver nuclei, microsomes and cytosol. Biochem. J. *316*, 401–407.

Parthasarathy, S., Inoue, M., Xiao, Y., Matsumura, Y., Nabeshima, Y., Hoshi, M., and Ishii, Y. (2015). Structural insight into an alzheimer's brain-derived spherical assembly of amyloid β by solid-state NMR. J. Am. Chem. Soc. *137*, 6480–6483.

Perez, R.G., Soriano, S., Hayes, J.D., Ostaszewski, B., Xia, W.M., Selkoe, D.J., Chen, X.H., Stokin, G.B., and Koo, E.H. (1999). Mutagenesis identifies new signals for β-amyloid precursor protein endocytosis, turnover, and the generation of secreted fragments, including Aβ42. J. Biol. Chem. *274*, 18851–18856.

Powell, S.K., Khan, N., Parker, C.L., Samulski, R.J., Matsushima, G., Gray, S.J., and McCown, T.J. (2016). Characterization of a novel adeno-associated viral vector with preferential oligodendrocyte tropism. Gene Ther. *23*, 807–814.

Rajendran, L., and Annaert, W. (2012). Membrane trafficking pathways in Alzheimer's disease. Traffic *13*, 759–770.

Ribak, C.E., Nitsch, R., and Seress, L. (1990). Proportion of parvalbumin-positive basket cells in the GABAergic innervation of pyramidal and granule cells of the rat hippocampal formation. J. Comp. Neurol. *300*, 449–461.

Rivett, A.J., Palmer, A., and Knecht, E. (1992). Electron microscopic localization of the multicatalytic proteinase complex in rat liver and in cultured cells. J. Histochem. Cytochem. *40*, 1165–1172.

Rodriguez-Navarro, J.A., Gomez, A., Rodal, I., Perucho, J., Martinez, A., Furio, V., Ampuero, I., Casarejos, M.J., Solano, R.M., de Yebenes, J.G., et al. (2008). Parkin deletion causes cerebral and systemic amyloidosis in human mutated tau over-expressing mice. Hum. Mol. Genet. *17*, 3128–3143.

Roychaudhuri, R., Yang, M., Hoshi, M.M., and Teplow, D.B. (2009). Amyloid β-protein assembly and alzheimer disease. J. Biol. Chem. *284*, 4749–4753.

Roychaudhuri, R., Zheng, X., Lomakin, A., Maiti, P., Condron, M.M., Benedek, G.B., Bitan, G., Bowers, M.T., and Teplow, D.B. (2015). Role of species-specific primary structure differences in Aβ42 assembly and neurotoxicity. ACS Chem. Neurosci. *6*, 1941–1955.

Sannerud, R., Declerck, I., Peric, A., Raemaekers, T., Menendez, G., Zhou, L.J., Veerle, B., Coen, K., Munck, S., De Strooper, B., et al. (2011). ADP ribosylation factor 6 (ARF6) controls amyloid precursor protein (APP) processing by mediating the endosomal sorting of BACE1. Proc. Natl. Acad. Sci. U S A *108*, E559–E568.

Sasaguri, H., Nilsson, P., Hashimoto, S., Nagata, K., Saito, T., De Strooper, B., Hardy, J., Vassar, R., Winblad, B., and Saido, T.C. (2017). APP mouse models for Alzheimer's disease preclinical studies. EMBO J. *36*, 2473–2487.

Schmidt, M.R., and Haucke, V. (2007). Recycling endosomes in neuronal membrane traffic. Biol. Cell *99*, 333–342.

Schneider, A., Rajendran, L., Honsho, M., Gralle, M., Donnert, G., Wouters, F., Hell, S.W., and Simons, M. (2008). Flotillin-dependent clustering of the amyloid precursor protein regulates its endocytosis and amyloidogenic processing in neurons. J. Neurosci. *28*, 2874–2882.

Schubert, U., Anton, L.C., Gibbs, J., Norbury, C.C., Yewdell, J.W., and Bennink, J.R. (2000). Rapid degradation of a large fraction of newly synthesized proteins by proteasomes. Nature *404*, 770–774.

Schwab, M.H., Bartholomae, A., Heimrich, B., Feldmeyer, D., Druffel-Augustin, S., Goebbels, S., Naya, F.J., Zhao, S., Frotscher, M., Tsai, M.J., et al. (2000). Neuronal basic helix-loop-helix proteins (NEX and BETA2/Neuro D) regulate terminal granule cell differentiation in the hippocampus. J. Neurosci. *20*, 3714–3724.

Sciaky, N., Presley, J., Smith, C., Zaal, K.J., Cole, N., Moreira, J.E., Terasaki, M., Siggia, E., and Lippincott-Schwartz, J. (1997). Golgi tubule traffic and the effects of brefeldin a visualized in living cells. J. Cell Biol. *139*, 1137–1155.

Serrano-Pozo, A., Frosch, M.P., Masliah, E., and Hyman, B.T. (2011). Neuropathological alterations in Alzheimer disease. Cold Spring Harb. Perspect. Med. *1*, a006189.

Sinha, S., and Lieberburg, I. (1999). Cellular mechanisms of β-amyloid production and secretion. Proc. Natl. Acad. Sci. U S A *96*, 11049–11053.

Szodorai, A., Kuan, Y.H., Hunzelmann, S., Engel, U., Sakane, A., Sasaki, T., Takai, Y., Kirsch, J., Muller, U., Beyreuther, K., et al. (2009). APP anterograde transport requires Rab3A GTPase activity for assembly of the transport vesicle. J. Neurosci. *29*, 14534–14544.

Tarassishin, L., Yin, Y.I., Bassit, L., and Li, Y.M. (2004). Processing of Notch and amyloid precursor protein by γ-secretase is spatially distinct. Proc. Natl. Acad. Sci. U S A *101*, 17050–17055.

Thayer, D.A., Jan, Y.N., and Jan, L.Y. (2013). Increased neuronal activity fragments the Golgi complex. Proc. Natl. Acad. Sci. U S A *110*, 1482–1487.

Tomiyama, T., Matsuyama, S., Iso, H., Umeda, T., Takuma, H., Ohnishi, K., Ishibashi, K., Teraoka, R., Sakama, N., Yamashita, T., et al. (2010). A mouse model of amyloid β oligomers: their contribution to synaptic alteration, abnormal tau phosphorylation, glial activation, and neuronal loss *in vivo*. J. Neurosci. *30*, 4845–4856.

Tomiyama, T., Nagata, T., Shimada, H., Teraoka, R., Fukushima, A., Kanemitsu, H., Takuma, H., Kuwano, R., Imagawa, M., Ataka, S., et al. (2008). A new amyloid β variant favoring oligomerization in alzheimer's-type dementia. Ann. Neurol. *63*, 377–387.

Tonoki, A., Kuranaga, E., Tomioka, T., Hamazaki, J., Murata, S., Tanaka, K., and Miura, M. (2009). Genetic evidence linking age-dependent attenuation of the 26S proteasome with the aging process. Mol. Cell. Biol. *29*, 1095–1106.

Tsubuki, S., Saito, Y., Tomioka, M., Ito, H., and Kawashima, S. (1996). Differential inhibition of calpain and proteasome activities by peptidyl aldehydes of Di-leucine and Tri-leucine. J. Biochem. *119*, 572–576.

Ubelmann, F., Burrinha, T., Salavessa, L., Gomes, R., Ferreira, C., Moreno, N., and Almeida, C.G. (2017). Bin1 and CD2AP polarise the endocytic generation of beta-amyloid. EMBO Rep. *18*, 102–122.

Vembar, S.S., and Brodsky, J.L. (2008). One step at a time: endoplasmic reticulum-associated degradation. Nat. Rev. Mol. Cell Biol. *9*, 944–957.

Walsh, D.M., and Selkoe, D.J. (2007). Aβ Oligomers - a decade of discovery. J. Neurochem. *101*, 1172–1184.

Wang, H., and Saunders, A.J. (2014). The role of ubiquitin-proteasome in the metabolism of amyloid precursor protein (APP): implications for novel therapeutic strategies for alzheimer's disease. Discov. Med. *18*, 41–50.

Wang, Y., Wei, J.H., Bisel, B., Tang, D., and Seemann, J. (2008). Golgi cisternal unstacking stimulates COPI vesicle budding and protein transport. PLoS One *3*, e1647.

Watanabe, T., Hikichi, Y., Willuweit, A., Shintani, Y., and Horiguchi, T. (2012). FBL2 regulates amyloid precursor protein (APP) metabolism by promoting ubiquitination-dependent APP degradation and inhibition of APP endocytosis. J. Neurosci. *32*, 3352–3365.

Weiner, M.W., Veitch, D.P., Aisen, P.S., Beckett, L.A., Cairns, N.J., Green, R.C., Harvey, D., Jack, C.R., Jagust, W., Liu, E., et al. (2012). The alzheimer's disease neuroimaging initiative: a review of papers published since its inception. Alzheimers Dement *8*, S1–S68.

Wilkinson, B., and Gilbert, H.F. (2004). Protein disulfide isomerase. Biochim. Biophys. Acta *1699*, 35–44.

Xiao, Y., Ma, B., McElheny, D., Parthasarathy, S., Long, F., Hoshi, M., Nussinov, R., and Ishii, Y. (2015). Aβ(1-42) fibril structure illuminates self-recognition and replication of amyloid in Alzheimer's disease. Nat. Struct. Mol. Biol. *22*, 499–505.

Xu, H., Sweeney, D., Wang, R., Thinakaran, G., Lo, A.C., Sisodia, S.S., Greengard, P., and Gandy, S. (1997). Generation of Alzheimer β-amyloid protein in the *trans*-Golgi network in the apparent absence of vesicle formation. Proc. Natl. Acad. Sci. U S A *94*, 3748–3752.

Yu, W.H., Kumar, A., Peterhoff, C., Kulnane, L.S., Uchiyama, Y., Lamb, B.T., Cuervo, A.M., and Nixon, R.A. (2004). Autophagic vacuoles are enriched in amyloid precursor protein-secretase activities: implications for β-amyloid peptide over-production and localization in Alzheimer's disease. Int. J. Biochem. Cell. Biol. *36*, 2531–2540.

Zhu, J.W., Nagasawa, H., Nagura, F., Mohamad, S.B., Uto, Y., Ohkura, K., and Hori, H. (2000). Elucidation of strict structural requirements of brefeldin a as an inducer of differentiation and apoptosis. Bioorg. Med. Chem. *8*, 455–463.

ISCI, Volume *13*

Supplemental Information

Alzheimer Aβ Assemblies Accumulate in Excitatory Neurons upon Proteasome Inhibition and Kill Nearby NAKα3 Neurons by Secretion

Hitomi Komura, Shota Kakio, Tomoya Sasahara, Yoshie Arai, Naomi Takino, Michio Sato, Kaori Satomura, Takayuki Ohnishi, Yo-ichi Nabeshima, Shin-ichi Muramatsu, Isao Kii, and Minako Hoshi

Supplemental Information

Supplemental Figures

Figure S1

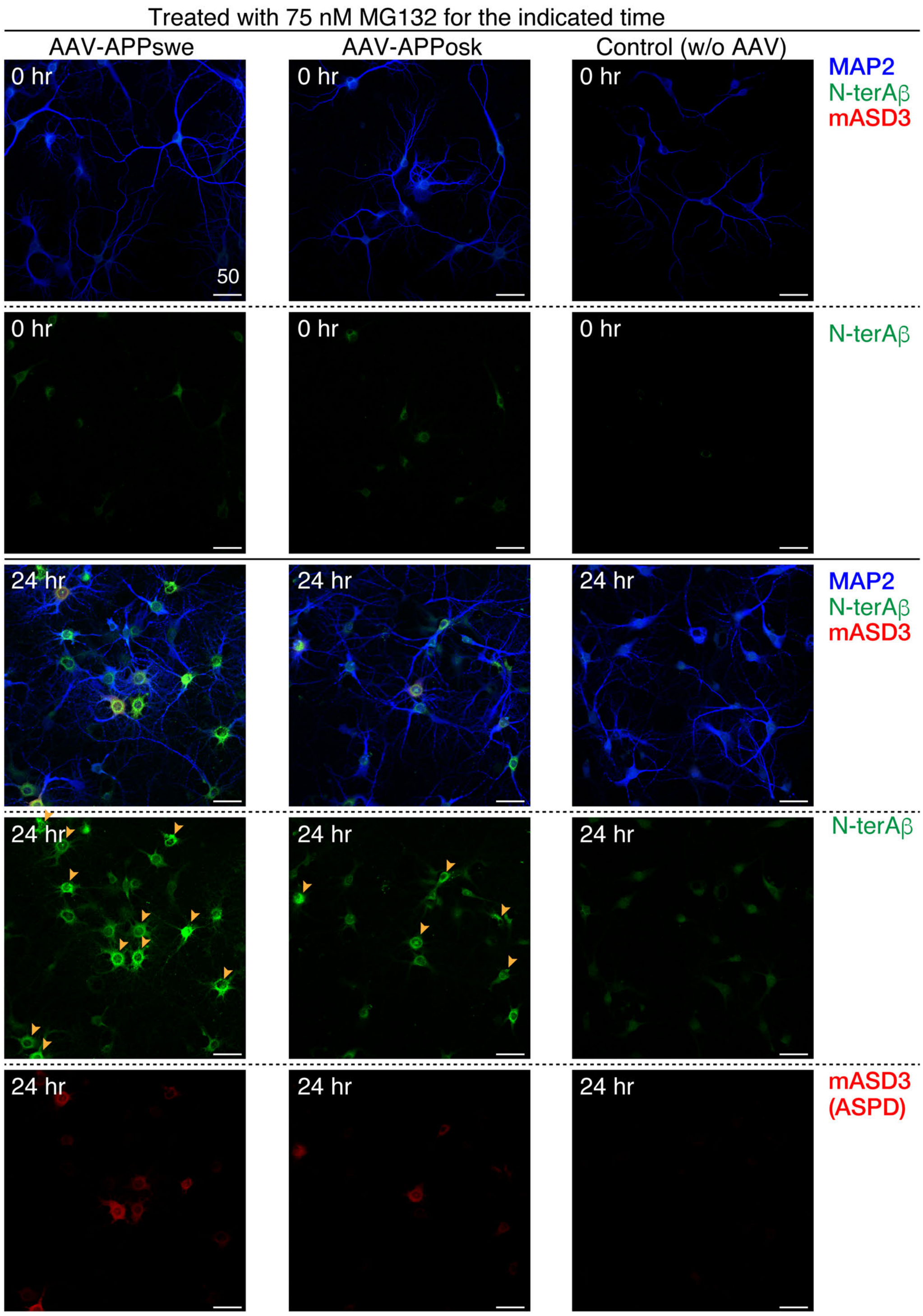

Figure S1 Effect of Proteasome Inhibition on Aβ and ASPD Accumulations, related to Figures 2, 4, and 11

Primary rat hippocampal neuronal cultures, with or without AAV-APP transduction, were treated with 75 nM MG132 for the indicated time. The cultures were triple-stained with antibodies against MAP2, Aβ N-terminal end (N-terAβ), and ASPD (mASD3). Representative images are shown. Single channel images of green or red are shown below. Scale bar = 50 μm. Arrowheads mark neurons with intense N-terAβ signals with ASPD staining.

Figure S2

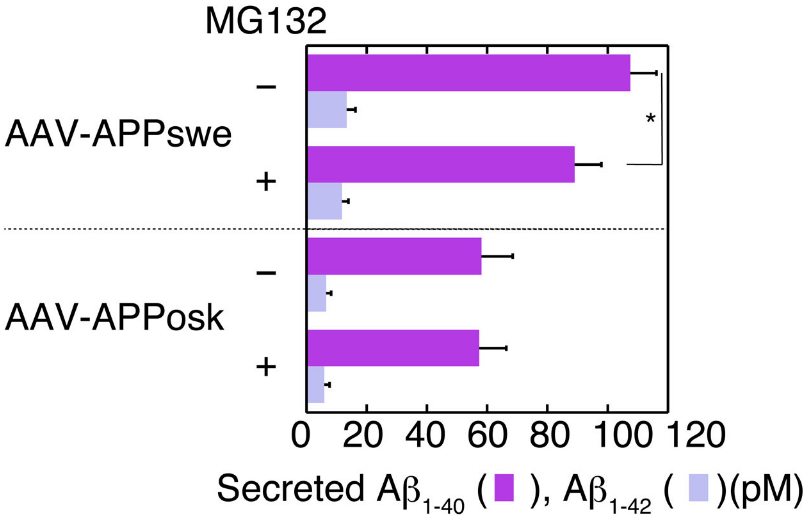

Figure S2 Proteasome Inhibition Does Not Affect Aβ Secretion, related to Figure 3
The culture supernates were obtained from APP-transduced primary rat hippocampal neuronal cultures, treated with or without 75 nM MG132 for 24 hr. $A\beta_{1\text{-}40}$ and $A\beta_{1\text{-}42}$ were quantified by using a WAKO ELISA system (Transparent Methods). (mean ± SD, n = 4; Scheffé *post hoc* test, *, $p = 0.04$)

Figure S3

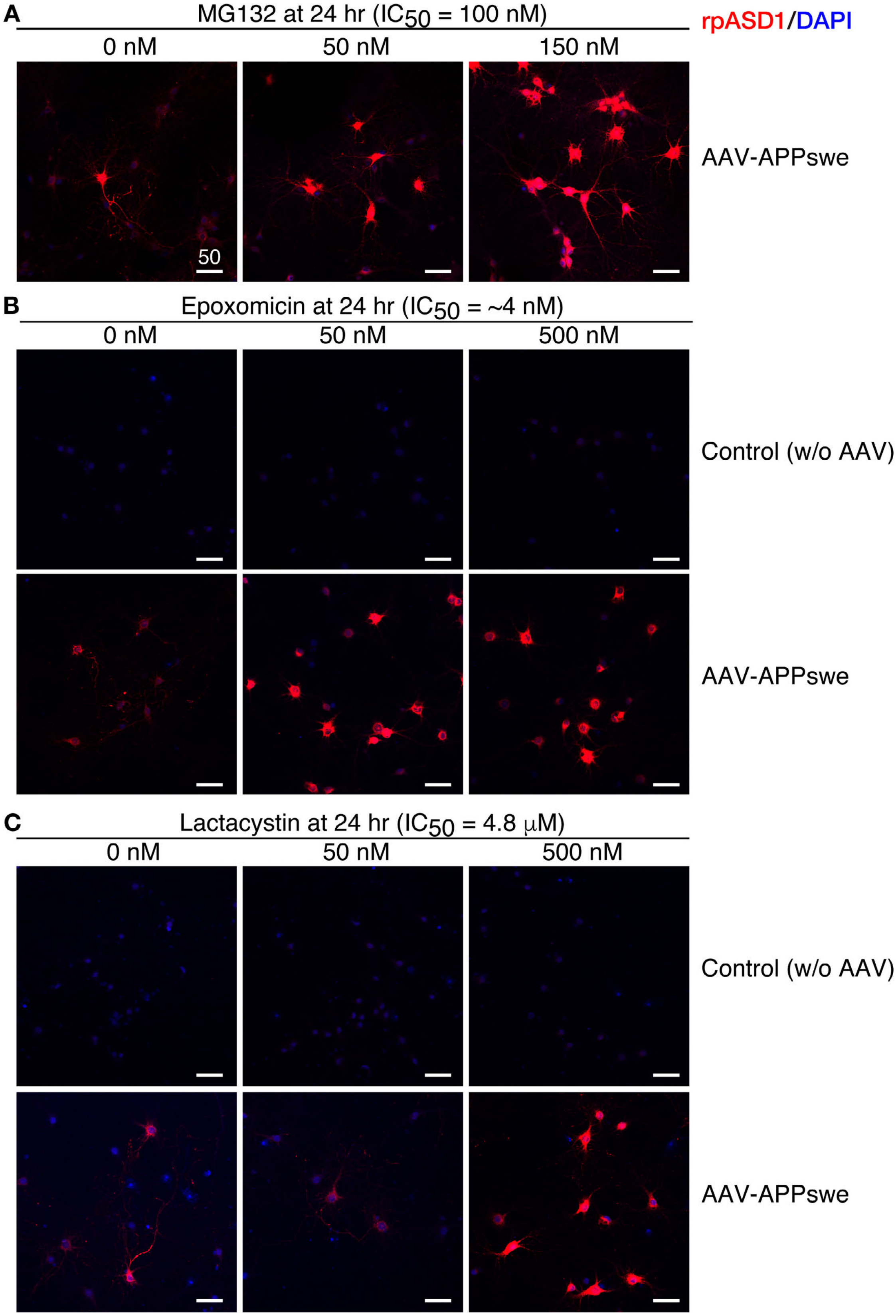
A
MG132 at 24 hr (IC_{50} = 100 nM)
rpASD1/DAPI
0 nM
50 nM
150 nM
AAV-APPswe
50
B
Epoxomicin at 24 hr (IC_{50} = ~4 nM)
0 nM
50 nM
500 nM
Control (w/o AAV)
AAV-APPswe
C
Lactacystin at 24 hr (IC_{50} = 4.8 μM)
0 nM
50 nM
500 nM
Control (w/o AAV)
AAV-APPswe

Figure S3 Effect of Mechanistically Different Proteasome Inhibitors on ASPD Accumulation, related to Figure 4

Primary rat hippocampal neuronal cultures, with or without AAV-APPswe transduction, were treated with MG132 (**A**), epoxomicin (**B**), or lactacystin (**C**) at the indicated concentration for 24 hr. The cultures were stained with anti-ASPD rpASD1 antibody and DAPI. Representative images are shown. Scale bar = 50 μm. All these proteasome inhibitors increased the neuronal ASPD staining at 24 hr, as shown in Figure 4A. The range of the dose-dependency of each inhibitor correlated reasonably well with the IC_{50} value.

Figure S4

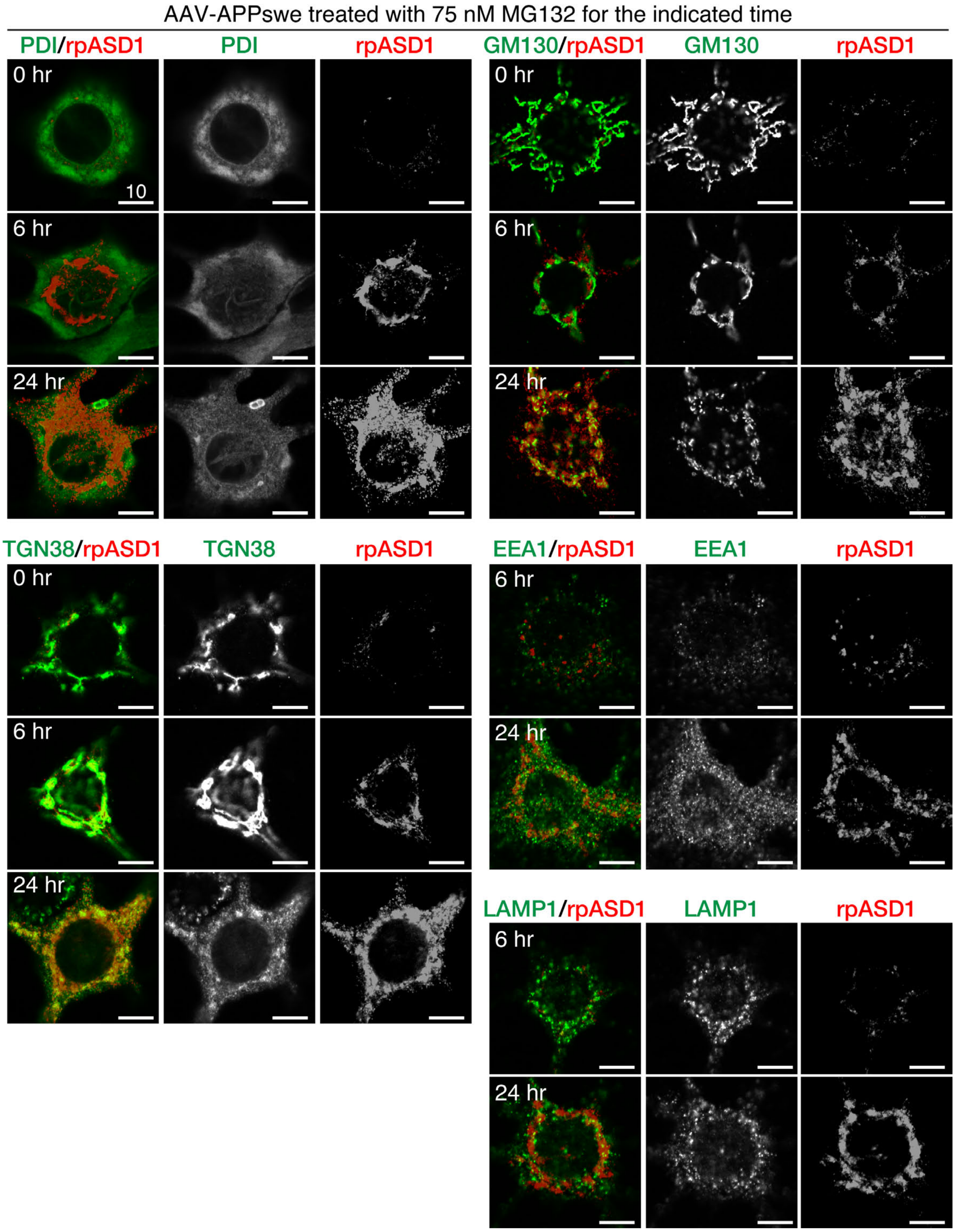

Figure S4 ASPD Accumulate in the Trans-Golgi of Mature Neurons, related to Figures 6 and 7

Primary rat hippocampal neuronal cultures with AAV-APPswe transduction were treated with 75 nM MG132 for the indicated time. The cultures were double-stained with anti-ASPD rpASD1 antibody and antibody against organelle marker protein (see Transparent Methods). Representative double-stained images obtained with a highly sensitive, direct photon-counting system with a 100x oil objective lens are shown, along with the corresponding single red or green images. Scale bar = 10 μm.

Figure S5

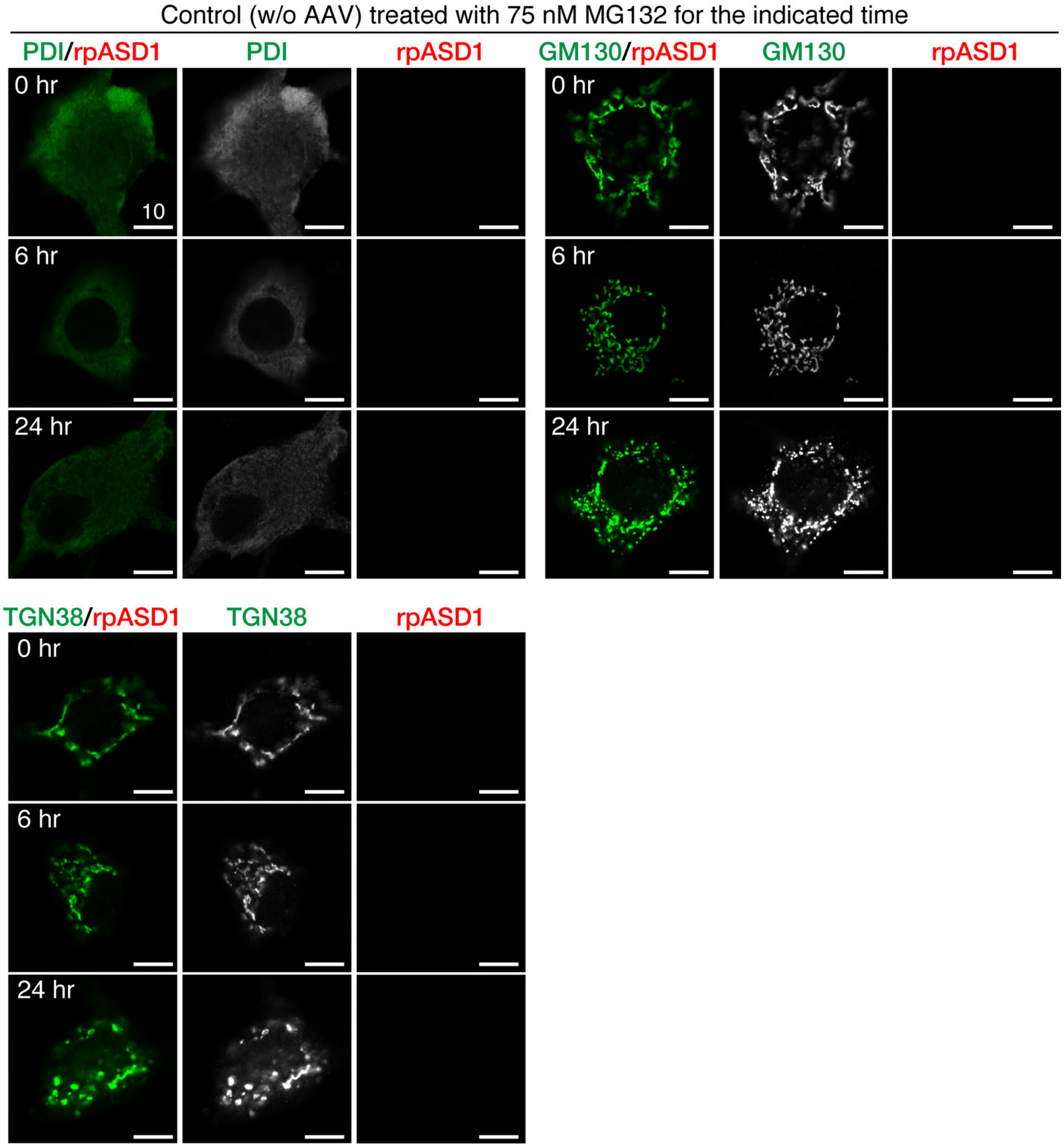

Figure S5 ASPD Rarely Accumulate without APP Transduction, related to Figures 6 and S4

Control experiment for Figure 6. Primary rat hippocampal neuronal cultures without AAV-APPswe transduction were treated with 75 nM MG132 for the indicated time and were double-stained with anti-ASPD rpASD1 antibody and antibody against organelle marker protein (see Transparent Methods) as in Figure 6. Representative double-stained images obtained with a highly sensitive, direct photon-counting system with a 100x oil objective lens are shown, along with the corresponding single red or green images. Scale bar = 10 μm.

Figure S6

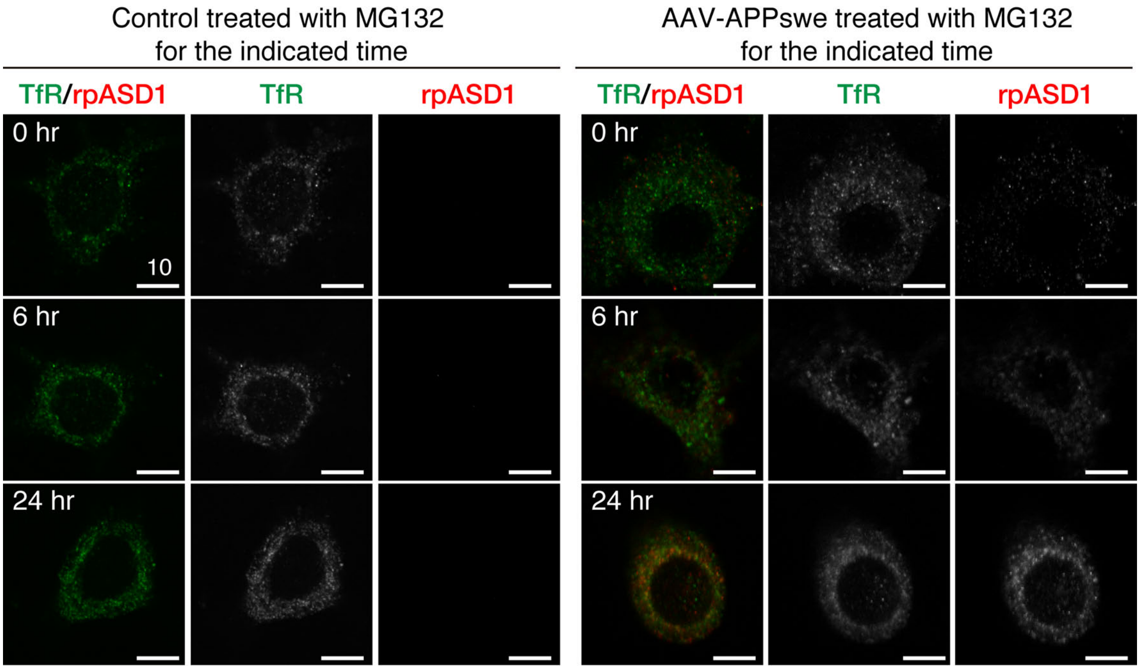

Figure S6 ASPD Accumulate in the Recycling Endosomes of Mature Neurons, related to Figure 8

Primary rat hippocampal neuronal cultures, with or without AAV-APPswe transduction, were treated with 75 nM MG132 for the indicated time. The cultures were double-stained with anti-ASPD rpASD1 and anti-TfR antibody (see Transparent Methods). Representative double-stained images obtained with a highly sensitive, direct photon-counting system with a 100x oil objective lens are shown, along with the corresponding single red or green images. Scale bar = 10 μm.

Figure S7

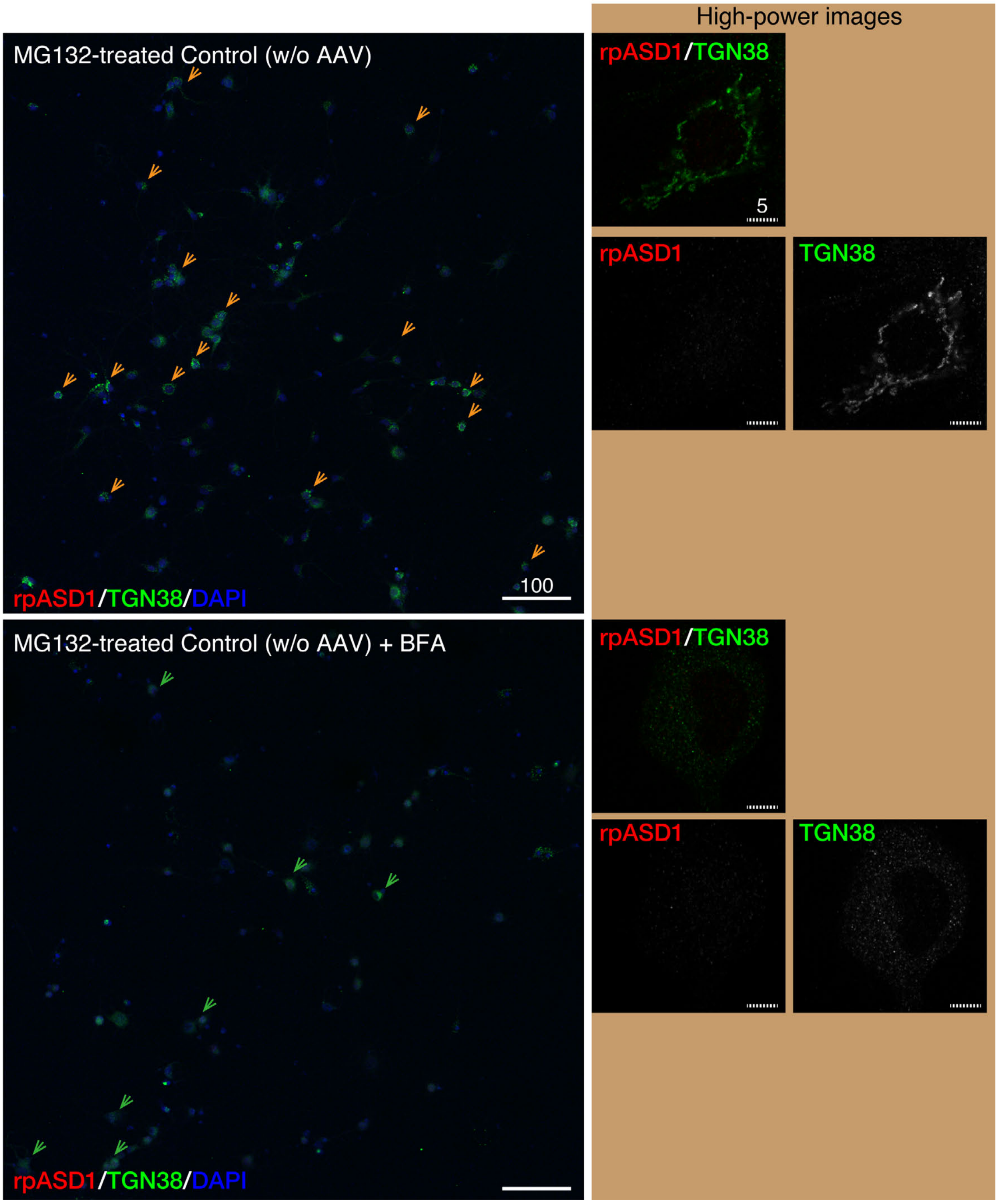

Figure S7 BFA Effects on the TGN in Control Mature Neurons, related to Figures 9 and S8

Control experiment for Figure 9 is shown. Primary rat hippocampal neuronal cultures without AAV-APPswe transduction were treated with 75 nM MG132 for 24 hr in the absence or the presence of 0.6 μg/ml BFA. The cultures were triple-stained with rpASD1, anti-TGN38 antibody (TGN marker), and DAPI. Representative images are shown. Orange arrows mark neurons that still appear to retain the Golgi structure, while green arrows mark neurons that show collapsed TGN staining. TGN38 staining was lost or diffusely spread throughout the cytoplasm in untransduced cells treated with MG132 and 0.6 μg/ml BFA together, indicating that BFA collapsed the Golgi apparatus (green arrows and high-power images in the right). In contrast, the Golgi structure appeared to be still preserved in some neurons of untransduced cells treated with MG132 in the absence of BFA (orange arrows and high-power images in the right). High-power images obtained with a highly sensitive, direct photon-counting system with a 100x oil objective lens are shown on the right. Solid and hatched scale bars are 100 and 5 μm, respectively.

Figure S8

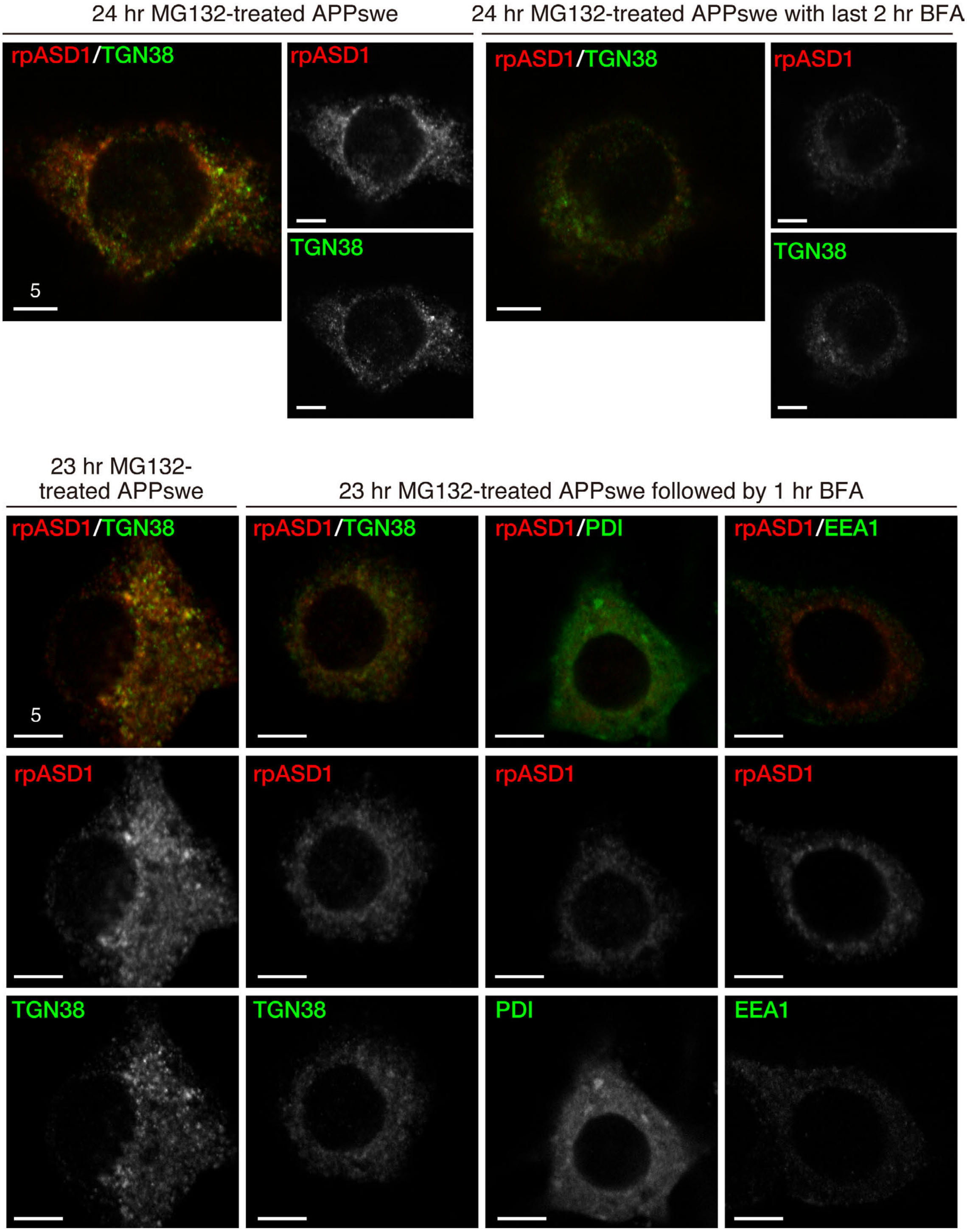

Figure S8 Effect of Brief BFA Treatment on the TGN in APPswe-Transduced Mature Neurons, related to Figures 9 and S7

Control experiment for Figure 9 showing the effects of brief treatment with BFA. APPswe-transduced primary rat hippocampal neuronal cultures were treated with 75 nM MG132 for 22-23 hr, followed by 0.6 μg/ml BFA treatment for another 1-2 hr. The cultures were triple-stained with rpASD1, an antibody against organelle marker protein, and DAPI. Representative images are shown. High-power images obtained with a highly sensitive, direct photon-counting system with a 100x oil objective lens are shown on the right. Scale bar = 5 μm. As shown in the images at 1 hr and 2 hr BFA treatment, the ASPD and TGN38 signals decreased substantially with increased duration of BFA treatment. In the case of 1 hr BFA treatment, ASPD signals still largely remained co-localized with TGN38 staining. However, more ASPD signals appeared in the ER, because BFA leads to retrograde transport from the Golgi apparatus to the ER (Nebenfuhr et al., 2002). In contrast, ASPD signals were only rarely co-localized with the EE, as was also observed before BFA treatment (see 24 hr EEA1/rpASD1 staining in Figure 6).

Figure S9

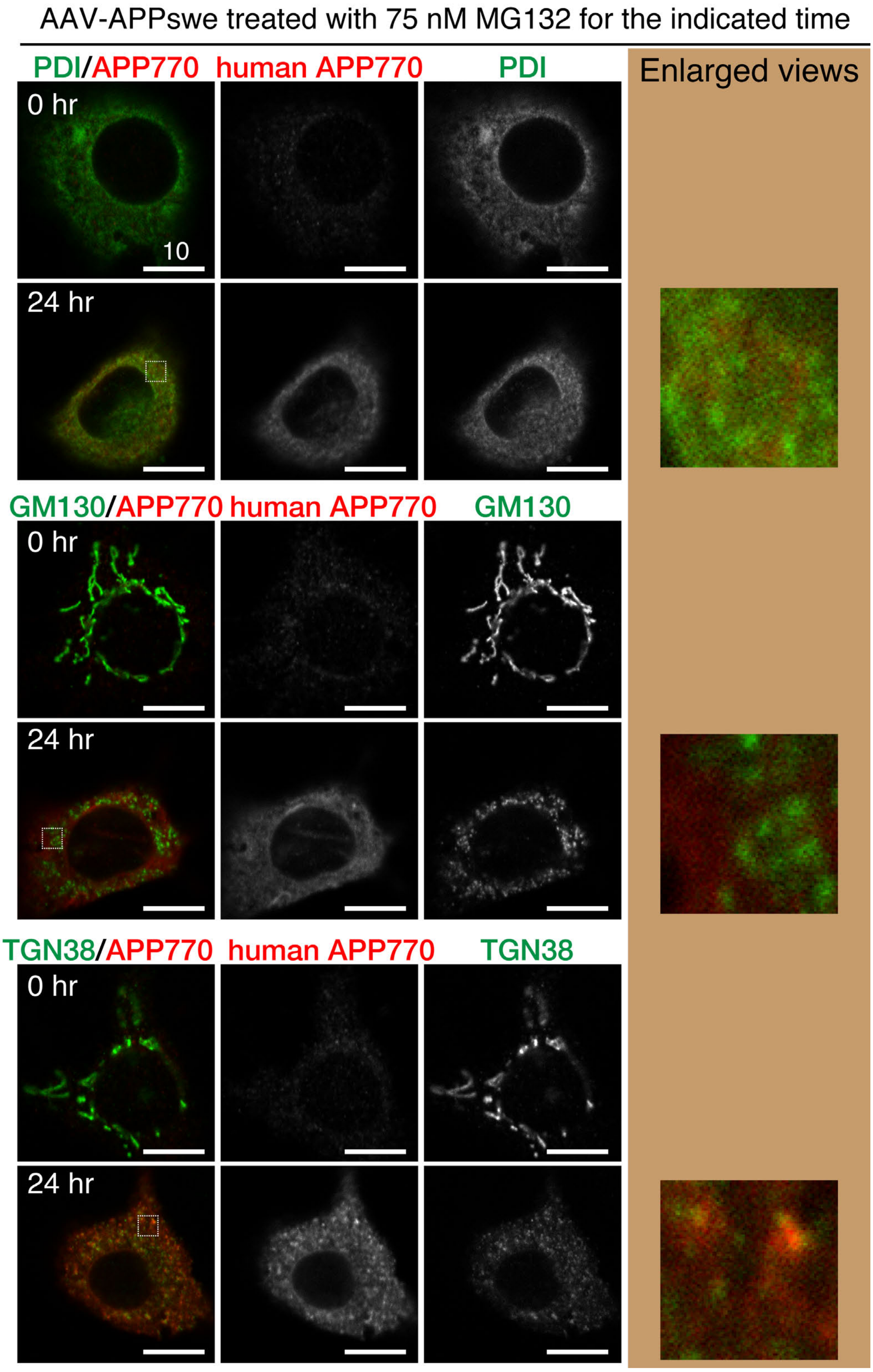
AAV-APPswe treated with 75 nM MG132 for the indicated time
PDI/APP770
human APP770
PDI
Enlarged views
0 hr
10
24 hr
GM130/APP770
human APP770
GM130
0 hr
24 hr
TGN38/APP770
human APP770
TGN38
0 hr
24 hr

Figure S9 Steady-State Distribution of human APP770, with or without Proteasome Inhibition, in APPswe-Transduced Mature Neurons, related to Figure 10

APPswe-transduced primary rat hippocampal neuronal cultures were treated with 75 nM MG132 for the indicated time. The cultures were double-stained with anti-human APP770 antibody and antibody against organelle marker protein (see Transparent Methods). Representative double-stained images obtained with a highly sensitive, direct photon-counting system with a 100x oil objective lens are shown, along with the corresponding single red or green images. An enlarged view of the field enclosed by a hatched line is shown on the right. Scale bar = 10 μm.

Figure S10

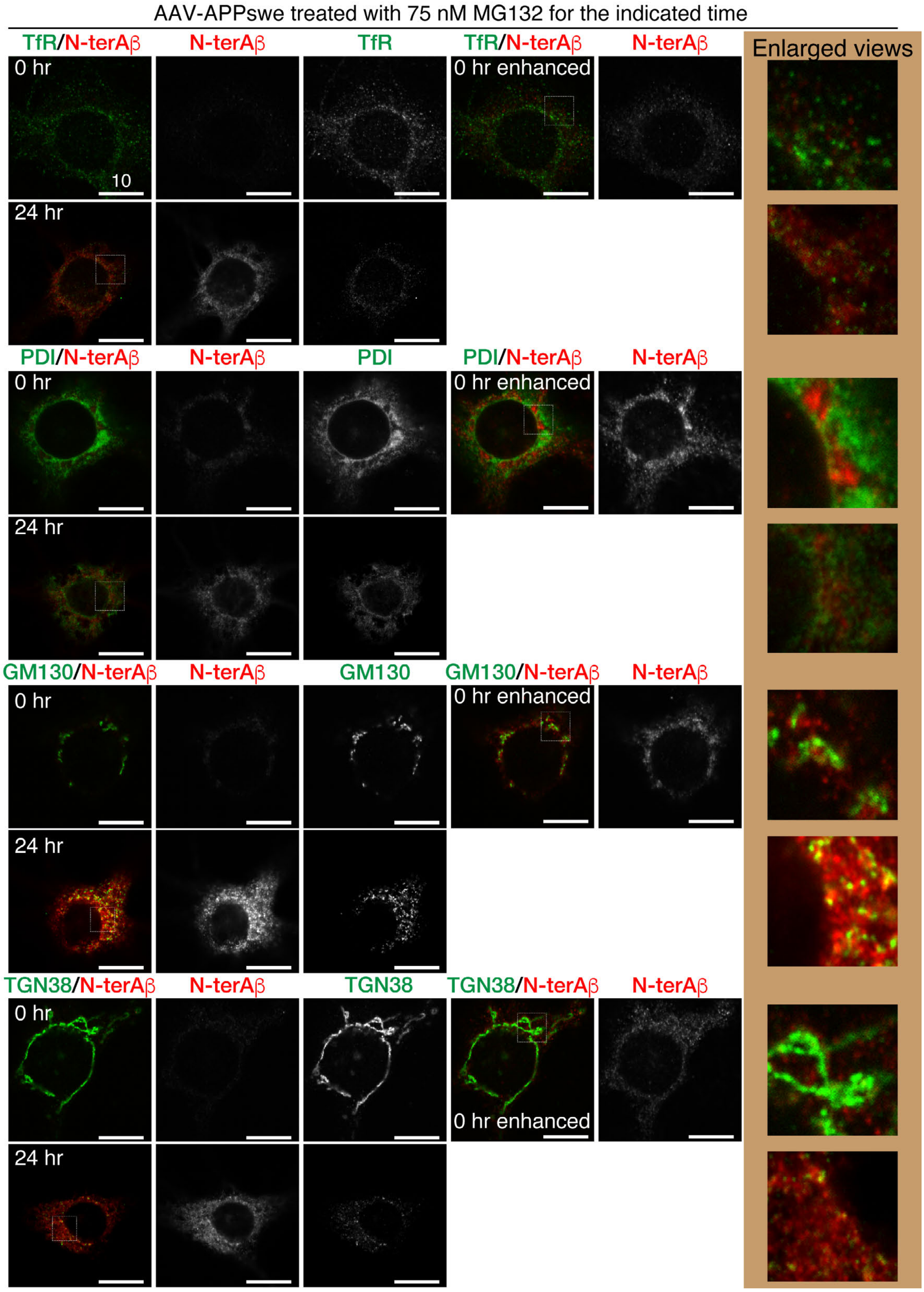

AAV-APPswe treated with 75 nM MG132 for the indicated time
TfR/N-terAβ
N-terAβ
TfR
TfR/N-terAβ
N-terAβ
Enlarged views
0 hr
10
0 hr enhanced
24 hr
PDI/N-terAβ
N-terAβ
PDI
PDI/N-terAβ
N-terAβ
0 hr
0 hr enhanced
24 hr
GM130/N-terAβ
N-terAβ
GM130
GM130/N-terAβ
N-terAβ
0 hr
0 hr enhanced
24 hr
TGN38/N-terAβ
N-terAβ
TGN38
TGN38/N-terAβ
N-terAβ
0 hr
0 hr enhanced
24 hr

Figure S10 Steady-State Distribution of N-terAβ, with or without Proteasome Inhibition, in APPswe-Transduced Mature Neurons, related to Figure 10

APPswe-transduced primary rat hippocampal neuronal cultures were treated with 75 nM MG132 for the indicated time. The cultures were double-stained with anti-ASPD rpASD1 antibody and antibody against organelle marker protein (see Transparent Methods). Representative double-stained images obtained with a highly sensitive, direct photon-counting system with a 100x oil objective lens are shown, along with the corresponding single red or green images. Scale bar = 10 μm. Without proteasome inhibition, the N-terAβ signal is weak. As a reference, red enhanced images are also shown. An enlarged view of the field enclosed by a hatched line is shown on the right. From the red enhanced images, the weak N-terAβ signal appeared to be present together with the ER or the cis-Golgi, but not with the TGN or the RE.

Figure S11

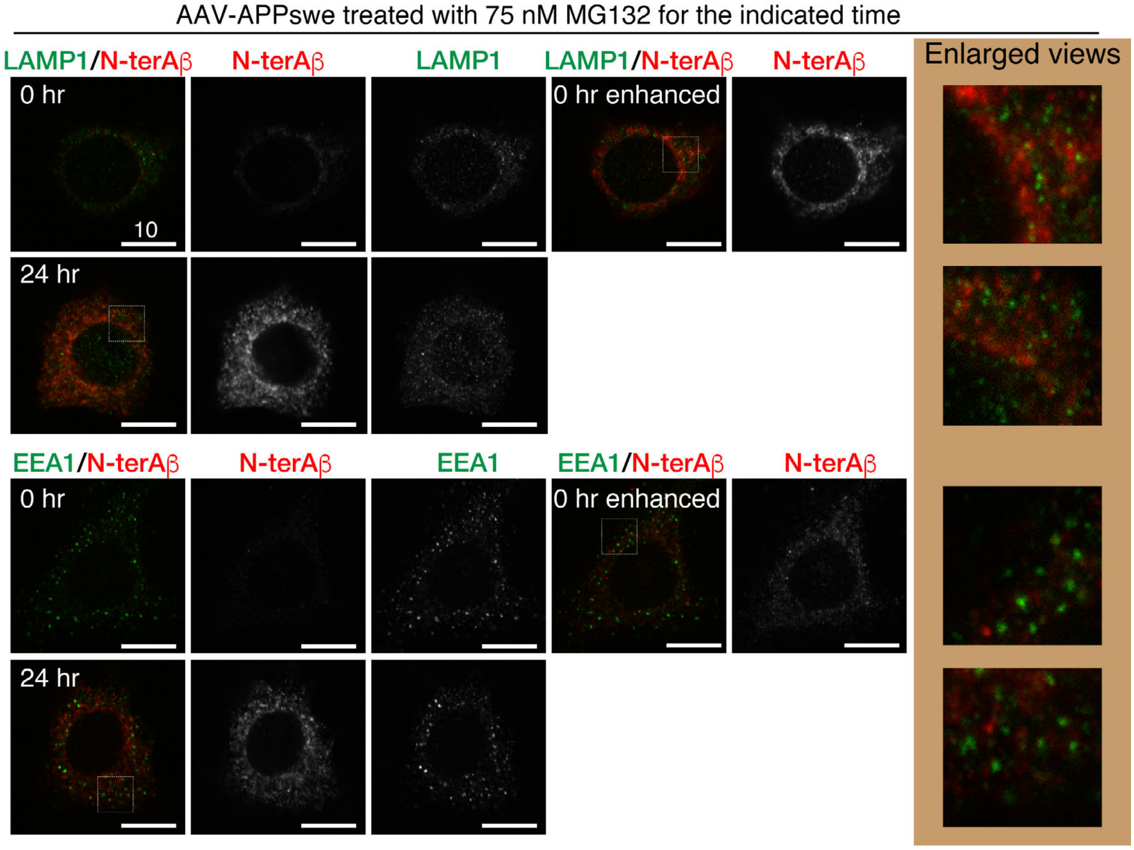

Figure S11 Steady-State Distribution of N-terAβ, with or without Proteasome Inhibition, in APPswe-Transduced Mature Neurons, related to Figure 10

APPswe-transduced primary rat hippocampal neuronal cultures were treated with 75 nM MG132 for the indicated time. The cultures were double-stained with anti-ASPD rpASD1 antibody and antibody against organelle marker protein (see Transparent Methods). Representative double-stained images obtained with a highly sensitive, direct photon-counting system with a 100x oil objective lens are shown, along with the corresponding single red or green images. Scale bar = 10 μm. Without proteasome inhibition, the N-terAβ signal is weak. As a reference, red enhanced images are also shown. An enlarged view of the field enclosed by a hatched line is shown on the right. From the red enhanced images, the weak N-terAβ signal didn't appear to be present together with the EE or the Lys.

Figure S12

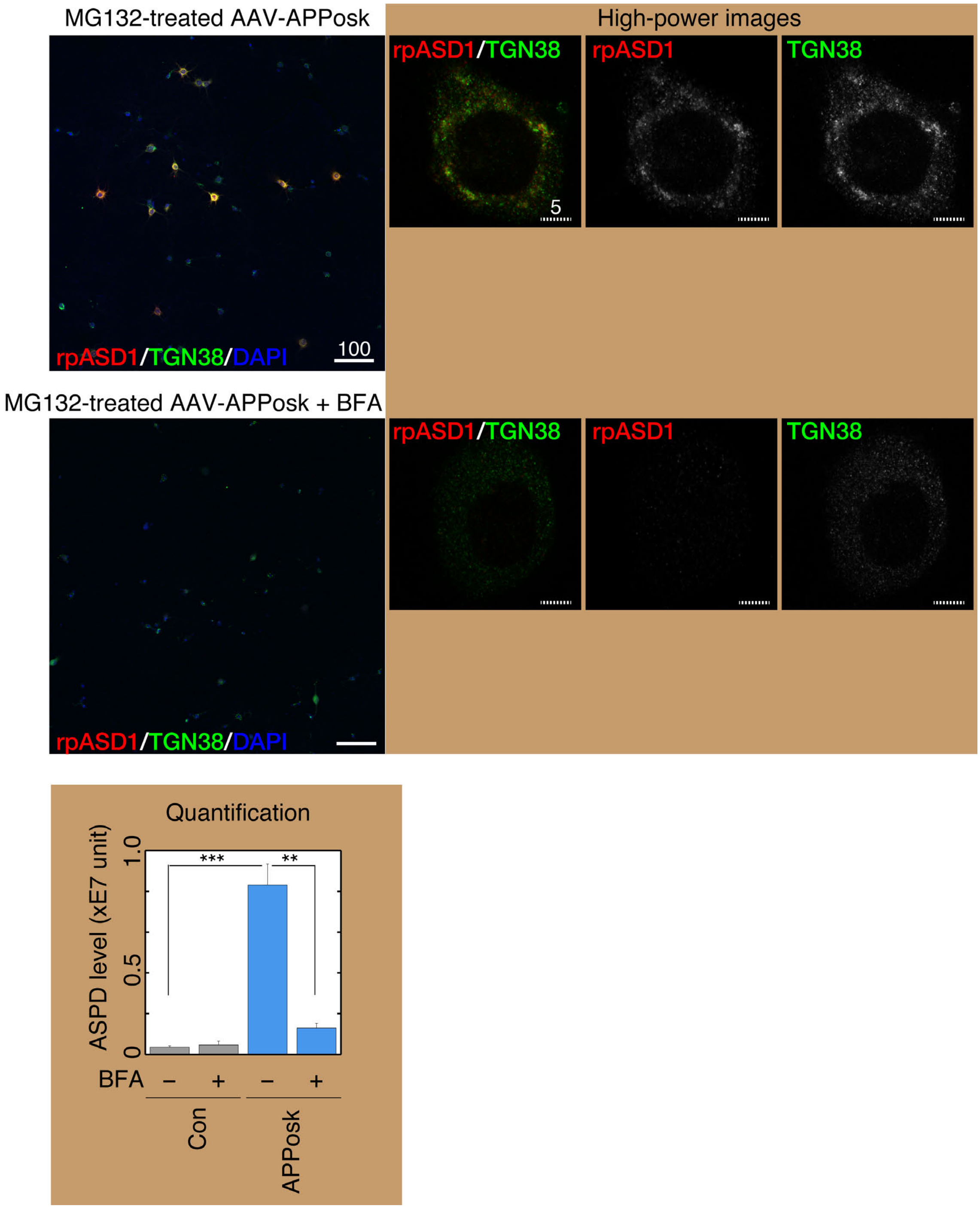

Figure S12 BFA Effects on the TGN in APPosk-Transduced Neurons, related to Figure 11

Primary rat hippocampal neuronal cultures with AAV-APPosk transduction were treated with 75 nM MG132 for 24 hr in the absence or the presence of 0.6 μg/ml BFA, as in Figure 9. The cultures were triple-stained with rpASD1 antibody, anti-TGN38 (TGN marker) antibody, and DAPI. Representative images are shown with scale bars in μm. The ASPD-staining of each culture was quantified using the In Cell Analyzer (*GE Healthcare Lifesciences*) as in Figure 9 (mean ± SD, n = 3; Scheffé *post hoc* test, ***, $p < 0.0001$; **, $p = 0.0004$). High-power images obtained with a highly sensitive, direct photon-counting system with a 100x oil objective lens are shown on the right. Single red or green images are also shown.

Figure S13

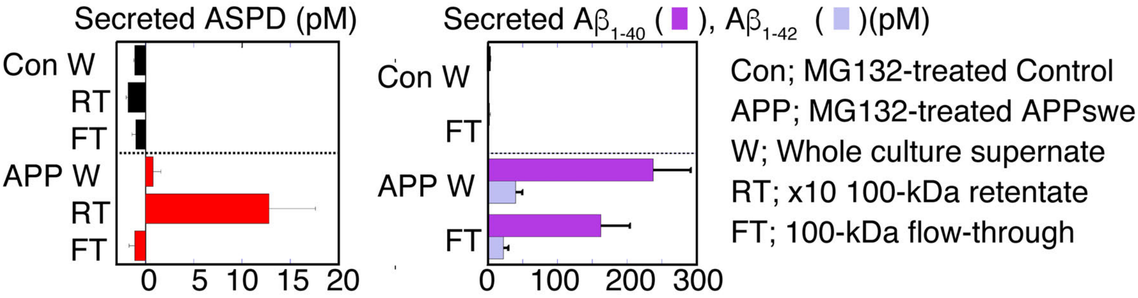

Figure S13 Intra-neuronal ASPD were Secreted and Showed Toxicity, related to Figure 12

The culture supernates were obtained from primary rat hippocampal neuronal cultures, with or without AAV-APPswe transduction, which were treated with 75 nM MG132 for 24 hr as in Figure 12B. A$\beta_{1\text{-}40}$ and A$\beta_{1\text{-}42}$ were quantified by using a WAKO ELISA system (details in Transparent Methods). Mean ± SD, n = 3.

Figure S14

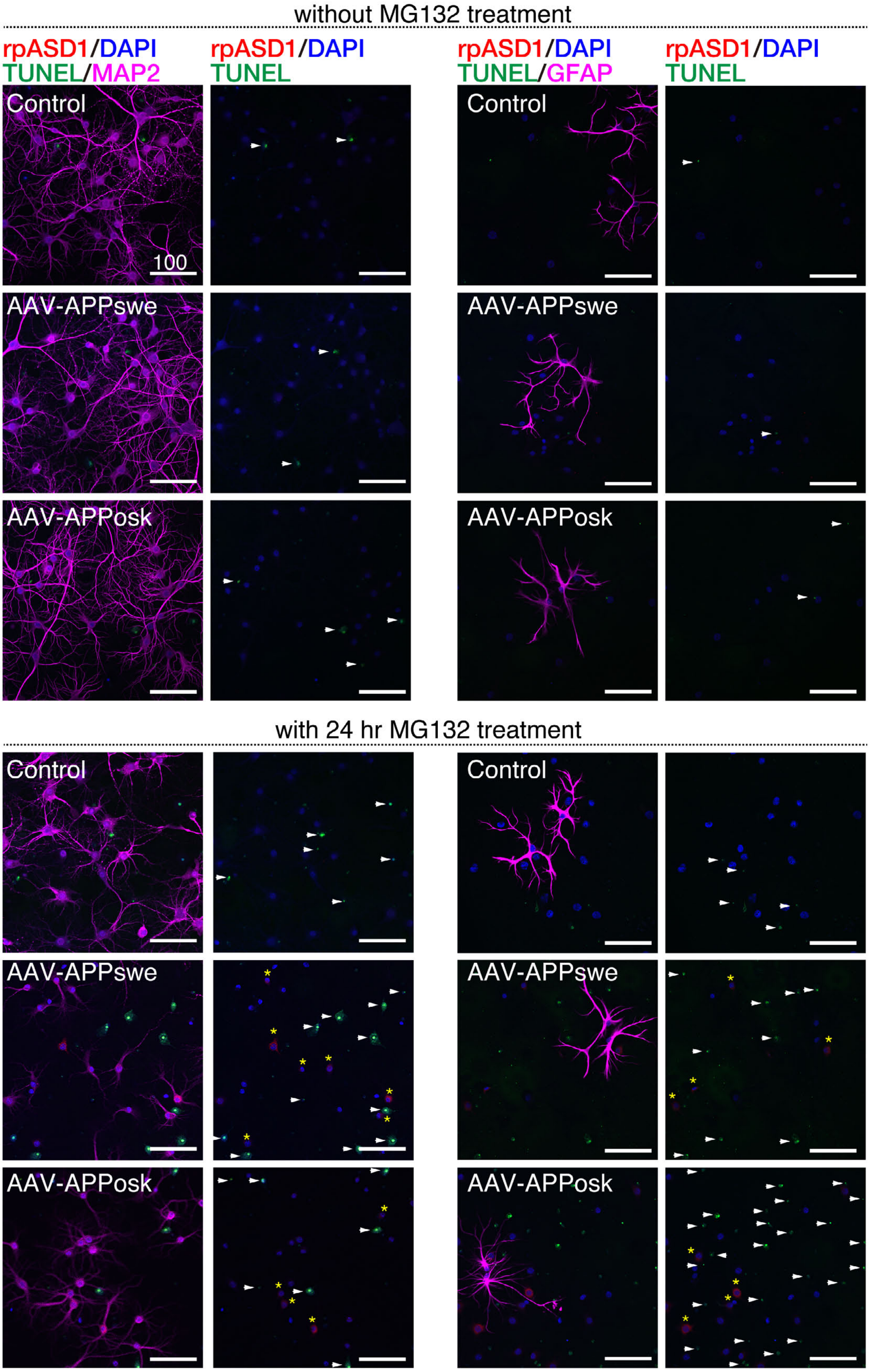
without MG132 treatment
rpASD1/DAPI
TUNEL/MAP2
rpASD1/DAPI
TUNEL
rpASD1/DAPI
TUNEL/GFAP
rpASD1/DAPI
TUNEL
Control
100
AAV-APPswe
AAV-APPosk
with 24 hr MG132 treatment
Control
AAV-APPswe
AAV-APPosk

Figure S14 Secreted ASPD Induced Apoptotic Degeneration of Surrounding Neurons, related to Figure 13

APP-transduced or untransduced control cultures were treated with or without 75 nM MG132 for 24 hr and quadruple-stained with rpASD1, DAPI, TUNEL, and MAP2/GFAP. Representative quadruple-stained images are shown, along with the corresponding triple staining of rpASD1(*), DAPI, and TUNEL (arrowheads) on the right, with 100 μm scale bars.

Figure S15

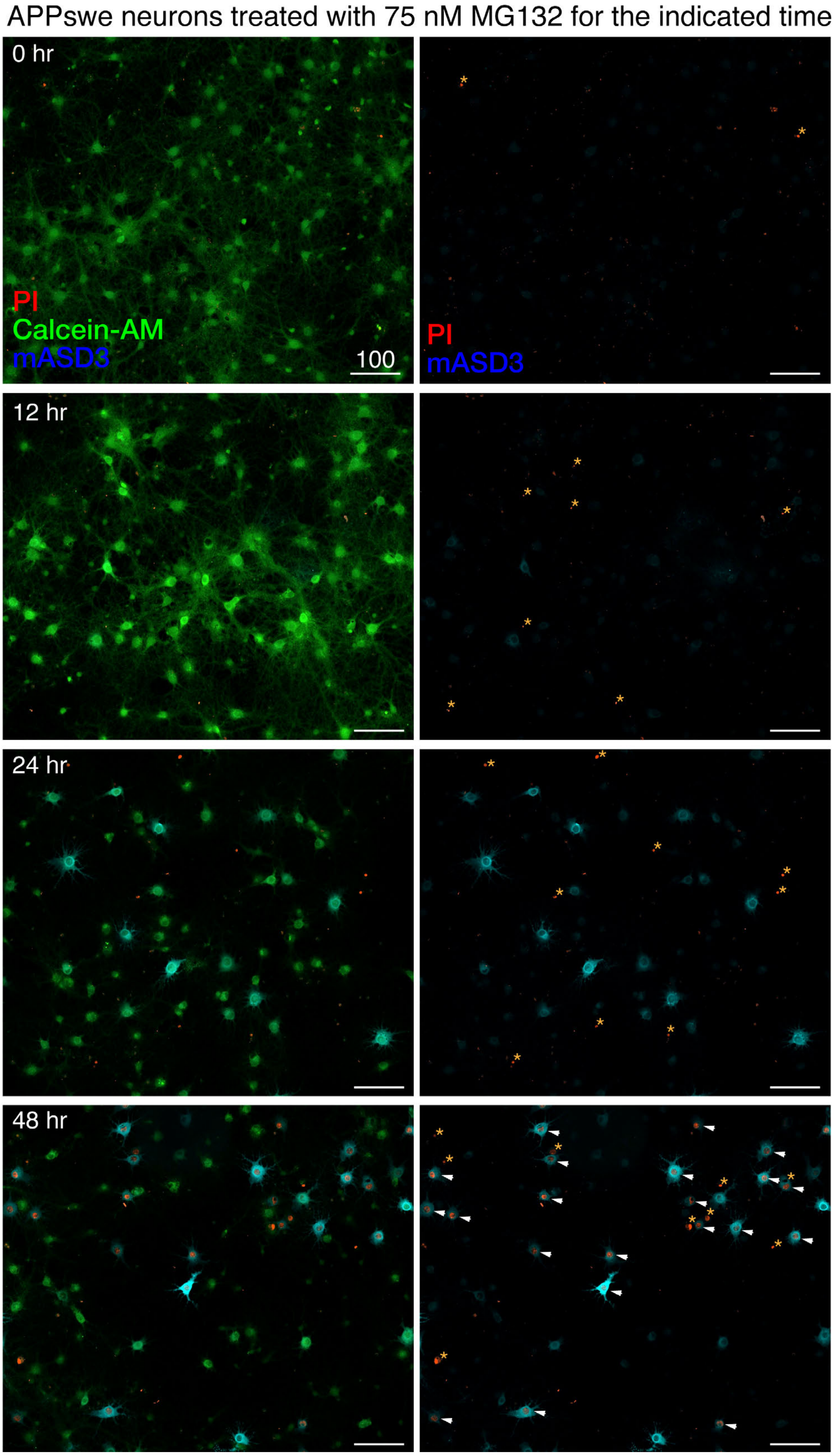
APPswe neurons treated with 75 nM MG132 for the indicated time
0 hr
PI
Calcein-AM
mASD3
100
PI
mASD3
12 hr
24 hr
48 hr

Figure S15 PI-Detectable, Non-Apoptotic Death Occurred in ASPD-Producing Neurons at 48 hr of MG132 Treatment, related to Figure 13

APPswe-transduced primary rat hippocampal neuronal cultures were treated with 75 nM MG132 for the indicated time, triple-stained with propidium iodide (PI), calcein-AM, and anti-ASPD mASD3 antibody (see Transparent Methods), and photographed. Left columns show triple staining and right columns show the corresponding PI/mASD3-staining. Representative images are shown with 100 μm scale bars. Asterisks show apoptotic nuclei detected by PI. Arrowheads show PI-detectable non-apoptotic death in ASPD-producing neurons.

Figure S16

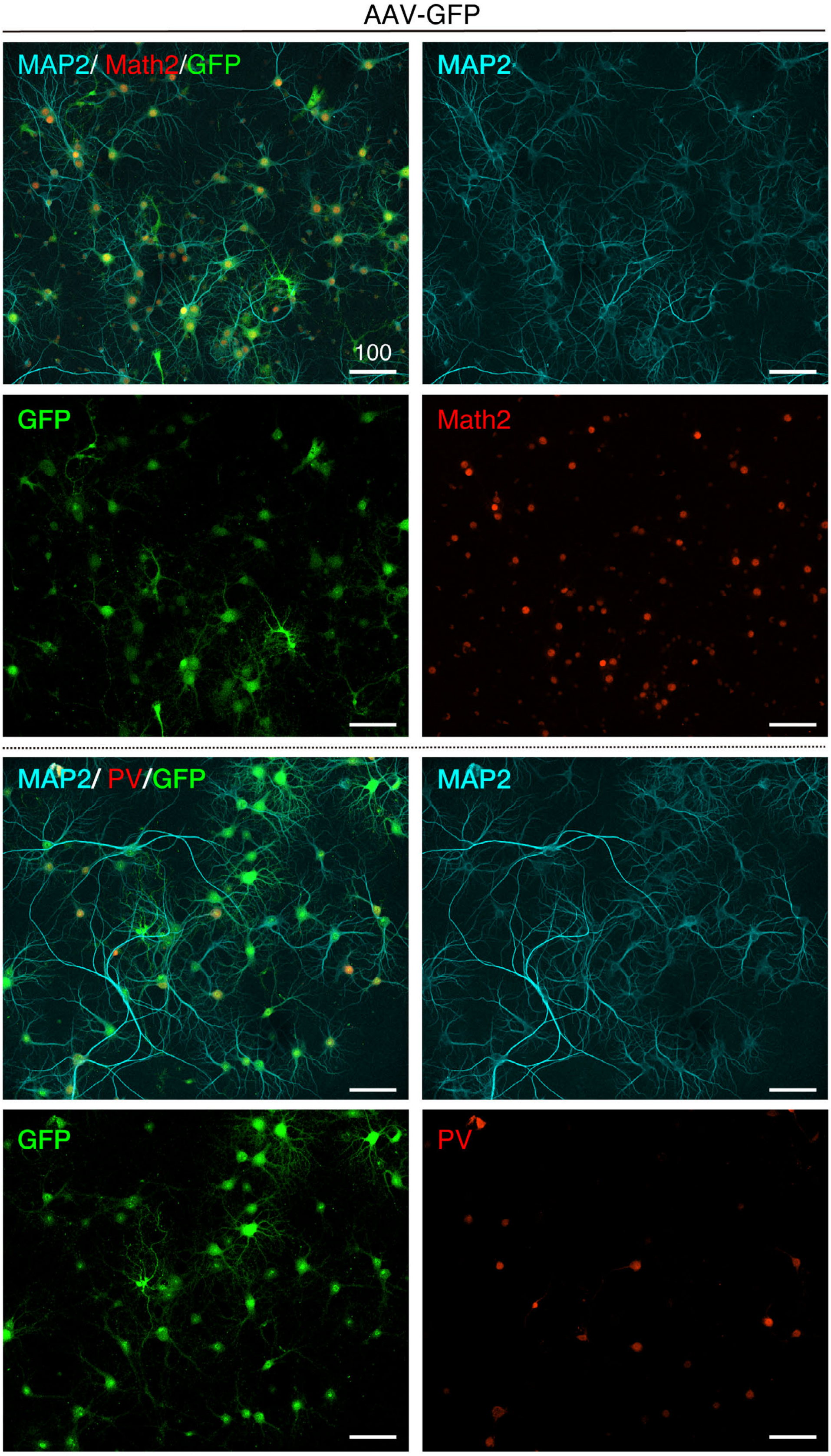
AAV-GFP
MAP2/ Math2/GFP
MAP2
100
GFP
Math2
MAP2/ PV/GFP
MAP2
GFP
PV

Figure S16 GFP was Transduced Both in Excitatory and Inhibitory Neurons with the Same Efficiency, related to Figures 14, S17, and S18

GFP-transduced neuronal cultures without MG132 treatment were triple-stained with MAP2, GFP, and Math2 or PV. Representative images are shown with 100 μm scale bars. Please note that GFP was transduced to almost all neurons, irrespective of Math2-positive excitatory neurons (Schwab et al., 2000) (99.1 ± 1.4 %, n = 30) or parvalbumin (PV)-positive GABAergic interneurons (97.0 ± 3.7 %, n = 30). The ratio of the GFP-containing neurons among either MAP2/Math2- or MAP2/PV-double-positive neurons was quantified using a Yokogawa CQ1 (see Transparent Methods; Inset, mean ± SD).

Figure S17

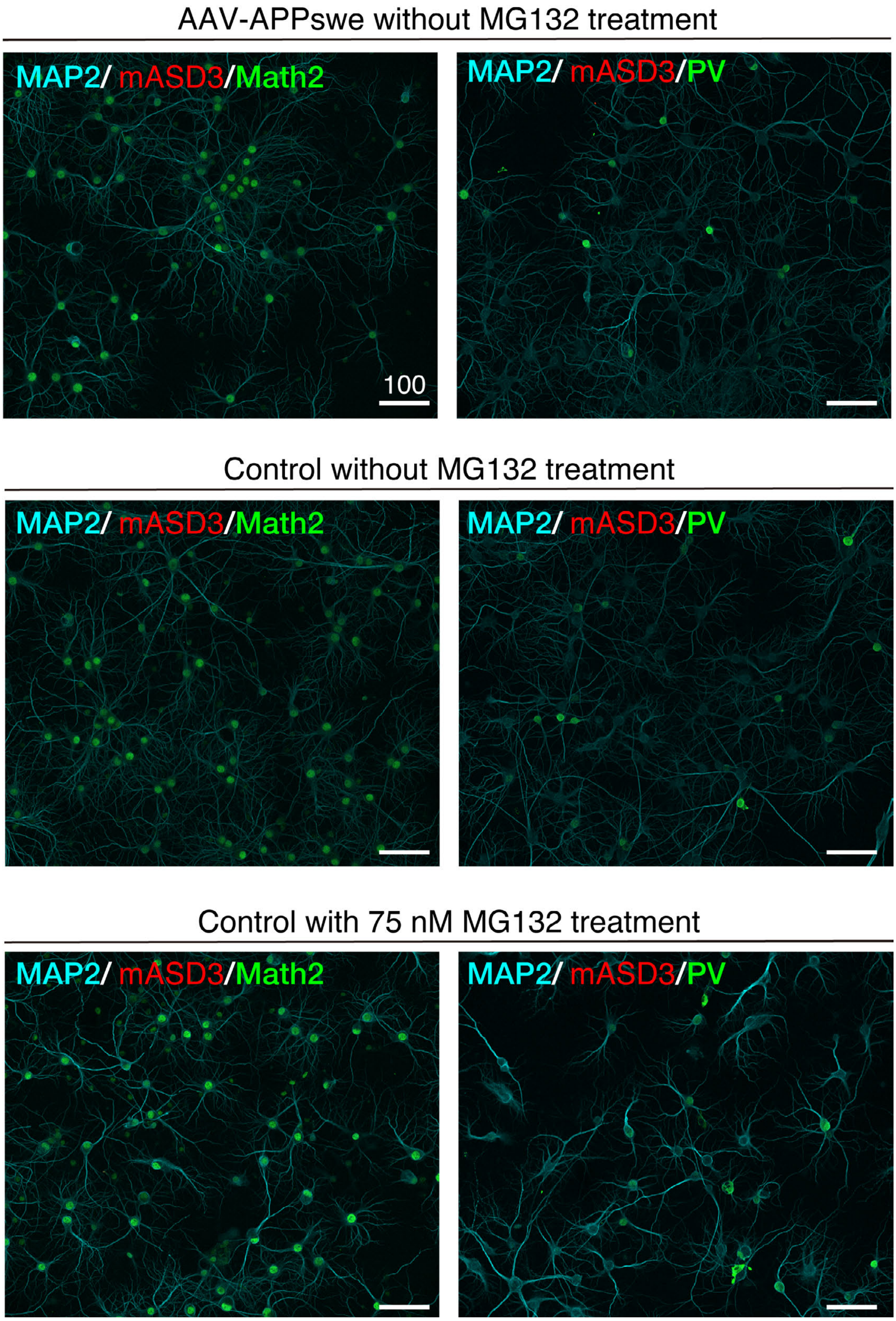
AAV-APPswe without MG132 treatment
MAP2/ mASD3/Math2
100
MAP2/ mASD3/PV
Control without MG132 treatment
MAP2/ mASD3/Math2
MAP2/ mASD3/PV
Control with 75 nM MG132 treatment
MAP2/ mASD3/Math2
MAP2/ mASD3/PV

Figure S17 ASPD Accumulate Only in Excitatory Neurons, related to Figures 14 and S18

APPswe-transduced or untransduced control neuronal cultures were treated with or without MG132 treatment for 24 hr and then triple-stained with MAP2, mASD3, and Math2 or PV. Representative images are shown with 100 μm scale bars.

Figure S18

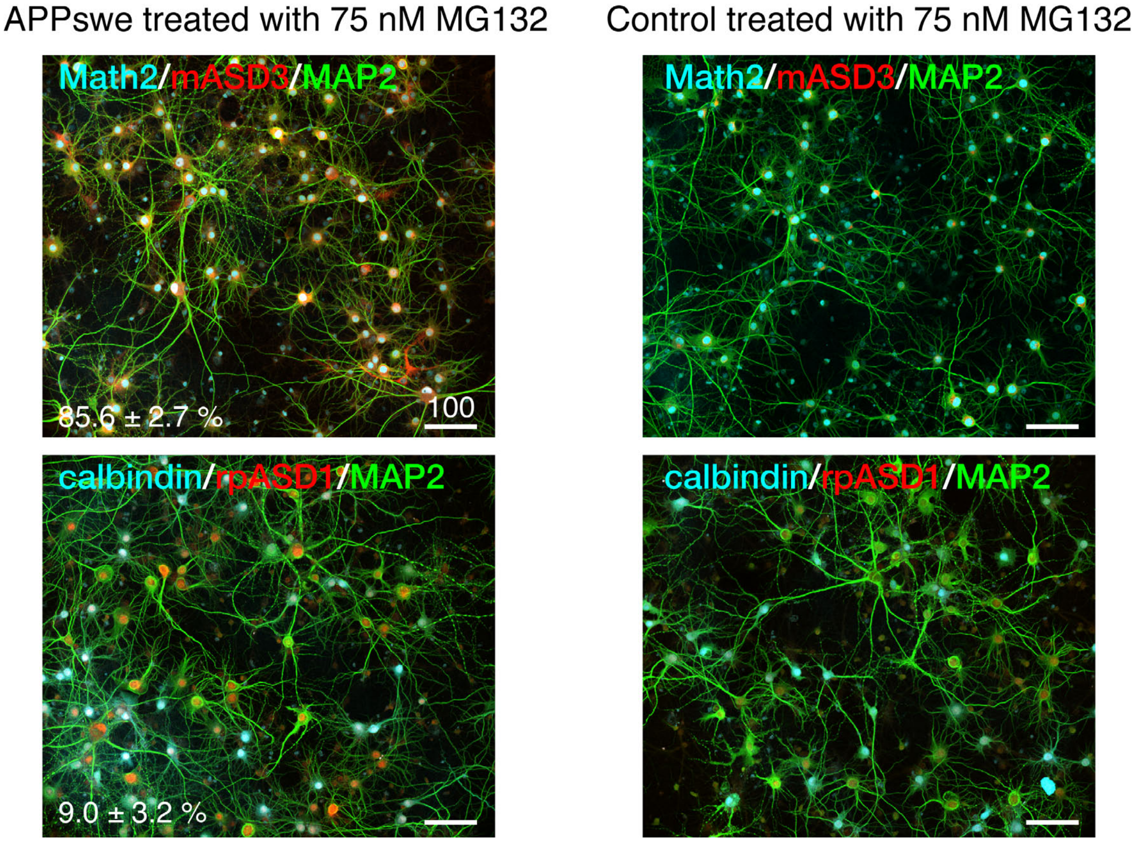

Figure S18 ASPD Accumulate Only in Excitatory Neurons, related to Figure 14
APPswe-transduced or untransduced control neuronal cultures with 24 hr MG132 treatment were triple-stained with MAP2, mASD3, and Math2 or with MAP2, rpASD1, and calbindin. The ratio of the ASPD-containing neurons among either MAP2/calbindin or MAP2/Math2-double-positive neurons was quantified using a Yokogawa CQ1 (see Transparent Methods; Inset, mean ± SD, n = 5). ASPD were detected by anti-ASPD rpASD1 or mASD3 antibody.

Figure S19

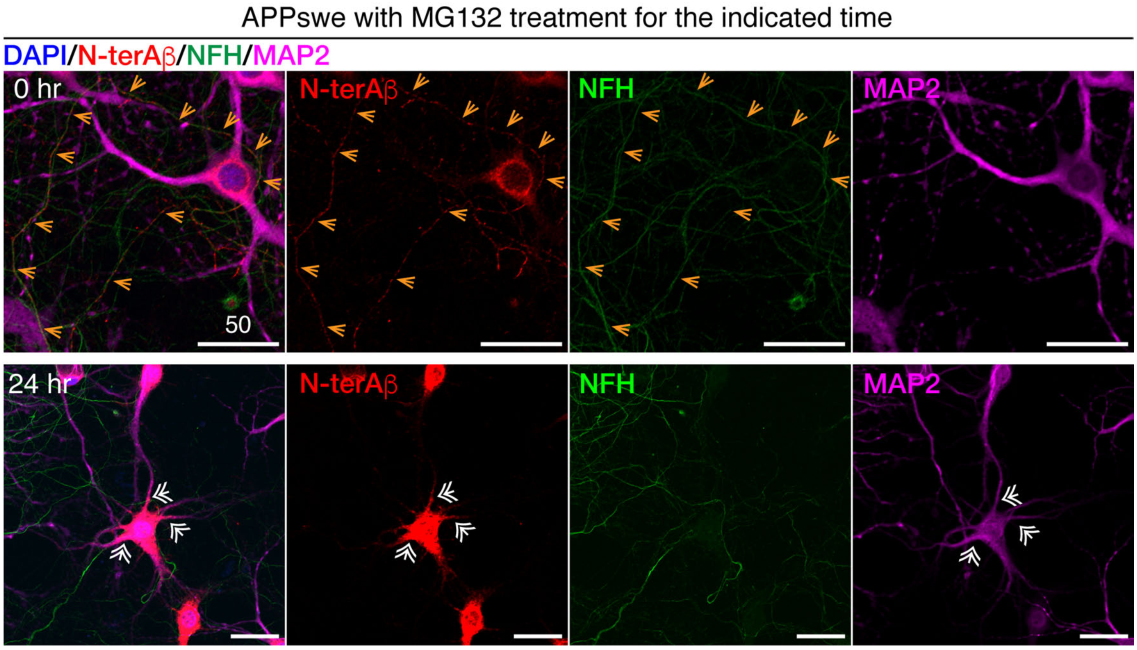

Figure S19 Aβ Distribution in MG132-treated APPswe-transduced Neurons, related to Figure 5

Primary rat hippocampal neuronal cultures with AAV-APPswe transduction were treated with 75 nM MG132 for 24 hr, and quadruple-stained at 22 DIV with the anti-ASPD rpASD1 antibody, anti-NFH antibody, anti-MAP2 antibody, and DAPI (see Transparent Methods). A representative image, along with the corresponding single red, green, or magenta image, is shown with 50 μm scale bars. Orange arrows mark axons, while white double-lined arrows mark dendrites. ASPD were co-localized with NFH (orange arrows) in the upper panels, but co-localized with MAP2 (white double-lined arrows) in the lower panels.

Transparent Methods

Ethics

The Animal Care and Experimentation Committees of MITILS, Kyoto University, FBRI, and TAO approved animal experiments.

Introduction of human APP770 genes bearing early-onset mutations into mature primary neuronal cultures by using an AAV vector

APP exists in several alternatively spliced isoforms, including APP695, APP751, and APP770. APP751 and APP770 contain a Kunitz-type protease inhibitor (KPI) domain (Nalivaeva and Turner, 2013). KPI domain-containing APP770 was used to establish a mature neuron-based system, because reports show that the protein and mRNA levels of KPI domain-containing APP isoforms (in particular APP770) are elevated in AD brains and are associated with increased Aβ deposition (Menendez-Gonzalez et al., 2005; Tanaka et al., 1988). It was also reported that prolonged activation of extrasynaptic NMDA receptor in neurons could shift APP expression from APP695 to KPI domain-containing APP isoforms, accompanied with increased production of Aβ (Bordji et al., 2010). Therefore, an adeno-associated virus 1-derived (AAV) vector expressing human APP770 gene with a familial AD mutation was produced as described previously (Li et al., 2006). The expression cassette contains a cytomegalovirus (CMV) immediate-early promoter, cDNA of human mutant APP, and simian virus 40 polyadenylation signal sequence between the inverted terminal repeats of the AAV2 genome. HEK293 cells were transduced with the vector plasmid, the AAV2 *rep* and AAV1 *vp* expression plasmids, and the adenoviral helper plasmid pHelper (Invitrogen). The recombinant viruses were purified by isolation from two sequential continuous CsCl gradients. Viral titers were determined by measuring the vector genome with quantitative PCR (Li et al., 2006). Primary rat hippocampal cultures were prepared from embryonic day 17 pups and plated at 4.1×10^4 cells/cm^2 (48-well plates), 2.7×10^4 cells/cm^2 (24-well plates), or 3.4×10^4 cells/cm^2 (cover glasses) in Neurobasal media containing B27 supplement and 2.5 μM L-glutamine (termed LC)(Ohnishi et al., 2015). At 10 DIV, the cultures were infected with the above AAV vectors, which were removed at 14 DIV. At 21 DIV, the medium was replaced with fresh LC, with or without MG132 (3175-v), lactacystin (4368-v), or epoxomicin (4381-v) as a proteasome inhibitor (Peptide Institute Inc.), dissolved in sterile

Hybri-Max™ dimethyl sulfoxide (Sigma-Aldrich). Brefeldin A (BFA)(Sigma-Aldrich B5936) was dissolved in LC containing 10% (v/v) ACM.

Evaluation of secreted ASPD toxicity

Two different lines of experiments were performed.

First, to examine whether ASPD secreted from neurons indeed exerted neurotoxicity against neighbouring neurons, AAV-APPswe transduced neurons (see above "Primary neuronal cultures") were pretreated for 2 hr with ASPD-specific mouse monoclonal mASD3 antibody (1 ng/ml), which we have established and shown to specifically block the neurotoxicity of patient-derived ASPD against mature neurons (Noguchi et al., 2009). Then, these neurons were further treated with 75 nM MG132 for 24 hr. As a control, untransduced neurons were treated in the same way.

Second, culture media were collected from untransduced or AAV-APPswe transduced neurons after 24 hr MG132 treatment. The ASPD-specific mASD3 antibody or normal mouse IgG (12 μg each) was covalently conjugated to 60 μl of *N*-hydroxysuccinimide (NHS)-activated magnetic beads (Thermo Scientific) according to the manufacturer's instruction. The collected culture media (1.2 ml) were incubated with the resulting mASD3-conjugated or normal mouse IgG-conjugated magnetic beads by slowly rotating the sample for 1 hr at room temperature (r.t.). Another primary rat hippocampal culture at 22 DIV without AAV transduction was treated with the immunodepleted medium for 24 hr.

In both experiments, the neurons were fixed and immunostained with appropriate antibodies, and quantification of NAKα3-expressing neurons was performed as described below: "Immunocytochemistry."

Immunocytochemistry and quantification

ASPD were detected by immunohistochemical staining with ASPD-specific rpASD1 antibody or mASD3 antibody (Noguchi et al., 2009), which has been used to detect ASPD in immunopathological studies of human brains (Noguchi et al., 2009; Ohnishi et al., 2015). Primary neuronal cultures were fixed with 4% (w/v) paraformaldehyde (PFA) for 15 min at 37 °C and rinsed three times with Dulbecco's phosphate-buffered saline without calcium and magnesium (PBS). The fixed cells were treated with 1 mg/ml $NaBH_4$ for 20 min at r.t., rinsed three times with PBS, permeabilized with 0.2%

(v/v) Triton X-100 for 5 min at r.t., and rinsed three times with PBS. The cells were pretreated with PBS containing 3% (w/v) BSA (Sigma-Aldrich) and 10% (v/v) normal goat serum (NGS)(IBL Co., Ltd.) for 30 min at r.t., and incubated overnight with primary antibody against APP (1:250, Millipore AB5988P), GFAP (1:400, Sigma-Aldrich G3893), MAP2 (1:5000 or 1000, EnCor Biotechnology Inc. CPCA-MAP2; 2 μg/ml, Sigma-Aldrich M4403), Neurofilament heavy polypeptide (NFH) (1:1000, abcam ab7795), ASPD (4.3 μg/ml rabbit polyclonal rpASD1; 1.3 μg/ml mouse monoclonal mASD3), Aβ N-terminal end (1:200, rabbit monoclonal D54D2, Cell Signaling Technology 8243), PDI (1:2000, Affinity BioReagents MA3-019), GM130 (1:100, BD Biosciences 610822), TGN38 (1:100, BD Biosciences 610898), EEA1 (1:300, BD Biosciences 610457), LAMP1 (1:100, Enzo Life Sciences ADI-VAM-EN001-D), TfR (1:1000, monoclonal H68.4, Invitrogen 13-6800), NAKα3 (0.4 μg/ml, Santa Cruz sc-16051-R), parvalbumin (1:250, Novus NB120-11427), calbindin (CB-955)(1:1000, abcam ab82812), Math2 (1:200, abcam ab85824), or Bassoon (1:500, Enzo Life Sciences ADI-VAM-PS003) at 4 °C. After three washes with PBS, the cells were incubated with a highly cross-adsorbed secondary antibody in PBS containing 3% (w/v) BSA and 10% (v/v) NGS (Alexa Fluor 546 (1:1000), Alexa Fluor 555 (1:1000), or Alexa Fluor 594 (1:1000) as anti-rabbit IgG; Alexa Fluor 488 (1:400), Alexa Fluor 555 (1:1000), or Alexa 647 (1:1000) as anti-mouse IgG; Alexa Fluor 405 (1:1000), Alexa Fluor 488 (1:1000) or Alexa Fluor 647 (1:2000) as anti-chick IgG, Molecular Probes) for 90 min at r.t. In some experiments, cells were counterstained with 4',6-diamidino-2-phenylindole (DAPI)(1:500, Dojindo Molecular Technologies, Inc.) along with the secondary antibodies. The cells were rinsed three times with PBS and mounted with Prolong Gold anti-fade reagent (Invitrogen). TUNEL staining was performed using a DeadEnd^{TM} Fluorometric TUNEL System (Promega) according to the manufacturer’s instructions. The TUNEL-stained cells were further immunostained with the anti-ASPD rpASD1 antibody, followed by DAPI counterstaining as described above. Live/dead dual cell staining was performed using PI and calcein-AM(Hoshi et al., 2003). Briefly, live cells were incubated with the solution containing PI (1:100, Dojindo Molecular Technologies, Inc.) and calcein-AM (1:500, Dojindo Molecular Technologies, Inc.) for 30 min at 37 °C, and immediately fixed with 10% (v/v) neutral buffered formalin for 30 min at 4 °C, then immunostaining was performed as described above. Low-magnification fluorescence images were acquired via x10-x20 objective lenses with a cooled CCD camera using photomultiplier tubes on a Zeiss LSM710 confocal microscope with constant laser intensity and signal detection settings (Ohnishi et al., 2015). High-power views were taken with an x100 oil immersion lens using a direct photon-counting ConfoCor 3 avalanche photodiode detection system on a Zeiss LSM710 confocal microscope with constant laser intensity and signal detection settings (Ohnishi et al., 2015). Neuronal images were taken at 0.4 μm intervals on the z-axis. ASPD formation detected by ASPD-specific rpASD1 antibody was quantitated by using a GE Healthcare Life Sciences "IN Cell Analyzer" system. Approximately 500 cells were randomly selected from seven different fields. The weighted colocalization coefficients were obtained using ZEN2009 software (Zeiss) exactly according to the manufacturer's instructions. The weighted colocalization coefficients consider the intensity value of the summed pixels and calculate values based on the estimated fluorophore population. In calculating the weighted colocalization coefficients, all imaging parameters that influence the intensity of the image remain the same for all data acquisitions, including the objective lens, laser power, filter sets, wavelength collections, acquisition speed, camera, and APD settings. The weighted colocalization coefficients represent the number of red pixels (rpASD1 or N-terminal end specific Aβ) that colocalize with green pixels (organelle markers) divided by the total number of red pixels. To quantify NAKα3-expressing neurons, a confocal quantitative image cytometer, CQ1 (Yokogawa Electric Corporation), was used to acquire 4 to 9 view fields/well. The NAKα3 area was calculated from the sum of areas stained by the anti-NAKα3 antibody. Co-localization of ASPD signals with either anti-parvalbumin/anti-calbindin or anti-Math2 signals was also quantitatively determined by using CQ1 as described above.

Viability

Viability was determined with a Cell Counting Kit-8 (Dojindo Molecular Technologies, Inc.) according to the manufacturer's instructions.

In house-developed ASPD CLEIA

ASPD-specific CLEIA was developed with two ASPD-specific antibodies, rpASD1 as a capture antibody and mASD3 as a detection antibody (Noguchi et al., 2009). rpASD1 antibody (500 ng/well) was applied to 96-well microplates, which were incubated overnight at 4 ˚C, and blocked with 3% (w/v) BSA in TBS for 30 min at r.t. The sample or the standard was added, and incubation was continued for 1 hr at r.t. The plates were washed, mASD3 antibody (100 ng/well) was added, and incubation was continued for 1 hr at r.t. The plates were rewashed and incubated with horseradish peroxidase-conjugated anti-mouse IgG (4 ng/well, Jackson ImmunoResearch Laboratories, Inc. 715-035-151) for 1 hr at r.t. Immunoreactions were detected by incubating the plates with a chemiluminescent substrate (Thermo Fisher Scientific Inc. QL227687) for 1 min in the dark. Luminescence was detected with a Berthold luminometer. ASPD were determined from a standard curve generated from serial dilutions of synthetic ASPD, the concentration of which was pre-determined by quantitative amino acid analysis (Ohnishi et al., 2015). As a negative control, solutions of A$\beta_{1\text{-}42}$ containing monomers and LMW-Aβ (such as dimers) were prepared (Ohnishi et al., 2015; Xiao et al., 2015). Briefly, lyophilized A$\beta_{1\text{-}42}$ was dissolved in 10 mM NaOH solution to give a 0.6 mM solution, followed by 10-fold dilution with 10 mM phosphate buffer (pH 7.4). The 50-kDa flow-through fraction (Vivaspin 500, Sartorius) obtained by centrifugation at $4.8 \times 10^3 \times g$ for 3 min contained mostly A$\beta_{1\text{-}42}$ monomers without pre-formed high-mass aggregates (Ohnishi et al., 2015; Xiao et al., 2015). Its concentration was also determined by quantitative amino acid analysis (Ohnishi et al., 2015). The ASPD-specific CLEIA system did not respond to this 50-kDa flow-through fraction of A$\beta_{1\text{-}42}$.

Quantification of ASPD, A$\beta_{1\text{-}40}$, and A$\beta_{1\text{-}42}$

The culture supernatant was collected and immediately filtered through a 0.22 μm Millex-GV filter. A$\beta_{1\text{-}40}$ and A$\beta_{1\text{-}42}$ in the supernatant were quantified using the WAKO sandwich ELISA systems specific to A$\beta_{1\text{-}40}$ (292-62301) and A$\beta_{1\text{-}42}$ (296-64401), respectively, according to the manufacturer's instructions. The 10-times-concentrated culture supernate was obtained from the above 0.22-μm filtered sample by recovering the 100-kDa retentates (Vivaspin 20, Sartorius). This filtration process eliminated Aβ monomers and LMW-Aβ (such as dimers and dodecamers) from the 100-kDa retentates (Noguchi et al., 2009). ASPD in the supernates was quantified using the in house developed ASPD-specific CLEIA system.

TEM

Samples were negatively stained with 4% (w/v) uranyl acetate solution on high-resolution carbon substrate on STEM 100Cu grids (HRC-C10, Okenshouji Co., Ltd) and analyzed immediately (Ohnishi et al., 2015).

Dot blotting

Dot blotting was performed (Ohnishi et al., 2015) using 40 ng/ml ASPD-specific rpASD1 antibody in 5% skim milk with membrane boiling, and 12.5 ng/ml anti-Aβ N-terminal 82E1 antibody in 10% skim milk without membrane boiling. Immunoreactions were detected with SuperSignal West Femto chemiluminescent substrates and quantified using a LAS-4000 Mini (Ohnishi et al., 2015).

ASPD Preparation

ASPD are neurotoxic, spherical Aβ assemblies of 10-15-nm diameter (measured by TEM) that are recognized by ASPD-specific antibodies (Ohnishi et al., 2015). Synthetic ASPD formed in 50 μM $A\beta_{1\text{-}42}$ solution (derived from wild-type $A\beta_{1\text{-}42}$ or $A\beta_{1\text{-}42}$-osk) using in house prepared highly soluble Aβ peptides (essential for obtaining ASPD; see "Aβ synthesis") in F12 buffer without L-glutamine and phenol red by slowly rotating the solution for ~16 hr at 4 ˚C (Ohnishi et al., 2015). ASPD quality was confirmed by dot blotting, TEM, amino acid analysis, and toxicity assays (Ohnishi et al., 2015).

Aβ synthesis

Highly soluble $A\beta_{1\text{-}42}$ and $A\beta_{1\text{-}42}$-osk peptides were synthesized in house, purified, finally lyophilized in a solution containing 0.1% (v/v) TFA and 30% (v/v) acetonitrile on ice (~150 μM), and kept at -30 ˚C (Ohnishi et al., 2015). Purity was confirmed by analytical HPLC, quantitative amino acid analysis, and matrix-assisted laser desorption/ionization time of flight/mass spectrometry. The peptides were completely dissolved in 1,1,1,3,3,3 hexafluoro-2-propanol (HFIP for HPLC; Kanto Chemical Co., Inc.) at ~80 μM and lyophilized (~40 nmol/tube)(Ohnishi et al., 2015). This step was repeated three times. The lyophilized peptide was kept at -30 ˚C. We have long used HFIP from Sigma-Aldrich, which we previously found contained ~1.3 mM bis(2-ethylhexyl)phthalate (DEHP)(Ohnishi et al., 2015). This means that solutions of peptide lyophilized in Sigma-Aldrich HFIP usually contained ~0.65 mM DEHP when the peptide concentration was 50 μM. Therefore, when we used HFIP in which DEHP was undetectable, we added DEHP (0.65 mM final concentration; Tokyo Chemical Industry Co., Ltd.)(Ohnishi et al., 2015) to ensure consistency with our previous conditions (Hoshi et al., 2003; Matsumura et al., 2011; Noguchi et al., 2009).

Western blotting

Whole-cell lysates were prepared by lysing the cells in a lysis buffer (50 mM Tris (pH 7.5), 107 mM NaCl, 5 mM EDTA, 0.1% SDS, 0.5% sodium deoxycholate, 1% NP40, 1 μg/mL pepstatin, and 1x EDTA-free complete protease inhibitor cocktail (Roche)) and collecting the supernatant by centrifugation (Ohnishi et al., 2015). In detecting APP, the supernatant (10 μg/lane) was separated under denaturing conditions on reducing NuPAGE 4-20% Tris-Glycine gels and transferred onto a 0.2-μm nitrocellulose membrane. The membrane was blocked with 5% (w/v) skim milk for 1 hr at r.t., followed by incubation with primary antibody (0.1 μg/ml anti-APP, IBL11090; 0.3 μg/ml anti-actin, Millipore MAB1501R). In detecting Aβ, the supernatant (8 μg/lane) was separated under denaturing conditions on reducing NuPAGE 4-12% Bis-Tris gels (Invitrogen) and transferred onto a 0.2-μm nitrocellulose membrane. The membrane was blocked with 5% (w/v) skim milk for 1 hr at r.t., followed by incubation with primary antibody (0.05 μg/ml anti-Aβ N-terminal end, CST8243; 0.3 μg/ml anti-actin). In both cases, bands were detected with Super Signal West Femto and quantified using a LAS-4000 Mini (Ohnishi et al., 2015).

Statistical Analyses.

Statistical significance was assessed at the 5% significance level using Scheffé *post hoc* tests with StatView®5 software.

Supplemental References

Bordji, K., Becerril-Ortega, J., Nicole, O., and Buisson, A. (2010). Activation of Extrasynaptic, But Not Synaptic, NMDA Receptors Modifies Amyloid Precursor Protein Expression Pattern and Increases Amyloid-β production. J. Neurosci. *30*, 15927-15942.

Hoshi, M., Sato, M., Matsumoto, S., Noguchi, A., Yasutake, K., Yoshida, N., and Sato, K. (2003). Spherical aggregates of β-amyloid (amylospheroid) show high neurotoxicity and activate tau protein kinase I/glycogen synthase kinase-3β. Proc. Natl. Acad. Sci. U. S. A. *100*, 6370-6375.

Li, X.G., Okada, T., Kodera, M., Nara, Y., Takino, N., Muramatsu, C., Ikeguchi, K., Urano, F., Ichinose, H., Metzger, D., *et al.* (2006). Viral-mediated temporally controlled dopamine production in a rat model of Parkinson disease. Mol. Ther. *13*, 160-166.

Matsumura, S., Shinoda, K., Yamada, M., Yokojima, S., Inoue, M., Ohnishi, T., Shimada, T., Kikuchi, K., Masui, D., Hashimoto, S., *et al.* (2011). Two distinct amyloid β-protein (Aβ) assembly pathways leading to oligomers and fibrils identified by combined fluorescence correlation spectroscopy, morphology, and toxicity analyses. J. Biol. Chem. *286*, 11555-11562.

Menendez-Gonzalez, M., Perez-Pinera, P., Martinez-Rivera, M., Calatayud, M.T., and Blazquez Menes, B. (2005). APP Processing and the APP-KPI Domain Involvement in the Amyloid Cascade. Neurodegener. Dis. *2*, 277-283.

Nalivaeva, N.N., and Turner, A.J. (2013). The amyloid precursor protein: a biochemical enigma in brain development, function and disease. FEBS Lett. *587*, 2046-2054.

Nebenfuhr, A., Ritzenthaler, C., and Robinson, D.G. (2002). Brefeldin A: Deciphering an Enigmatic Inhibitor of Secretion. Plant Physiol. *130*, 1102-1108.

Noguchi, A., Matsumura, S., Dezawa, M., Tada, M., Yanazawa, M., Ito, A., Akioka, M., Kikuchi, S., Sato, M., Ideno, S., *et al.* (2009). Isolation and characterization of patient-derived, toxic, high mass amyloid β-protein (Aβ) assembly from Alzheimer disease brains. J. Biol. Chem. *284*, 32895-32905.

Ohnishi, T., Yanazawa, M., Sasahara, T., Kitamura, Y., Hiroaki, H., Fukazawa, Y., Kii, I., Nishiyama, T., Kakita, A., Takeda, H., *et al.* (2015). Na, K-ATPase α3 is a death target of Alzheimer patient amyloid-beta assembly. Proc. Natl. Acad. Sci. U. S. A. *112*, E4465-4474.

Schwab, M.H., Bartholomae, A., Heimrich, B., Feldmeyer, D., Druffel-Augustin, S., Goebbels, S., Naya, F.J., Zhao, S., Frotscher, M., Tsai, M.J.*, et al.* (2000). Neuronal basic helix-loop-helix proteins (NEX and BETA2/Neuro D) regulate terminal granule cell differentiation in the hippocampus. J. Neurosci. *20*, 3714-3724.
Tanaka, S., Nakamura, S., Ueda, K., Kameyama, M., Shiojiri, S., Takahashi, Y., Kitaguchi, N., and Ito, H. (1988). THREE TYPES OF AMYLOID PROTEIN PRECURSOR mRNA IN HUMAN BRAIN: THEIR DIFFERENTIAL EXPRESSION IN ALZHEIMER'S DISEASE. Biochem. Biophys. Res. Commun. *157*, 472-479.
Xiao, Y., Ma, B., McElheny, D., Parthasarathy, S., Long, F., Hoshi, M., Nussinov, R., and Ishii, Y. (2015). Aβ(1-42) fibril structure illuminates self-recognition and replication of amyloid in Alzheimer's disease. Nat. Struct. Mol. Biol. *22*, 499-505.